Development of a Hybrid Offshore Wind and Wave Energy System

Muhammad Waqas Ayub

This thesis is submitted in partial fulfillment

of the requirements for the degree of

Doctor of Philosophy in Engineering

January 2024

Lancaster University

Engineering Department

Declaration

I declare that this dissertation consists of original work undertaken solely by myself at Lancaster University and not been submitted in substantially the same form towards the award of a degree or other work, and affirm that acknowledgement has been made to assistance given and that all major sources have been appropriately referenced.

Muhammad Waqas Ayub

January 2024

Abstract

The proposed research aims to fulfil the growing demand for sustainable energy solutions by developing a hybrid offshore wind-wave energy (HOWWE) system. The project intends to contribute to the optimisation of power outputs and the reduction of infrastructure costs by harnessing the potential of both sources individually and synergistically. Key performance indicators (KPIs), including output power optimization and the efficiency of control algorithms, serve as crucial metrics for assessing the project's success. This project is in line with global initiatives to shift to cleaner, more efficient energy sources. This research's novitiates are focused on overcoming significant development issues relating to efficiency and power output maximisation. To improve the system efficiency by integration using converters with the implementation of a maximum power-point tracking algorithm (MPPT). A comprehensive numerical model that includes the permanent magnet synchronous generator (PMSG), linear generator, and HOWWE system serves as a basic novitiate for achieving the hybrid system. The research's principal goals are twofold: First, create an analytical model that integrates numerical and analytical approaches, focusing on power modelling and various power calculation case studies. Second, to optimise offshore wind and wave energy output power, various control strategies such as feedback linearization (FBL), proportional integral derivative (PID), sliding-mode control (SMC), super-twisting algorithm (STA), and integral-based real twisting algorithm (IBRTA) will be investigated and evaluated. STA and IBRTA algorithms have been carefully tested in comparison to conventional PID, FBL, and SMC algorithms, confirming their efficiency in increasing power generation. In the case of wave energy, single point absorber (SPA) and multipoint absorber (MPA) solutions are investigated using real-time data.

Furthermore, by developing MPPT techniques for both energy sources, the research contributes to the seamless integration of offshore wind-wave energy. Maximum power extraction is ensured by the use of voltage source converters (VSC) for both sources. The integration strategy, which employs VSC for AC-DC and voltage source inverter (VSI) for DC-AC, is tested using real-time data from the North West, Silverstone lightship and Greenwich lightship of the United Kingdom on a semi-submersible platform equipped with one PMSG and nine linear generators. The proposed system was successfully constructed and rigorously tested in MATLAB, with real-time data used to ensure accuracy and reliability in realistic situations. The findings of this study have the potential to considerably augment the field of HOWWE and contribute to the creation of long-term energy solutions for a cleaner and greener future.

Acknowledgment

The authors appreciatively acknowledge the funding provided by Lancaster University in terms of the Ph.D. studentship. To pursue the PhD degree and of finalising Thesis, I express gratitude to all Professors and friend for their great help.

Heart fully thankful to first supervisor, Dr Xiandong Ma, who provides and helps me to build PhD research idea from scratch to implementation by his suggestion and motivations. He is the best teacher, mentor, professional guider for research. He is enduring and cooperative scholar, and always inspires me when I meet complications in my academic life.

Many thanks to Professor George Aggidis, who also contributes with his useful supervision for my PhD. He motivates and persuades me for my research in appraisal meetings. I am thankful to my family as well, specially my parents and wife. My wife is a doctor and she left her job to look after my twin's children and helped me to complete PhD journey.

Table of Contents

Abbreviations

AC: Altering Current

AI: Artificial Intelligence

AWS: Archimedes Wave Swing

CA: Cluster Analysis

DFIG: Doubly-Fed Induction Generator

DC: Direct-Current

EMF: Electromotive Force

EU: European Union

FA: Factor Analysis

FBL: Feedback Linearization

FLC: Fuzzy Logic Control

FFNN: Feed Forward Neural Network

FWT: Floating Wind-Turbine

GBS: Gravity Base Support

GSC: Grid Side-Converter

GSVSC: Grid-Side Voltage-Source-Converter

HCS: Hill Climb Search

HSS: High Speed Shaft

HOWWE: Hybrid Offshore Wind-Wave Energy

HVDC: High-Voltage Direct-Current

IBRTA: Integral based real twisting algorithm

JWWE: Joint Wind Wave Energy

KPIs: Key Performance Indicators

KE: Kinetic Energy

LG: Linear Generator

LCC: Line Commutated Converter

LPMG: Linear Permanent Magnet Generator

MPA: Multipoint Absorber

MTDC: Multi-Terminal HVDC

MPPT: Maximum-Power Point Tracking

MPP: Maximum-Power Point

NDA: Non-Uniformly-Distributed-Array

OWC: Oscillating Water Column

OWT: Offshore-Wind Turbine

OWF: Offshore Wind Farm

OWHE: Offshore Wave Energy

PCA: Principle Component Analysis

PDA: Peripherally Distributed-Array

PID: Proportional-Integral Derivative

PI: Proportional-Integral

PLL: Phased Loop Locked

PSF: Power Signal Feedback

PWM: Pulse-Width Modulation

PV: Photo Voltaic

RES: Renewable Energy-Sources

RSC: Rotor Side-Converter

SPA: Single Point Absorber

SFC: Semi-Submersible Flap-Combination

SG: Synchronous Generator

SMC: Sliding-Mode-Control

STA: Super-Twisting-Algorithm

TSR: Tip-Speed-Ratio

UDA: Uniformly-Distributed-Array

VSC: Voltage-Source Converter

VSI: Voltage-Source Inverter

VSWECS: Variable Speed Wind Energy Conversion System

Acronyms

$qd0$	Direct-quadrature-zero
F_L	Input-torque of the linear-motion
T_L	Input-torque of the rotary-motion
J	Rotary inertia
M	Mover weight
T_e	Electromagnetic torque
F_e	Thrust
B_r	Transmission friction of rotary part
B_l	Transmission friction of linear part
r	Pearson's coefficient
μ_x	Observation mean value
σ_x	Standard deviation
N	Total number of sample
U_{10}	Speed of wind at 10m height
$\in$	Wind shear exponent
ω_h	Shaft speed
ω_{ref}	Reference speed
e	Error
R_b	Radius of WT blade
v_{wd}	Wind speed
ρ	Mass density of air
C_{pr}	Power-coefficient

w_{sh}	WT shaft angular-speed
q	Gear-transmission-ratio
$C_T(\lambda)$	Torque coefficient
R_{stator}	Stator-resistance
L_d	Inductances
Ω_h	Angular speed
Φ_m	Flux of permanent magnets
J	Generator shaft inertia
$R_{chopper}$	Equivalent chopper-resistance
D	Drop of DC voltage
F	Force
H	Magnetic field strength
i_{as}	Stator current for the ‘a’-phase
i_{bs}	Stator current for the ‘b’-phase
i_{cs}	Stator current for the ‘c’-phase
i_{abcs}	Stator-current matrix
J	Rotational inertia
$qd0$	Transformation matrix
L	Generator inductance
LC	Inductance across capacitance
p	Poles numbers
P	Generated power

List of Figures

List of Tables

Chapter 1 Introduction

In this chapter, a brief definition, problem statement, objectives, advantages, innovation and knowledge contribution of HOWWE is explained. This chapter starts with a brief overview of the HOWWE system and Section 1.1 covers the definition of HOWWE. Section 1.2 is the problem statement and then the problems required to solve in HOWWE research are identified and the associated solutions are discussed in 1.3. Section 1.4 is the aim and objectives of the research. Furthermore, Section 1.5 is the novelty of this research and 1.6 is the selected approach. Section 1.7 is summarized, the structure of the thesis.

1.1 Definition of HOWWE

In recent decades, power generation from oceanic energies, which includes offshore wind and wave energy, has ascended to prominence. As the global community grapples with increasing energy demands and the depletion of natural resources, there has been a discernible pivot towards exploring and deploying sustainable energy resources [1]. Notably, offshore and marine energy sources have captivated attention as potent, alternative solutions to meet burgeoning energy needs sustainably. The rising demand of electricity can be achieved by advanced renewable energy methods such as hybrid offshore wind and wave energy (HOWWE). HOWWE is the novel combination of two energy resources, first is the offshore-wind and the second is the wave energy. It also synergistically merges the both resources functionalities. This approach targets to capitalize balancing nature of HOWWE, generating consistent energy output. Consequently, amalgamated configuration improves the dependability and reliability of the power supply. The offered area also covers different parts such as power conversion and inversion, both energy sources coupling, the cogeneration to combine the both resources and classification of the system. Due to the increase in global warming, the depletion of natural resources, and the fact that HOWWE is more environmentally friendly, it has been fairly popular in recent years. There are following advantages of the HOWWE system such as continuous power supply, cost-effective energy source, low maintenance cost, linking to the electric grid by same electric cables, area-efficient and the power generation from both sources at one point. The offshore wind speeds tend to be faster than on land and the wave energy is the reliable source of energy due to the continuous motion of the sea waves. The proposed area of this PhD research is to develop the HOWWE. To harvest the supreme power from the stated hybrid renewable energy system, a

permanent magnetic synchronous generator (PMSG) and linear generator are needed to operate the variable speed consistently at their maximum power point (MPPs). Because of their low efficiency and incompatibility with fluctuating wind conditions, conventional induction generators are frequently not chosen for offshore wind power. The key development issues to be addressed are associated with energy efficiency and optimal production. Most of the problems concerned with the prior techniques have been solved by implementing some hybrid control schemes. The control contributes many advantages, such as better convergence, insensitivity to variation in parameters. The combination of two different control techniques constitutes a hybrid technique, which utilizes the benefits of one technique to mitigate the problems of others.

Currently, the power generation from the wave energy system is low due to the lack of design consideration, controller design, generator selection and higher levelised costs [2]. The unsuitable design coupling between wind and wave makes the system heavy. Wave energy converters (WECs) come in a variety of designs and technologies; therefore the generators used in wave energy systems can range from linear generators to hydraulic generators. There are following advantages of unidirectional motion of linear generator with the wind turbine such as it produces more power and low cost of construction. The joints of linear generator on the wind turbine tripod support the system from heavy sea wave. The structure of wave energy generation on HOWWE is based on the buoy, linear generator, coupling rod and cables. Moreover, the state-of-the-art infrastructure is also studied for the system. In Fig. 1.1, the flow chart shows the development of HOWWE using individual power conversions and joint inversion and battery storage units respectively.

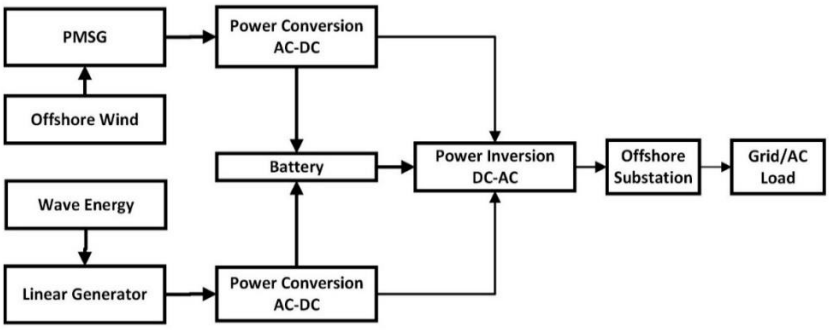

Figure 1.1 PMSG and linear generator-based HOWWE system

1.2 Problem identification

The current structures of HOWWE are lack of efficiency and power conversion process that are required to be improved at their optimal level. The hybrid system model needs careful understanding to maximise the power output, it can be achieved by improving, adding or changing the existing hybrid parameters, parts, structural design, cogeneration, correlation and control strategies to integrate both sources. Considering the real time example, doubly fed induction generator (DFIG) and synchronous generator are used for offshore wind system and to select the ideal generator for HOWWE is important to maximise the output power.

The main agenda is to improve the current structure of the hybrid model by using appropriate generators for both sources. Similarly, different techniques used for power generation from wave energy such as oscillating water column in chamber but this technique is not suitable for the hybrid system. Design of hybrid system also needs improvement. Existing design covers separate panel of offshore wind and separate array of wave energy separate, hence cogeneration and coupling of both wind-wave sources is important. Furthermore, integration approach of both system is important and the analysis method to convert outputs from both sources.

1.3 Problem solution

In HOWWE, the wind source is more dominant source with percentage of 70 % as compared to wave energy with generation capacity of 30 %. So, to optimise the overall performance of HOWWE, the offshore wind needs more consideration for power optimisation. In our scenario, the ideal generator for wind power generation is the PMSG and for wave power generation is linear generator. The combination of both generators for the hybrid system provides a more efficient and sustainable model. The novel method is the optimization of the current infrastructure to produce a cost-effective and more efficient model. For harnessing of marine resources, a HOWWE is a new technology that can provide an alternative approach in the energy sector. In particular, the research will develop a novel HOWWE power conversion with controllers using maximum power point tracking (MPPT). A robust controller is required to run the system continuously at the MPPs. The PMSG is a preferable choice due to maximum reliability, gearless transmission capability, maintenance cost is loss and ease of control. The reasonable choice at the present is the co-located systems and semisubmersible platform that merge the both sources. The power optimisation is also based on the control algorithm. In this work, MPPT schemes will be developed via proportional integral derivative (PID) controller, sliding mode control (SMC), super twisting algorithm (STA) and integral based real twisting algorithm (IBRTA) to get maximum power from a PMSG. On the other hand, single point absorber (SPA) is implemented to couple with hybrid system. Moreover, new proposed technique for wave energy is carried out called as multipoint absorber. Finally, integration of both sources is carried out using voltage source converter and voltage source inverter. In particular, the research is based on facts and figures that are used for research development of a novel HOWWE system. Thus, using different

techniques and methodologies it is aimed that the HOWWE current structure will be improved.

1.4 Aim and objectives of research

The aim of this research work is to explore, develop, and optimize hybrid systems that combine two distinct technologies, aiming to enhance renewable energy contribution, system efficiency, and promote sustainable energy solutions. Our research undertakes a thorough assessment of the resource potential of both resources, examining the availability and variability of output power. We attempt to devise innovative designs and configurations that blend both energy sources into a singular, efficient hybrid system. Furthermore, control algorithms are applied to each energy source independently, ensuring optimal power output while maintaining system stability. Through the development of numerical models and conducting simulations, we evaluate the performance of HOWWE systems under various conditions, aiming to maximize overall energy output and increase system reliability by utilizing energy converters. The specific objectives are mention below:

- Assess existing OWT and WEC technologies, focusing on generators and power conversion for HOWWE farms.
- Model and simulate wind turbines with PMSG generators and wave power generation using linear generators to develop a hybrid system model.
- Implement various control strategies PID, FBL, SMC, STA an AI-based IBRTA for OWT and conduct comparative analysis of control strategies.
- Test wave energy conversion using SPA and MPA.
- Implement power conversion and inversion with VSC and VSI.

- Evaluate HOWWE systems using real-time data from North West, Silverstone and Greenwich lightship UK.

1.5 Novelties

In renewable energy sector the HOWWE is the development of existing pathway. This research is used to overcome challenges in the generator selection by studying different parameters of the generators, the ideal design to combine both sources, the optimal power solution by using conversion and inversion techniques. The proposed solutions make the system at optimal level for output power generation. The sub sections explain further optimisation in the different parts of HOWWE are categorised on the optimisation of individual source and combination of the both sources.

- **Innovation in offshore energy**

To increase the effectiveness and responsiveness of OWT, we have implemented a number of control methods and strategies. The power can be optimized with different control strategies such as PID, FBL control and model-based SMC. The model-based STA and IBRTA are designed and implemented to get maximum power. The suggested IBRTA is anticipated to result in more efficient power optimisation, making it particularly advantageous for remote or off-grid applications.

- **Innovation in wave energy**

For wave energy, we have tested single, multipoint absorber using real time data. The output power can be analysed using MPA approach that enhanced to merge two wave generators output for wider range of operating conditions. The key differentiators of this wave energy harvesting technology compare to present designs are the following. Using multiple

generators coupled with the base of offshore turbine and with three point energy generation this device is capable of generating energy from every movement of a buoyant structure and thus can harvest 3-4 folds more energy from comparable single-point energy harvesting system.

- **Innovation in HOWWE**

To generate steady and continuous energy output from HOWWE, VSCs and VSIs, can be used as an inventive solution to this problem. Moreover, this research also fills gap in the following sections of HOWWE as shown in the Fig. 1.2.

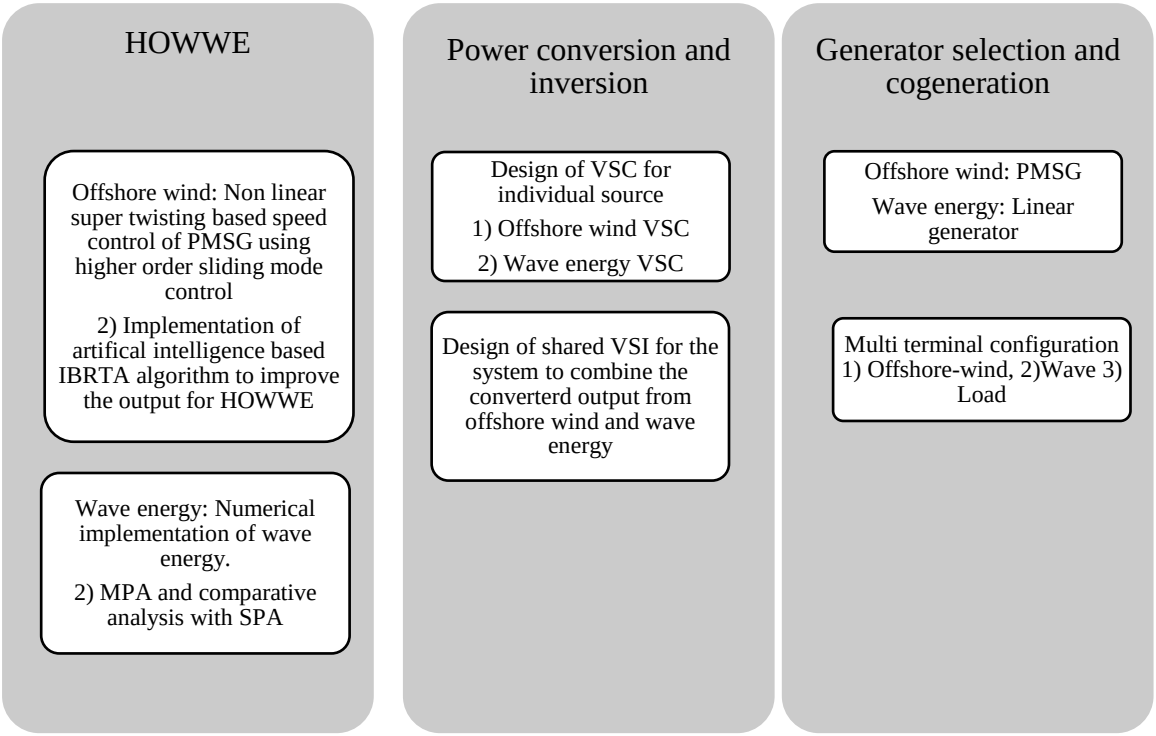

Figure 1.2 Novelty in three phases of project

1.6 Selected approach

There are challenges in the HOWWE system such as design, generator selection, control algorithms, power conversion and inversion. These challenges might be overcome by using appropriate techniques such as using PMSG generator, AI based IBRTA control algorithm and integration using VSC-VSI. The selected approach of the system is identified by farms, structure and generator selection as shown in Fig. 1.3. The most suitable system selection is colocated with multiple generators using PMSG and linear generator. The existing techniques are separate sources with monopole structure for offshore wind and oscillating water columns for wave energy. The study identifies major research gaps in the HOWWE, emphasizing the need for more investigation and comprehension.

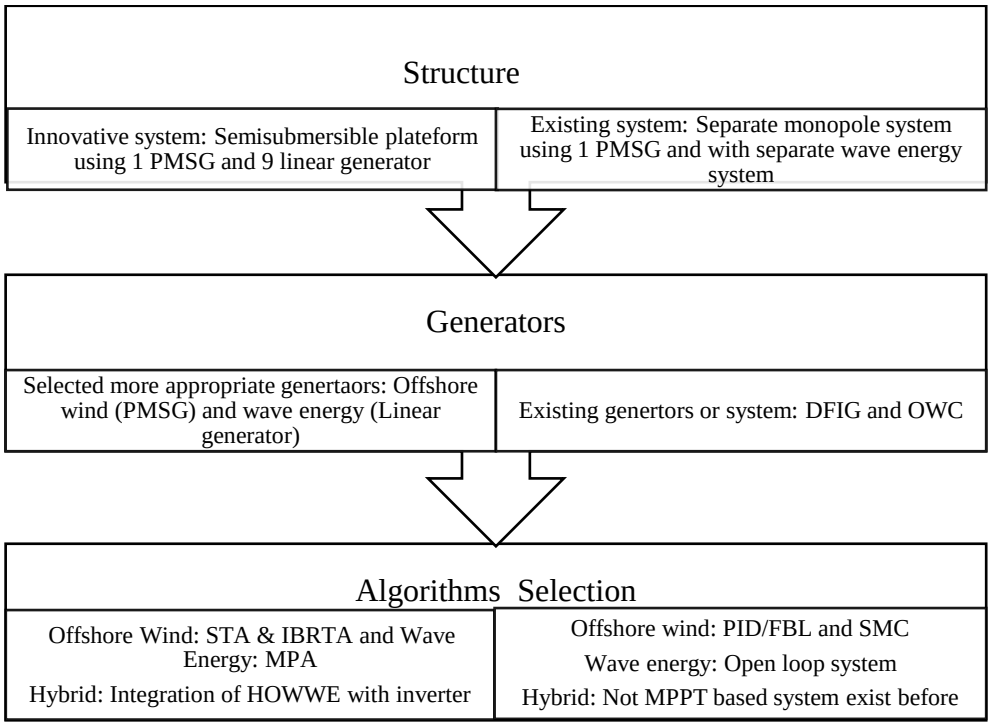

Figure 1.3 Classification of HOWWE system

The lack of comprehensive studies addressing efficiency and power output maximization difficulties in HOWWE systems is one of the most significant research gaps. While power

converter integration and the invention of a MPPT methods are novelties, there is a gap in knowledge of their practical implementation and efficacy in real-world circumstances.

1.6.1 Design considerations

The semi-submersible platform, incorporating an offshore wind turbine and nine linear generators, three on each side of the platform, represents a pioneering advancement in offshore renewable energy technology. This hybrid platform combines the output power stability of a semi-submersible structure, which floats partially submerged in water, with energy capture from both an offshore wind turbine and multiple linear generators. The wind turbine yokes wind power to generate electricity, while the strategically placed linear generators convert the linear motion induced by waves into additional electrical energy. This multifaceted approach not only amplifies total energy production efficiency but also enhances platform stability under challenging offshore conditions. Such integrated systems signify substantial potential in augmenting the viability of offshore wind energy, simultaneously improving sustainability and reliability. This methodology is notably superior, producing three times more energy compared to the existing technique, which employs a monopole with a single linear generator.

1.6.2 Resourceful generators for wind and wave

The generator selections are also useful task for making system efficiency better and effectiveness for energy extraction, particularly in wave energy systems. PMSG wind turbines and linear generators in tandem to maximize energy output, reduce maintenance costs, and display a strong commitment to improving the area of renewable energy, ultimately contributing to a more sustainable and eco-friendly energy landscape in real world. The existing generator used for the offshore wind is DFIG and wave energy is water chamber or

oscillating water column. These generators are quite difficult to combine and integrate in real world.

1.6.3 Control algorithms for wind and wave energy

The creation of novel algorithm IBRTA is a critical driver of innovation in a wind energy domain. This algorithm frequently reflects breakthroughs in optimization of power more efficiently and precisely. The IBRTA is a significant breakthrough in control systems, especially in terms of resilience and adaptability. IBRTA, in contrast to traditional control algorithms such as PID, provides a fresh way to dealing with complex and uncertain offshore wind systems. It uses STA concepts but expands on them by introducing higher-order terms to improve performance and precision. This breakthrough is especially useful in offshore wind where standard control systems struggle to maintain stability and accuracy. IBRTA capacity to deal with nonlinearities and uncertainties outperforms many existing control algorithms such as PID and SMC, making it an ideal controller for high-performance offshore wind system. It has ability to handle dynamic operation of offshore systems and provide robust management in the presence of disturbances. On the other hand, multipoint absorber makes major contributions to wave energy progress and practical applications.

1.6.4 Power integration for wind and wave

The integration of HOWWE makes a substantial contribution to the field of renewable energy. The voltage source converter (VSC) and voltage source inverter (VSI) system present grid connected HOWWE with power conversion for individual energy sources and shared power inversion of both energy sources. Similarly, power converter mixtures can be utilized in such frameworks in combination of on-location battery storage, thus providing the continuous output supply.

1.7 Thesis layout

The arrangement of chapter for PhD research thesis are given below:

The Chapter 1 covers the definition, problem statement and solution of the HOWWE system. The objectives and novelties section cover different important aspects and improvement in the HOWWE. Moreover, the importance of combining the HOWWE system and motivation of the projects is discussed. Furthermore, the objectives related with the investigation and the layout arrangement of the research dissertation are presented.

The Chapter 2 is based on literature review. The power conversion of the HOWWE system, the response coupling of HOWWE where spar torus wind-wave floating systems spar are discussed as the examples.

In the Chapter 3, the analytical analysis of overall system is presented. The offshore wind energy conversion is based on two sections; the OWT and modeling of PMSG. The state equation of the system with stability of zero dynamic term is used for wind conversion. The wave energy conversion using linear generator is carried out using variable equations. In order to find the translator variables for linear generator, the translator reference frame using dq0 variables is used. The final section of this chapter is the hybrid system modeling.

The Chapter 4 covered the design and control techniques for offshore wind such as PID, SMC, FBL, STA and IBRTA. These algorithms are tested on the offshore wind to make the performance better for the HOWWE. In this chapter, a comparative analysis is performed among PID, SMC, FBL, STA and IBRTA to extract maximum power.

In the Chapter 5, design and control techniques for wave energy are implemented and tested. The first section is about SPA an existing technique and the multi-point absorber a new

innovative technique for HOWWE have been proposed in this chapter. The power take off from multipoint absorber for the wave energy is proposed and MPA algorithm are tested under case study of real time data using two linear generators.

The Chapter 6, is the based on an integration of HOWWE using VSC and VSI. This system is developed using MATLAB Simulink. The system is tested using different case studies using multi-terminal AC and DC. The system is tested with improved VSI using real world applications. The Chapter 7 summarizes the conclusion and limitation of the thesis. Future work that can be carried out following the findings of this work is also discussed.

Chapter 2 Literature Review

This chapter covers all possible primary aspects of the HOWWE. The chapter starts with the brief explanation of the power conversions of offshore-wind, wave-energy and the power conversion from HOWWE. The HOWWE system is presented at end of the chapter, covering integration methodologies, designs, structures and farm types. This chapter is organized as follows. Section 2.1 is the introduction and 2.2 presents the power conversion of the HOWWE system. Section 2.3 classifies the response coupling of HOWWE where spar torus wind-wave floating systems are discussed as the examples. The control scheme for co-generation and complimentary generation are presented in Section 2.4 while the colocation of HOWWE is presented in Section 2.5. Section 2.6 reviews the possible integration methodologies and synergies are presented in 2.7.

2.1 Introduction

According to the contemporary scientific research, around 78–80% of the world's electricity used for commercial purposes is produced from fossil fuels [1]. However, there are many negative effects on the environment due to high carbon sources, such as affected rain and air. In light of this, the countries around the world have been consciously transferred to use of low-carbon energy sources. Energy production from wind-wave energy, tidal power, solar-PV energy and biomass are copious sources that can harvest affordable and clean energy. HOWWE are plentiful resources, which can be exploited without compromising the needs for future energy. HOWWE is measured as an innovative technology for producing electricity due to its abundant availability of both winds and sea waves at one same location. The global distribution of HOWWE is shown in Fig. 2.1 [2].

The UK has outstanding wave energy resources and progressive methods that are essential to be promptly advanced to attain the target of 22 GW by 2050 [3]. The UK has the prospective to produce electricity over 48 GW from offshore wind-energy by 2050 [3]. The development of HOWWE systems in the world are also studied and defined to highlight the significant support in obtaining net zero target. It is evident that HOWWE can contribute to the de-carbonization, thus helping to attain net zero target.

The benefit of power production from HOWWE is because electricity can be generated from both wind and wave with high capacity. They can be offshore wind-wave jointly or separate devices complementarily. Therefore, there is same grid to use this output energy. There are some practices applied for HOWWE to certify output-power, stability and grid interconnection.

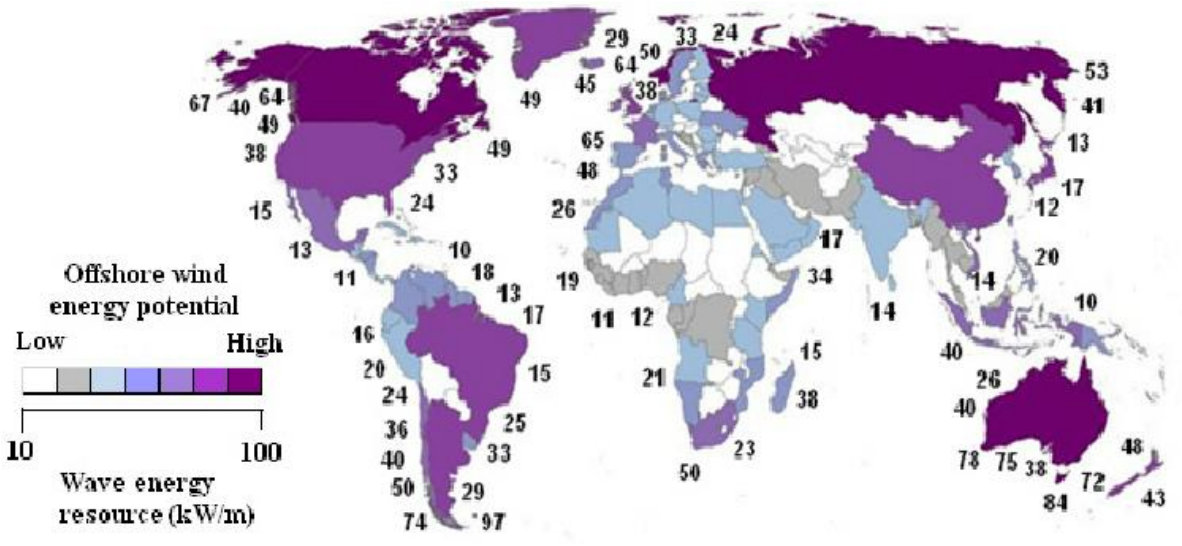

Figure 2.1 Global distribution of HOWWE [2]

The research and development of the HOWWE has practically experienced productive and significant progress over the past two decades. The hybrid system has a prodigious potential for improvement and creates a vital part in the EU and global energy policy [4]. By 2050, a global target capacity of 188 GW of wave energy and 460 GW of offshore wind energy has been set [5]. Due to its increased eco-friendliness, the acceleration of global warming, and the depletion of natural resources, HOWWE has recently attracted more attention [6, 7]. On average, the wind blows more quickly in water than on land. Because sea waves are always moving, they provide a dependable source of energy. Due to the integration of power from both sources at a single place, the system is space-efficient [8]. The same cables that connect to the electric grid for the HOWWE device can be used for this connection [9]. It is noted that the distributed generation system comprising wind, wave, solar and hydro-power has also received the increasing attentions. The advanced power conversion techniques by using shared inverter can be an excellent choice for combining the DC output from multiple sources such as HOWWE.

2.2 Power conversion

2.2.1 Offshore wind

Power conversion is the key part of the OWT used to change mechanical-rotations into electrical power-energy to meet regulations of voltage and current [10]. A detailed review of power conversion of offshore wind is presented in [11]. Wind power needs to provide continuous maximum power by implementing MPPT technologies. The challenges and prospects facing in the conversion process of OWT are discussed in [12]. The usage of power-converters is attractive to build efficient power while working in harsh conditions. In this manner, power circuits are probably going to supplant the silicon-based power switches [13], which will not just offer high unwavering quality due to high temperature. The evaluation of converters in enormous scopes essentially relies upon the type of generators utilized. The power conversion with PMSG and DFIG is presented in [14]. Fixed speed wind turbines have historically been preferred due to their ease of installation and manufacturing, as well as their simplicity and cheaper initial costs. But because they only run at one pace, they are not as effective in different wind situations and might even gather less energy. On the other hand, variable speed turbines have the benefit of being able to modify the speed of their rotor in response to variations in wind speed, which maximize energy capture and raises overall efficiency. Variable speed turbines also offer improved grid compatibility and the ability to supply ancillary services like voltage control and frequency regulation. Notwithstanding these benefits, variable speed turbines usually have more intricate control and design systems, which raise the cost of upkeep and operation. In addition, their initial installation expenses are typically higher than those of fixed speed turbines. By allowing for variable wind speeds and minimizing mechanical stress, a three-stage gearbox improves torque amplification and

speed adjustment, maximizing the efficiency of a doubly fed synchronous generator in wind turbines. The GSC and RSC conversion is explained in [15]. With regards to the power transmission, the VSC with high voltage direct current (HVDC) has been developed as an attractive method for the long-transmission of offshore-wind. The VSC HVDC has taken over the HVAC transmission system in offshore sectors because HVDC system is more efficient for transferring power over long distance [16]. The numerous upcoming choices are discussed in [17] to upsurge offshore wind power by minimizing investment and re-pairing expenses for such power conversion solutions. The power conversion can implement MPPT and hence regulate voltage and frequency control. An OWT conversion system has become a reliable HOWWE part for electric power generation. An example of wind turbine and its connection to the grid are shown in Fig. 2.2. Learning about offshore wind generators is a necessity for grid connection because numerous generators are selected and each generator type has a unique interconnection system. The likings of PMSG for HOWWE comprise exceptionally different speed ranges and improved efficiency from squirrel cage induction generators (SCIG) and DFIG, as shown in Fig. 2.2. The wind energy industry makes extensive use of induction generators. The first wind turbines were powered by squirrel cage generators, which were grid connection directly using full-rated-power converters operating at varying speeds. When wind turbine generators are first connected, there may be mechanical stress and inrush current. A soft starter made of thyristor equipped electronics was employed to address this issue. Switched capacitor banks or specially built power converters can be used for power factor correction. Reactive power can be supplied by switching capacitor banks for fixed speed generators to increase power factor. With the capacitor bank, the soft starter is frequently used with SCIG.

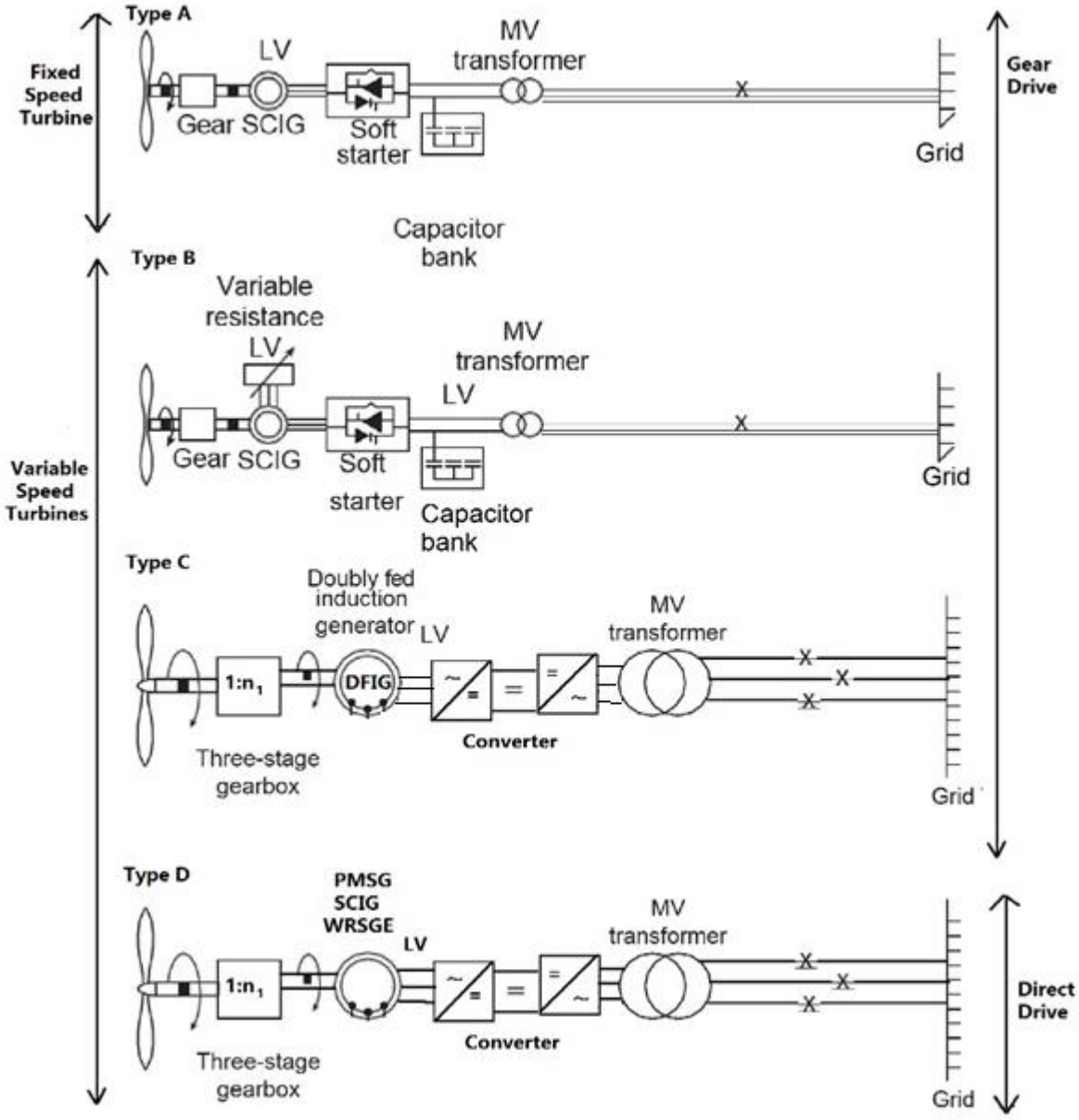

Figure 2.2 Power conversion of fixed speed, SCIG, DFIG and PMSG wind turbines [17]

In Table 2.1, advantages and disadvantages of different wind generators are analyzed.

Table 2.1 The advantages and disadvantages of different wind generators with respective conversion system [17].

Wind turbine generators	Advantages	Disadvantages
Fixed speed induction generator	Maximum power production is possible Low cost	Minor variation in speed can cause large-torque. Low efficiency when TSR changes. Difficult to control the generator torque. Aerodynamic fluctuation is moved to the grid side causing grid faults. High power-driven stress and power losses.
DFIG with partially rated power converter	Torque of generator is entirely under control of the power conversion. Speed can be improved by 40 %, therefore MPPT is achievable. Very rapid torque control, response time of the torque is from 5 to 50 ms. Aerodynamic fluctuation can be filtered before entering the generator.	Magnetizing current is delivered via the rotor terminal affecting loss of efficiency. High maintenance requirements of slip rings. Aerodynamic fluctuations may cause grid faults. As with PMSG, power-converters are required to connect the grid. 25-30% is fed to the grid through converter.
PMSG with fully rated power converter	Voltage with reactive power are accessible without upsetting the dynamics of generator. Gearbox can be avoided.	PMSG cannot be straight joined to the grid. Power conversion is required between the generator and the grid. High cost.

With technological advancements, the evaluation of generators used in offshore wind power generation changes. Due to the significant reactive-power consumption that requires essential compensation, SCIG was substituted. In demand to fulfill power electronics interface with the rotor currents, the DFIG, a type of variable-speed WT, was invented. The generators are

composed of a rotor and a stator, which work based on the theory of Faraday's law of electromagnetic induction.

Rotor speed for synchronous generators is influenced by operating frequency. As compared to the DFIG and SCIG, the PMSG is more appropriate choice for OWT production due to the positive aspects such as gearless transmission, low cost of maintenance, and high reliability with ease of power conversion control.

2.2.2 Wave energy

The power takeoff (PTO) is required to extract power and transform it into the useable electricity. The following types are used for power generation from wave energy by combining the OWT. Mainly, there are six types of wave energy converters (WECs); single-point-absorber, rotating mass system device, oscillating-water-column (OWC), terminators, submerged pressure differential device, and attenuators. The relative efficiency of a linear generator and a rotary generator depends on a number of variables, including the particular application, design considerations, and operating circumstances. WECs use linear generators to directly convert the linear motion of waves into electrical energy. When used in these kinds of applications, linear generators have the potential to be more efficient than rotary generators in terms of simplicity, dependability, and effective wave energy capture.

While sharing the same structure for combining HOWWE resources, point absorber might be an ideal choice because it attaches with the bottom of semisubmersible and tripod OWT. The OWC device is ideal for the hybrid system if WEC arrays are added separately with the offshore wind platform. The OWC moves up and down due to sea waves, in response to the air which comes out from the chamber and pushes the chamber back into its position. The high-velocity air is produced due to the repeating processes of the reversing stream. These

systems appear simpler and more reliable than the other system such as rotating mass device. In the OWC air turbine, there has no moving parts. These systems are suited for any type of environments such as offshore, shoreline and near the shoreline. The PTO is used to convert ocean wave energy into electrical energy, as shown in Fig. 2.3. The PTO is divided into hydraulic, pneumatic, hydro, and direct drive system categories, each of which incorporates a suitable linear generator. The PTO analysis of the wave energy system is presented. According to the survey [18], 58% of current WECs use linear generators, while 42% use water-powered PTOs. A system designed to move the oils to the accumulator and cylinders is the hydraulic PTO. The apparatus includes rams or cylinders that can convert the mechanical energy from the oscillating body's movement into hydraulic energy. The pneumatic PTO is ex-changed with a conventional connection between the airflow rate and the OWC pressure [19].

The linear generator can be straightforwardly joined to a vertical chamber, which is regularly utilized in the oscillating systems. In wave energy, the linear generators are most likely thriving because of their high energy density and more effectiveness at low speeds. There are two types of generators that are utilized in WECs: linear and rotatory generators [20]. The WEC with linear generator is simpler and less expensive for power yield [21]. The rotatory generator is expensive to build.

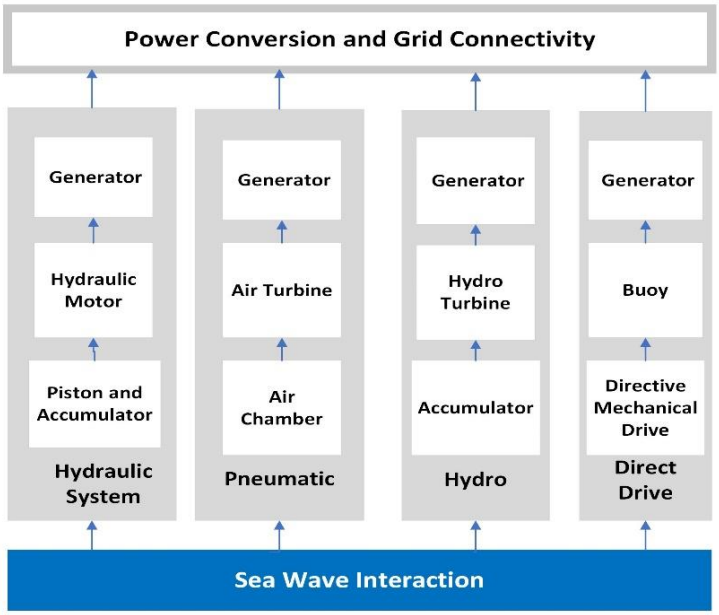

Figure 2.3 Typical PTO systems used in the wave energy devices

In [23], WEC PTO is based on a drive train technology by using linear Vernier and the experiment is carried out using a direct drive machine with 3-dimensional finite element technique. A unique bistable X-structured WEC is proposed and examined in [24]. The sea waves drive the buoy to up and down, and due to the moment of buoy the base excitation is produced for the supporting X-structure, which produces the relative motion to generate electricity [24].

2.2.3 Power conversion of HOWWE

The power conversion is a crucial part to increase the stability of the HOWWE. The power output from HOWWE is harvested separately, such as wind power conversion using synchronous generator is carried out using AC-DC-AC conversion by using control algorithms and MPPT techniques while wave power conversion is made based on PTO and the associated conversion process. The detailed power conversion from HOWWE is investigated in [25] [26]. A HOWWE system based on hywind and wavestar is presented in

[27]. In [28], explains the likelihood of integrating HOWWE for commercial gain and methods for reducing fluctuation impacts from such a merger. According to [29], wave energy can provide power at a range of 22% to 29% efficiency, but offshore wind energy can produce power at a range of 30% to 50% efficiency. According to [30], an onshore grid system based on VSC receives power from a micro-grid based on HOWWE resources. Also suggested and utilised in a DC microgrid is a HOWWE system [31]. As seen in Fig. 2.4, the hybrid power generation system is incorporated into the bidirectional DC microgrid by means of the hybrid system. According to Fig. 2.4, the hybrid power generating system is incorporated into a bidirectional DC microgrid that is running in an is-landed mode. This is accomplished by connecting the hybrid system. The bi-directional grid-tie inverter is used to link the AC grid to the linear permanent magnetic generator (LPMG) and PMSG, respectively. In [31], a 2 MW system was used to examine the coupling between the linear generators and an Archimedes wave swing (AWS) based WEC system. The voltage DC-link is produced and shared in the micro-grid by employing VSC control techniques in order to maximize power sharing in DC micro-grid from wind and wave [30]. An effective power converter is necessary to determine the maximum energy requirements between the battery and capacitor. Therefore, the DC-DC bi-directional converter was suggested to incorporate the intermittent and uncertain characteristics of the wind and wave [31]. Either High voltage alternating current (HVAC) or high voltage direct current (HVDC) technologies can be used to transfer the electricity produced by HOWWE systems. Since HVDC transmission can carry huge amounts of electricity over longer distances with fewer electrical losses than HVAC transmission, it is frequently chosen for long-distance transmission. In the end, HOWWE systems' decision between HVAC and HVDC transmission is influenced by a number of variables, including cost, grid infrastructure, power capacity, and distance.

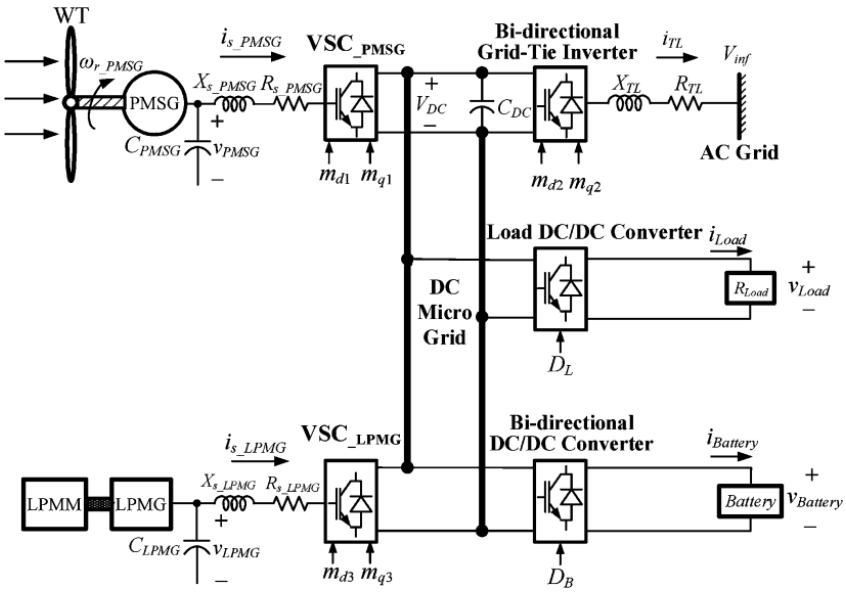

Figure 2.4 Schematic of a hybrid wind-wave energy system for DC power supply [31]

The linear permanent magnetic generator LPMG-VSC and PMSG-VSC connect the hybrid system to the DC grid, respectively. Both DC and AC micro grids are covered in [31]. A battery is connected via a bi-directional grid-tied inverter to the DC grid in order to meet load demand and maintain consistent power [32]. The charged batteries are used to feed the HOWWE power into the DC micro-grid, and the inverter then transfers the excess power to the AC grid. A renewable energy system, such a hybrid wind and solar system, can provide more power when two resources are combined [33, 34]. In order to improve microgrids by incorporating renewable resources, hybrid renewable energy systems and their applications based on wind and solar are presented in [35, 36]. The minimum downtime period from both wind and wave farms as well as the smooth output power of HOWWE are presented in [37, 38]. The design of the farm is crucial for power conversions as well; co-located farms can produce more power from both resources with less maintenance and at a lower cost. Offshore wind and wave co-exploitation is becoming increasingly important [39], although there are

still a lot of difficulties with it, including cost, risk, and complexity, which are discussed in [40].

2.3 Response coupling of HOWWE

The HOWWE system depends on response coupling in several ways. In addition to controlling current and voltage, it also controls power flow and provides structural protection. Wind and wave models are typically used to study HOWWE capacities, while atmospheric wave and ocean (AWO) dynamical coupling methods are disregarded [41]. A completely AWO coupled model is used to evaluate the AWO coupling control strategies for simulating HOWWE potentials. Similar to this, [42] investigates the synergy and connection between HOWWE. Regarding linked dynamic analysis techniques, an analysis is carried out in [43] to use a WEC as a motion suppression device for FWTs. This analysis uses the passive damping approach for FWTs to dissipate the wave-induced energy, thereby lowering the global platform motions. Real-time hybrid model testing is carried out in [44] using the aero-hydro-servo-elastic simulation program SIMO-RIFLEX-Aero Dyn. The authors in [44] analyzed the aerodynamic loads on the FWT in a wave basin using concurrent simulations. The aerodynamic-loads have been calculated using coefficients using this method [45]. A novel joint-wind-wave-energy (JWWE) is proposed in [46], where a dual-stator-linear and rotary-permanent-magnet-generator (DSLRPMG) is deployed to convert the wave and wind energy, respectively. The joint offshore wind and wave energy power conversion is directly employed to convert mechanical-to-electrical energy. The DSLRPMG system can be deduced by using the vector control techniques. The flux-power decoupling method are presented, as shown in Fig. 2.5, where the linear and rotary motions of the DSLRPMG magnetic field presents strong coupling effects.

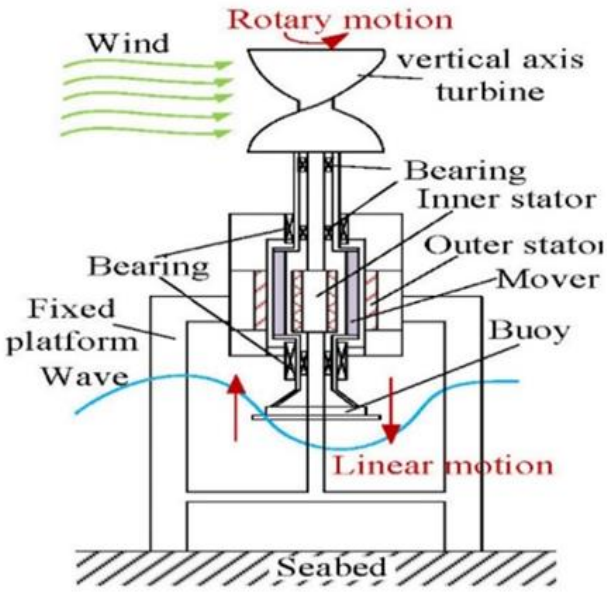

Figure 2.5 Coupling of the hybrid wind and wave energy conversion [46]

Since the back electromotive force and flux linkage are both sinusoidal, by ignoring the magnetic saturation, hysteresis loss and influence of the temperature, the linear-motion $\boldsymbol{v_1}$ and rotary-motion $\boldsymbol{\omega_r}$ are expressed by the equations below [46].

$$\begin{cases} \mathbf{T_L} = \mathbf{J}\frac{\mathbf{d\omega_r}}{\mathbf{dt}} + \mathbf{B_r\omega_r} + \mathbf{T_e} \\ \mathbf{F_L} = \mathbf{M}\frac{\mathbf{dv_1}}{\mathbf{dt}} + \mathbf{B_1 v_1} + \mathbf{F_e} \end{cases} \quad (1)$$

where $\mathbf{F_L}$ is input torque of the linear motion and $\mathbf{T_L}$ is the input-torque of rotary-motion. **J** represents the rotary inertia and M represent the mover weight. $\mathbf{T_e}$ is the electromagnetic-torque and $\mathbf{F_e}$ is the DSLRPMG thrust. The coefficient of transmission friction of rotary and linear parts is represented by $\mathbf{B_r}$ and $\mathbf{B_1}$, respectively.

In [47], the OWC type WEC is combined with the monopole wind turbine. The main formation is to integrate a monopole with cylindrical OWC chamber. The chamber is fastened to an offshore monopole turbine, free at the bottom, and connected to a wind turbine at the

top. In order to increase the size and design of WECs in the system so that the larger WECs create more energy in a designated region, floating wind and WECs are combined in [37]. A numerical model is put to the test in [48] to determine the HOWWE's rational size. By studying different PTO structures in the hydrodynamic model and their influence on WEC performance under different conditions, finest damping coefficient is achieved. Hydrodynamic performance is mathematically examined and then evaluated experimentally with a monopole OWT being integrated to the OWCs [48]. Moreover, the linear potential flow theory in a 3D time-domain is also numerically developed in [48].

In [49], the structure shape of OWC is coaxial cylindrical cylinder with two parts. The internal cylinder signifies the OWT mono-pile while the outer cylinder has a skirt whose range is to monitor the wave energy flux. In [50], an innovative HOWWE system is proposed and the initial feasibility study of both FWT and OWCs is achieved by applying numerical simulation of aero-hydro-servo-mooring. The significant impacts of the WEC PTO system on the hybrid system are also studied.

In [51], a combined HOWWE model comprising a 5 MW FWT is coupled with a torus-type. The dynamic study of the tension leg platform (TLP) for OWT with point absorber WEC is examined. Joint coupling between torus-shaped WECs and spar-type FWTs is examined in [52]. In [53, 54], numerical simulations of the linked HOWWE with a beneficial synergy between spar floating wind and WEC are shown. A floating system that moors into TLP and supports a 10 MW wind turbine is proposed [55]. It includes a variety of hydrodynamically related OWC technologies. The hybrid platforms are proposed in [48, 56] with the WECs positioned at downwind and upwind directions being analyzed to study the system stabilization problem. The time-frequency analysis for a point absorber is carried out to

measure the non-linear dynamic responses in [57, 58]. Similarly, in [59], a point absorber linked with semi-submersible system and a prototypical experiment is then carried out. A numerical representation is designed to optimize of the size of WEC installations in HOWWE system in [60]. The existing wind-wave coupling models are summarized in [61].

2.3.1 Spar-torus-combination

For the Spar-torus-combination (STC), the parts such as spar, torus and wind turbine are usually rigid bodies and mooring lines are represented by linear springs. The spar operates based on hydrodynamic loads, such as the drag force and first-order wave loads, while the wind turbine operates based on aerodynamic loads. In [62], the numerical modelling of the two models for the semi-submersible flap combination (SFC) and the STC is explored. For both STC and SFC, comparisons are made between numerical and experimental data. The excitation of wind and wave energy model is tested at a 50:1 scale, where the HOWWE conversion is achieved using the STC.

The floating spar-type OWT combined with SPA is reported in [63]. In this configuration, the point absorber WEC is slid across the spar to extract energy from waves while at the same time the FWT extracts energy from winds. This is a comparatively simple and stable model and thus understandingly presents many feasibility problems. However, the current system still has the potential to achieve the maximum performance. Moreover, this system needs to be designed for fatigue limit test and ultimate limit test in the operation mode. Fig. 2.6 shows the detailed numerical analysis model of STC conceptual sketch with different survival modes [64].

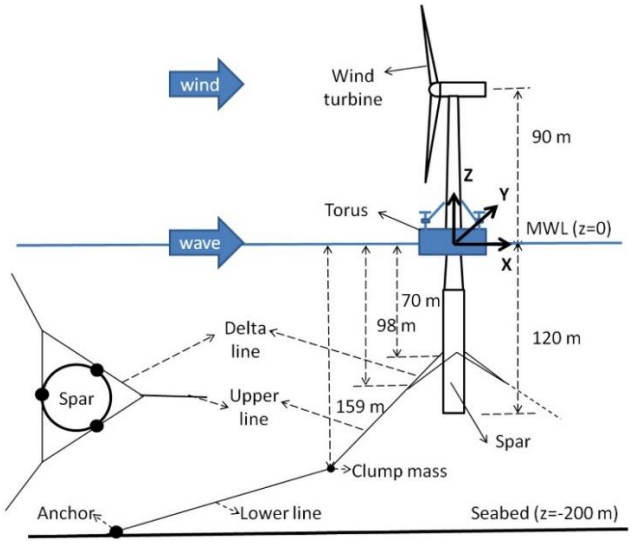

Figure 2.6 Spar torus combination conceptual sketch [64]

2.3.2 Wind wave float

In [65], presents various hybrid wind-wave floating systems. A tri-floater wind turbine and point absorber WECs are suggested for a hybrid system [66]. This model generates energy by exploiting the oscillation of moving flaps, which has received more attentions in recent years. The basic functions of sea wave spectra produced by winds and waves reveal a typical plus-minus mark related to change of the severe spectral peak to minimum frequencies [67]. In [68], the power performance of the FWT and WEC combination is examined. The Froude scale model is tested for FWTs under HOWWE load distribution in [69] using a unified approach. It is shown that the Fraud scaling interactions are active for the location and floater. For an array of FWTs, the stand motions and fatigue damage due to wind-wave misalignment effects are examined under typical operative circumstances. The dynamic floating wind-wave effect is fully examined using the innovative geometrically scaled national-renewable-energy-laboratory (NREL) of 5 MW OWT at top three floating platforms, i.e., a TLP, a spar-buoy, and a semisubmersible, to demonstrate the application [70].

2.4 Control scheme for co-generation and complimentary generation

In HOWWE, an independent blade pitch controller is employed to independently move the blades in order to reduce wind turbine fatigue [71, 72]. In [73], the fixed coordinate system is based on cosine-cyclic, sine-cyclic, and collective coordinates, and the multi-blade coordinate is examined. The individual pitch control is employed to reduce the variation in wind torque. However, because these two requirements involve competing aims, it is challenging to construct a control scheme to ensure both efficiency and dependability at the same time [73]. Since incoming wind is stochastic, to find the unknown disturbance state of the system it is compulsory to use output measurements. Utilizing various control techniques, the wind speed variation, unmodeled dynamics, and nonlinearity are examined. For a variable-speed turbine, the rotational speed of the turbine rotor is checked and adjusted using a disturbance accommodating controller [74, 75]. A stochastic disturbance accommodating controller is also described in [76] to stabilize the system with unknown external disturbance and unmodelled dynamics. The ability to cancel the disturbance can be made by using a modified direct model reference accommodating controller [77].

The output of HOWWE can be tracked by using controllers, which determines the maximum aerodynamic efficiency. The MPPT will improve the output power efficiency by tracking the optimum aerodynamic torque by using the conventional MPPT including perturb and observe, optimal torque, and TSR. The MPPT algorithms for the optimal power coefficient of the system can be referred in [78]. As an example, the nonlinear sliding mode control is used to optimize output power for variable DFIG turbine [79]. Two controllers are used to implement the system, one of which tracks the rotor speed while the other monitors the rotor

flux and generator torque. The generator toque can also be controlled using the Lyapunov controller and the optimal-direct-shooting control approach to optimise power [80].

2.5 Colocation of HOWWE

The HOWWE co-location is robust as compared to hybrid wind and solar energy due to energy harvesting on one platform. The HOWWE is the advanced type as compared to other marine energy resources in terms of the infrastructure policies, industrial manufacturing, worldwide commercialization, installed capacity and technical improvement.

By adjusting a wind turbine's specifications, such as its huge rotors and wave generator with an effective mechanical and electrical design interaction and the water depth, one can develop an efficient HOWWE solution [81]. Several scholars have suggested a thorough examination of HOWWE colocation between wind and wave [82, 83]. [84, 85] present the enhanced output power from pooled energy resources employing minimal cost structural design. Italian [63] and the Mediterranean region of [86] have both explored the HOWWE. In Table 2.2, different site locations are discussed where the potential deployment of the HOWWE are evaluated and tested. According to EEA (European Environment Agency) [87], offshore wind for energy production potential in the Mediterranean is at 20 %, Baltic at 29 % and the North Sea at 25 % by 2030 of approximately 7100 TWh covering these areas. In the Baltic and North Sea, HOWWE has received significant investment. Due to the waves' brief periods, the Baltic Sea, Mediterranean Sea, and Black Sea are known for having low power densities (5 kW/m) in terms of wave energy [88]. A third-generation wave model was used between 1988 and 2009 to monitor the HOWWE in the China Sea. In offshore and coastal areas, the third-generation wave model forecasts wave climates [89]. Each resource in [37] is subjected to pairwise comparisons using geographic information systems. In the Maldives, it was

discovered that the yearly wave energy ranged from 8.46 to 12.75 kW/m, and the mean wind power density ranged from 0.08 to 0.16 kW/m2. Based on wind-wave speeds and their forecast data, for the combined exploitation, the best areas are situated in the Aegean Sea north east coasts, Gulf of Loins, coasts of Sardinia and in the Sicily Straits [63, 87].

Table 2.2 The site location of HOWWE

Wind-Wave resources	**Sea**	**Coasts and Islands**
Europe	The Mediterranean	The Blue-Coast of French, some sides Tunisia and islands of Greeks [63]
	North Baltic belt	The north side of Scottish islands, Norway, West side of Denmark [87]
	The Atlantic	Atlantic Arc
UK	Celtic Sea	Celtic sea power [85]
	Irish-Sea bounded Scotland	Danish outfit Floating Power Plant
China	South China Sea	Paracel Islands

2.5.1 Statistical methods for correlation

The leading concern when applying HOWWE resources is their inconsistency and intermittency. The correlation of HOWWE in deeper seas is explored in [91]. The Pearson's coefficient $\boldsymbol{r}$ [6]: describes the HOWWE connection at various locations:

$$\boldsymbol{r} = \frac{\mathbf{1}}{\boldsymbol{N}}\sum_{\boldsymbol{k=1}}^{\boldsymbol{N}} \frac{[\boldsymbol{x(k)}-\boldsymbol{\mu_x}][\boldsymbol{y(k)}-\boldsymbol{\mu_y}]}{\boldsymbol{\sigma_x\sigma_y}} \tag{2}$$

where N is the total number of samples, N, $\boldsymbol{\mu_x}$, $\boldsymbol{\mu_y}$ denotes the mean value of the observations x and y, and $\boldsymbol{\sigma_x}$ **and** $\boldsymbol{\sigma_y}$ their standard deviation. The meteo-climate datasets had to be reduced in dimensionality for feature extraction, which necessitated the use of cluster analysis (CA), factor analysis (FA), and principal component analysis (PCA) [6]. By removing the

eigenvectors and eigenvalues from the covariance matrix, the PCA and FA appear to be the best options to reduce the dimensionality.

Among them, the PCA and FA appear the most suitable choice to minimize the dimensionality by extracting the eigenvectors and eigenvalues from the covariance matrix. The groups of Meteo-climatic data are also analyzed by CA, which has k means of hierarchical and non-hierarchical control.

2.5.2 Site selection

To find an appropriate site location for HOWWE, the offshore wind is calculated by Bulk aerodynamic method that is based on the 10m standard height with the shift of wind measurements. This height is used because the height of the anemometer results in increase in the chattering level of wind turbine, thus causing un-stability [37]. The accurate offshore wind speed can be derived by a power law and is expressed by equations (3) and (4) [92].

$$\frac{U_{10}}{U_2} = \left(\frac{z_{10}}{z_2}\right)^{\in} \tag{3}$$

where the $\boldsymbol{U_{10}}$ and $\boldsymbol{U_2}$ refer to the speed of wind at height of 10m and 2m, respectively. The wind shear exponent is symbolically represented by $\in$ and is expressed as:

$$\in = \frac{1}{ln\left(\frac{z_{10}}{z_0}\right)} \tag{4}$$

where $\boldsymbol{z_0}$ to $\boldsymbol{z_{10}}$ depend on the wave characteristics and represent the aerodynamics roughness-length. The power law exponent factor in Equation 4 is used to estimate offshore wind speeds in order to determine the best sites for the HOWWE system. The wind shear exponent (ε), which measures the variation in wind speed with altitude, is defined in Equation 4. Based on the ratio of the heights at which wind speeds are measured $\frac{z_{10}}{z_0}$, where $\boldsymbol{z_0}$ is the

aerodynamic roughness length, this exponent is computed. Wind speeds are normally recorded using the bulk aerodynamic approach at a standard height of 10 metres above sea level in order to reduce surface roughness interference and guarantee stability when operating wind turbines. Moreover, Table 2.3 shows different sites where offshore wind and wave energy are abundantly present. The Table 2.3 which is divided into the North and South Hemispheres according to geographic location, shows several global zones that are well-known for having an abundance of offshore wind and wave energy resources. Because of their favorable offshore surroundings and wind conditions, areas in the North Hemisphere with great potential for offshore wind energy generation include the European Atlantic coast, the United States, Greece, China, and Japan. As the European Atlantic coast, Iceland, Greenland, the United States, and the Canadian coasts all see abundant wave activity, these regions are also excellent for capturing wave energy. On the other hand, areas in the South Hemisphere that are known for their appropriate offshore surroundings and good wind conditions include the southern portion of New Zealand, Chile, Kerguelen, Heard Island, and the McDonald Islands.

Table 2.3 Site selection based on northern and southern hemispheres are presented for offshore-wind and wave-energy, respectively**.**

Worldwide zones	Offshore wind	Wave energy
North Hemispheres	European Atlantic coast [88], US, Greece, China [37], and Japan	European Atlantic coast [88], Iceland, Greenland, United States, Coasts of Canada [94]
South Hemispheres	Southern part of New Zealand, Chile, Kerguelen, the Heard Island and McDonald Islands	Australia, New Zealand, Western coast of South-America [94]

Furthermore, wave energy projects are drawn to regions with abundant wave energy resources, such as Australia, New Zealand, and the western coast of South America. Stakeholders can use this thorough overview as a useful resource to help them make well-informed decisions about the global selection and development of offshore renewable energy projects.

2.6 Integrated conversion system

According to the technology development, the system can be categorized in terms of water depth (deep water, transitional, and shallow-water waves) and the location near to the shoreline (offshore, near-shore, shoreline). The system can also be classified according to its connectivity. The hybrid connectivity between FWT and WECs can be made via hybrid, co-located and island system modes. Furthermore, the co-located system can be considered as the bottom-fixed and floating-system. The integration of wind-wave energy using co-located array with grid management system is discussed in [94]. The independent and combined arrays are the two categories of co-located systems. Fig. 6 presents the co-located HOWWE's representative structural designs. Based on separate FWT and WECs, the independent separate arrays are shown [8]. The co-located offshore wind and wave devices at the same farm, sharing the same ocean area and the other infrastructures, are recommended as combined arrays to create a single array [29]. The combined arrays of co-located systems are further broken down into three sub-types: the peripherally dispersed array (PDA), the non-uniformly distributed array (NDA), and the uniformly distributed array (UDA). In the PDA, the WECs are distributed as per the prevailing wave direction while in UDA the WECs and offshore wind turbines are geometrically distributed uniformly. In the NDA arrangement, the WECs are geometrically distributed non-uniformly throughout the offshore wind farm. The

best method of the distribution array among them is NDA because this arrangement is able to maximize the WECs performance by interacting with the wind turbines.

Diverse maritime industries, such as offshore wind, aquaculture, marine recreation, and marine transportation, combine with offshore constructions [95]. The hybrid systems are divided into bottom fixed and floating hybrid systems according to how they are installed. When developing the construction for the bottom fixed system, offshore wind turbines are used to adjust the WECs. WEC can be integrated into a wind turbine on the same platform to make the substructure strong; however, a lot of improvements are required to adjust the WECs onto an existing wind turbine. Numerous researchers have been working on this problem recently. For instance, Danish wave energy is creating the Wave Star, while Green Ocean Energy is developing the Wave Trader [8]. The HOWWE technologies are also arranged to operate as an island system. The island system combines the hybrid utilization of wind-wave sources on the one island. This system can be classified into two categories: artificial-island and floating-islands. The artificial islands are made by utilizing dykes or a large reef. The most recent work on artificial island system is undertaken by KEMA Energy Island and Dutch DNV KEMA Consulting. A floating island, as another type of island system, is built based on large multipurpose floating platforms. More details about the industrial hybrid wind and wave system are shown in Table 4 and further summarized as follows.

2.6.1 Bottom fixed system

The bottom fixed system can be independent or not. For the independent bottom fixed system, the WECs and the wind turbine are deployed in the same platform by sharing the same grid connections [8]. The WECs are distributed as a wave array accordingly in line with the wind

turbines. However, the independent bottom fixed system is not a good choice for co-located system designs because of high risk of collision between wind turbine and WECs. For the bottom fixed system, the platform is shared between wind turbine and WECs; however, there are no wind turbine floating bodies. The system's cost is also minimized due to the sharing platform and the high yield of energy [97].

2.6.2 Floating system

Both wind and wave energy converters are floating structures. This option is beneficial because the floating system can float easily on deeper water. The submersible floating systems are categorized as the TLP, barge and spar. The use of barge and TLP has been increased in recent wind-wave structure developments for ultra-deep underwater activities. These systems require the slack mooring system against their instability. The conventional approach was used by FWT, which introduces spar-buoy, TLPs and pontoon type (barge-type).

The barge is a long surface type WEC that uses a huge water plane area and shallow draft to maintain stability. This type of system is well-known in hybrid offshore structures. Spar is another well-known platform used for the floating platform, which is used in a shallow sea. They have a basic layout of legs that are used for buoys and can be used in long term energy production. The use of spar is based on the specific design that allows the use of wind, wave and currents more efficiently. Due to the large diameter of the spar platform, it is built in a vertical cylindrical shape based on a supporting deck, with the bottom being constructed with material that is denser than water, hence allowing to be floating underwater. There are three basic types of the spar: classical, cell and truss spar. Truss spar is used in hard tank configuration with a shorter cylindrical shape, which is different from a classical structure

where the truss spar is connected to the bottom. The truss spar structure used in literature [8] is based on four large orthogonal legs which are separated by X-braces and damping structures between each plane are achieved using heave plates. Immediately after the truss structure, there is the soft keel that allows the housing of heavy blasting material, which is commonly used in the floating systems.

For the large floating systems, the first concept barge was required to maintain the system's stability. The option with a water depth of 80m is to use the semi TLP. The semi type floating system is better than the TLP because the tidal elevation is very sensitive due to tether and buoyancy tensions of the TLP. Semi-floating structure is made based on decks, multi-column, pontoons and bracing members [98], as shown in Fig 2.7. The connection of columns in the semi-floating structure by using decks and pontoons is supported by the bracing members. On the top of every column, the wind turbine is installed. The WECs are placed between the structure of decks and pontoon. Due to strong wind pressure and strong sea waves on the system, the system reaches the unstable state, which decreases the performance of the system as well as increases the additional operating cost due to damage and fatigue [99].

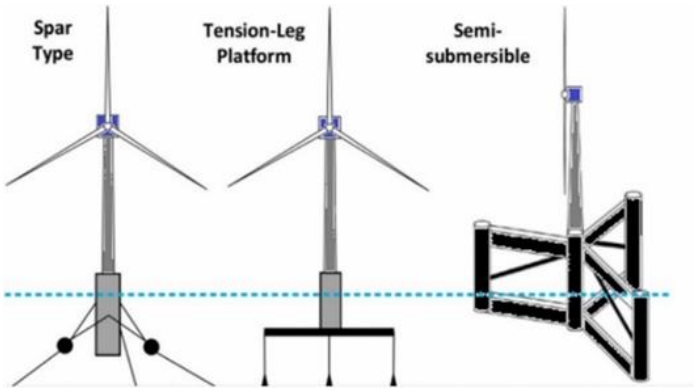

Figure 2.7 Spar-TLP-semisubmersible wind-wave devices

To generate the continuous output power from the system, the International Electro-Technical Commission is working on reviews of the additional maintenance, capital and operation costs for the FWT [100]. It is a challenging task to minimize the operational and maintenance cost, which requires suitable control techniques [101]. Many companies are working to minimize the cost of maintenance and their names are mentioned in Table 2.4. Although HOWWE projects are a relatively new idea, some companies and academic organizations are already investigating the possibilities of fusing offshore wave and wind generating technology. In Table 2.4, offshore wind platforms coupled with wave energy are presented.

Table 2.4 The cogeneration pattern and the industry working on offshore wind and wave [8]

Type of the System	Cogeneration Pattern	Companies Name
Co-located	Independent array	WindEurope
	Combined array	
Hybrid	Bottom fixed	WEGA, WaveStar, Wave-Trader
	Floating	OOES, WindWaveFloat, Poseidon, W2Power, OWWE
Island system	Artificial reefs	Kema Energy Island
	Floating	Hexicom, OTEC Energy Island, Hydrogenase

2.7 Synergies

Various synergies have been tried to create the integrated HOWWE framework. These efforts have improved energy yield, better consistency, smoothed power supply, shared platform, maintenance, shadow impacts and environmental advantages. The higher output is the result of the power unit device's size and dynamic motion expanding [102]. The integrated framework decreases power fluctuations in wind-wave energy sources [103]. Also reduced are environmental consequences [85], noise [104], visual effects, and marine transit thanks to the integrated HOWWE. HOWWE is in the early stages of development [105–107], which can be enhanced by using control algorithms like super twisting [108]. By examining the

characteristics of the site region, the environmental effects on the wind-wave turbine are evaluated [109]. Numerous restrictions are triggered by the deeper water, including turbulence and environmental concerns like endangered animals. The environmental implications also include bird collisions with wind farms, effects on marine life, and disturbance to other life forms; nevertheless, with the right safeguards and a careful investigation of the relevant aspects, a cautiously hopeful approach could change these circumstances and simplify the procedure as a whole. The oceanic environment may be harmed by the offshore farms' avian collisions, noise [109], and electromagnetic fields [110–112]. The predominant planning methodology up to this point for the integrated HOWWE installations has been quantitative spatial planning [113]. A new model is developed in [114] based on semi-submersible Nautilus, where the offshore wind turbine is integrated with four-point absorber WECs.

Multipurpose platform (MPP) is used to fulfil the demands of cogeneration and colocation for the offshore energy resources. MPPs would also endorse an optimization, efficient design, and integrated solution. MPPs have noteworthy prospective in economizing offshore energy sectors and minimizing the cost for the HOWWE by doing combined spatial planning. Control system of every generator offer voltage-frequency regulation. A MPP strategy is consequently essential to deliver the functioning stabilization. The management of the power network is formed based on the MPP's size and the kind of interconnection, such as isolated or grid-connected. [115] studies a variety of MPP systems with the goal of assigning the multidisciplinary feasibility responsibilities. A thorough analysis of Blue-Growth and MPP is given in [116], and both strategies are evaluated in strategy plans along with the wide spectrum of current information being analysed. Although the words multi-use platform

(MUP) and multi-purpose platform (MPP) are sometimes used synonymously, MUP refers to a method of integrating cooperative maritime economic activities within a small geographic area, whilst MPP denotes a structure capable of fostering synergies between various aquaculture systems. The frequency/voltage regulation and load control of the wind-wave system form the foundation of the MUP control system. In addition, it is required to tune the network of MUP grid or HOWWE with the main control grid. To deliver the output power efficiently at the system level is also a challenge, which can be improved by using a hierarchical control of HOWWE. This can be made based on three levels: supervisory, central and local controller, with the lower level being local and the highest level being supervisory. The local controllers can be categorized as microcontrollers (MC) and load controllers (LC).

2.8 Summary

This chapter has offered a main analysis of the most related aspects linked to the combined HOWWE systems. An extensive review of the different control concepts related to wind-wave systems is presented. This study has focused on the power conversion and advanced control coupling implementation of HOWWE systems. The technologies of wind turbine generators are compared in order to shed light on the benefits and drawbacks of each for HOWWE systems. In a similar vein, although the OWC devices emphasizes their ease of use and dependability, a critical assessment of their drawbacks, such as difficulties with installation and scalability, would offer a more impartial viewpoint. Furthermore, a summary of current research efforts is provided in the section on power conversion in HOWWE systems; nevertheless, a more thorough critical assessment of methodology, experimental findings, and practical consequences is necessary. A straightforward choice at the present phase for improvement of HOWWE technologies is the collocated systems by merging the OWT with a WEC array. For the offshore-wind power conversion, different generators and their working principle are covered, while for the wave power conversion, different PTO systems are analysed with sea wave interactions. The control scheme for co-generation and complimentary generation are presented by analysing their positive and negative aspects, respectively. The colocation deployment is a feasible solution to maximize the energy output from both resources by selecting a suitable location and therefore different approaches for site selection of HOWWE are also re-viewed. By comparing both wind and wave operation and the design, it is found that the control design and structural load reduction are important for the system to be able to maximize the power output while keeping stability. Furthermore, the coupling between the winds and waves is crucial for the site colocation, in order to

achieve the efficient energy generation from both energy resources. This chapter provides closely-relevant knowledge of the HOWWE system. Considerable research is required in control designs, efficient power conversion and reliable grid integration to harness power from the integrated HOWWE system.

Chapter 3 Analytical Analysis for HOWWE

In this chapter, analytical analysis for HOWWE is presented. OWT and wave energy numerical modelling are carried out in Sections 3.2 and 3.3. The OWT is categorized further with two subsections wind turbine modelling and PMSG modelling. Similarly, wave energy is based on linear generator where translator and stator equations are formulated. The mathematical conversion of both sources using state space method and dq0 transformation is also presented in this chapter. The Section 3.4 is the hybrid system modelling and the Section 3.5 presents an analytical approach to calculate the power output based on power modelling.

3.1 Introduction

OWT is the most solid, inexhaustible, reliable and environmentally friendly power energy source. Therefore, it tends to be utilized as one of the wellsprings of elective energy in future [117]. In view of speed, OWT are characterized as fixed speed OWT and variable speed OWT. The wind turbine based on variable speed gives 10–15% further energy output, decreased fluctuation in power, and decreased mechanical-stress than the fixed-speed [118]. A variable-speed turbine requires power conversion and MPPT [119]. The principal preferences of PMSG for offshore wind and wave energy include extremely broad speed range, greater efficiency and high density of power. This prompts a smaller and compact design, petty scale turbine with the capacity to work at minimum speeds [120]. Right now, more companies are using PMSG instead DFIG [121].

3.2 Wind energy conversion

In this study, the offshore-wind ECS essentially represents wind turbine based on PMSG, where GB is gearbox, RE is a rotational encoder, ω_h is shaft speed, ω_{ref} is reference speed and *e* represents the error, as shown in Fig. 3.1.

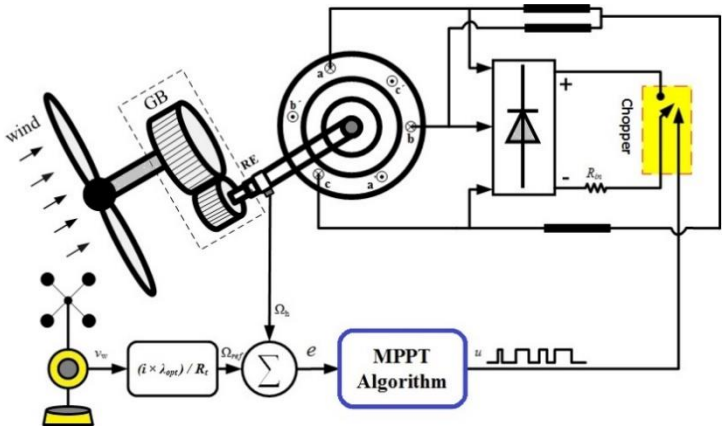

Figure 3.1 Schematic diagram for PMSG-ECS

3.2.1 OWT aerodynamic Model

The power is present at the turbine shaft is represented with expression [122]:

$$P_m = \frac{1}{2}\rho\pi {R_b}^2 {v_{wd}}^3 C_{pr}(\lambda). \quad (5)$$

where R_b is the radius of WT blade, wind speed is denoted by v_{wd}, ρ shows the mass density of air, λ is the tip speed ratio while C_{pr} represents the power-coefficient and it is represented as:

$$C_{pr}(\lambda) = [\lambda(0.0059 - 0.0013\,\lambda + 0.0081\lambda^2 - 0.00097477\lambda^3] \quad (6)$$

From the above equation, variations in λ are associated with distinct wind turbine operating circumstances, which impact the turbine's power output and aerodynamic efficiency.

The value of tip speed ratio λ is:

$$\lambda = \frac{w_{sh}R_b}{v_{wd}q} \quad (7)$$

where the symbol w_{sh} depicts the WT shaft angular-speed while, q is the gear-transmission-ratio.

Similarly, one can represent the shaft torque of turbine as a function of coefficient of torque as:

$$T_{mec} = \frac{1}{2}\rho\pi {R_b}^3 {v_{wd}}^2 C_T(\lambda) \quad (8)$$

The torque coefficient $C_T(\lambda)$ is expressed as:

$$C_T(\lambda) = \frac{C_{PR}(\lambda)}{\lambda} \quad (9)$$

3.2.2 Modeling of PMSG

A PMSG is modelled in dq-axis reference frame and all the details are presented as follows [122].

$$\left.\begin{aligned} \dot{i_d} &= \frac{-R_{stator} i_d + p(L_q - L_{chopper})\omega_h i_q - R_{chopper} i_d}{L_d + L_{chopper}} \\ \dot{i_q} &= \frac{-R_{stator} i_q - p(L_q + L_{chopper})\omega_s i_d - R_{chopper} i_q}{L_q + L_{chopper}} + p\Phi_m \Omega_h \\ \dot{\omega_s} &= \frac{1}{J}\left(-p\Phi_m i_q + \frac{b_1 {v_{wd}}^2}{q} + \frac{b_2 v_{wd}\omega_s}{q^2} + \frac{b_3 {\omega_s}^2}{q^3}\right) \end{aligned}\right\} \quad (10)$$

where R_{stator}, L_d, L_q, and i_d, i_q are the stator-resistance, inductances and currents of dq axis respectively while p expresses the pole number, ω_h is angular rotor speed and ω_s denotes the shaft angular speed of the generator. The Ω_h and Φ_m represent the angular speed and flux of permanent magnets. The symbol J represents the generator shaft inertia, $R_{chopper}$ represents the equivalent chopper-resistance and b_1, b_2, b_3 are constant parameters.

Table 3.1 Constant terms specifications [123]

Constant	Value	Constant	Value	Constant	Value
$l_1 = m_1$	27.147	l_2	0.94866	$l_3 = m_4$	8.2264
m_2	3	m_3	1.3146	n_1	9.945
m_3	0.1332	n_3	0.00506	n_4	23.806

State-variables are simplified by putting the constant parameters as mentioned in [123]. These parameters are tested and developed for the real world problem. These constant values are tested by tuning these parameters. $x_1 = i_d, x_2 = i_q \; and \; x_3 = \omega_s$.

$$\begin{bmatrix} \dot{x_1} \\ \dot{x_2} \\ \dot{x_3} \end{bmatrix} = \begin{bmatrix} -(l_1 + l_3 R_{chopper}) - (l_3 x_3) + 0 \\ -(m_2 x_3) - \left(m_1 + m_4 R_{chopper}\right) + m_3 \\ -\frac{n_1 {v_{wd}}^2}{x_1} - n_4 - (n_2 v_{wd} + n_3 x_3) \end{bmatrix} \begin{bmatrix} x_1 \\ x_2 \\ x_3 \end{bmatrix} \quad (11)$$

where $l_1, l_3, m_1, m_2, m_3, n_1, n_2, n_3$ and n_4 are the constant terms and their values are mentioned in the Table 3.1.

3.2.3 State equation of the system

The model of wind ECS represented in (11) can be written as:

$$\dot{x} = A(x) + B(x)u$$

$$y = h(x) = x_3 = \omega_h \quad (12)$$

where *A(x)* and *B(x)* donates the input matrixes and *x* describes the vector, while *u* defines the control-input.

$$A(x) = \begin{bmatrix} A_1 \\ A_2 \\ A_3 \end{bmatrix} = \begin{bmatrix} l_1 x_1 - l_2 x_2 x_3 \\ -l_1 x_2 - m_2 x_1 x_3 + m_3 x_3 \\ -n_1 {v_{wd}}^2 - n_2 v_{wd} x_3 + n_3 {x_3}^2 - n_4 x_2 \end{bmatrix}; B(x) = \begin{bmatrix} -l_3 x_1 \\ -l_4 x_2 \\ 0 \end{bmatrix}; u = R_{chopper}$$

The output value, y=x_3, is used to specify which state variables are available for use by the controller. Therefore, it is convenient to transform (11) into normal form (i.e., input-output form conversion) by the following way [122]:

$$G_1 = y = x_3; G_2 = L_A h(x) = \frac{\partial h(x)}{\partial x} A(x) = -\gamma_1 - \gamma_2 x_3 - \gamma_3 {x^2}_3 - \gamma_4 x_2; G_3 = {L_\mathrm{A}}^2 h(x) = \frac{x_1}{x_2}$$

where

$$\gamma_1 = n_1 {v_{wd}}^2, \gamma_2 = n_2 v_{wd}, \gamma_3 = k_3, \gamma_4 = k_4 \quad (13)$$

As the order of our system is larger than the relative-degree where $n\ and\ r\ are\ 3\ and\ 2$, therefore:

$$\dot{G_1} = G_2$$

$$G_2 = {L_\mathrm{A}}^2\, h(x) = L_B L_A h(x) u \tag{14}$$

where ${L_\mathrm{A}}^2\, h(x)$ is the lie-derivative of *h(x)* in the position of *A(x)* and *B(x)*.

$$\dot{G_3} = \frac{\gamma_4}{\gamma_1}\left(-\frac{l_1 G_3 \gamma_1}{\gamma_4} - \frac{l_2 G_1 \gamma_1}{\gamma_4} - \frac{l_1 x_1 G_3 \gamma_1 u}{\gamma_4}\right) - \left(\frac{G_3 \gamma_1}{\gamma_4}\right)\left(\frac{\gamma_4^2}{\gamma_1^2}\right)\left(-\frac{l_1 \gamma_1}{\gamma_4} - \frac{m_2 l_1 G_3 G_1}{\gamma_4} + n_4 G_1 - \frac{l_3 x_1 \gamma_1 u}{\gamma_4}\right) \tag{15}$$

where

$${L_\mathrm{A}}^2\, h(x) = -\gamma_2 A_2(x) - (\gamma_2 + 2\gamma_3 x_3) A_3(x)$$

$$L_B L_A h(x) = l_3 x_1 \gamma_4 x_2 \tag{16}$$

where the zero-dynamic-state (G_3) has no substantial effects. Consequently, one can neglect it as long as it is stable. It is convenient to show the stability of the zero dynamic term.

3.2.4 Stability of zero dynamic term

Zero dynamics are essential to the stability analysis of dynamical systems. The term "zero dynamics" describes how a system behaves when its input is zero, and it can provide important information about the entire system's performance and stability. By looking at the poles and zeros of the transfer function, one can comprehend the zero dynamics in the context of control systems represented by the transfer function. Zeros indicate the behavior of the system when the input is zero, whereas poles show the dynamics of the system. To be more precise, the zero dynamics match the dynamics connected to the transfer function's zeros.

One can find the stability by finding the position of zeros called as internal dynamics [124]. So, arranging G_1, G_2 and u=0 in Equation (9), we have:

$$\dot{G_3} = -G_3(n_1 - l_1) \tag{17}$$

where as long as $n_1 > l_1$, the internal dynamics are stable. Control system design and analysis require an understanding of the zero dynamics. In the absence of outside disruptions, stable zero dynamics suggest that the system will behave predictably and revert to equilibrium. On the other hand, unstable zero dynamics imply that the system can behave erratically or possibly lose control. Therefore, maintaining the overall stability and effectiveness of control systems depends on managing or stabilizing the zero dynamics.

3.3 Wave energy conversion using linear generator

In the preceding sections, the numerical modelling for wave energy system is assessed. The initial target is to find the maximum power for wave energy, which can be accomplished by appropriate generator selection and MPPT control technique. This is done via using linear generator for HOWWE.

3.3.1 Linear generator variable equations

It is simple to model linear generator by using rotating machine or generator variables and equations [125]. The torque is linked to force by:

$$P = \tau\omega_{rm} \tag{18}$$

and

$$P = FV \tag{19}$$

where F represents force, V represents velocity and P represents power. So, output-power can be calculated by:

$$P = v_{xs}i_{xs} + v_{ys}i_{ys} + v_{zs}i_{zs} \tag{20}$$

The stator voltage equation of the linear generator the stator side voltage can be defined by:

$$v_{xyzs} = r_s i_{xyzs} + \frac{d}{dt}\lambda_{xyzs} \tag{21}$$

where v_{xyz} , i_{xyz} and λ_{xyzs} are generalized in the form:

$$f_{xyzs} = \begin{bmatrix} f_{xs} \\ f_{ys} \\ f_{zs} \end{bmatrix} \tag{22}$$

where f_{xs} , f_{ys} and f_{zs} are the stator voltage, current linkage and flux linkage phases of x, y and z. The flux depend on translator electrical angle θ_{re} .The position of translator θ_{re} is linked with the mechanical translator-angle θ_{rm} by the no. of poles. The θ_{re} is defined as:

$$\theta_{re} = \theta_{rm}\frac{p}{2} \tag{24}$$

Therefore, the flux linkage matrix is represented as:

$$\lambda_{xyzs} = L_s i_{xyzs}\lambda'_m \begin{bmatrix} \sin\theta_{re} \\ \sin\theta_{re} - \frac{2\pi}{3} \\ \sin\theta_{re} + \frac{2\pi}{3} \end{bmatrix} \tag{25}$$

where λ'_m is the peak flux linkage. The stator self-inductance matrix is defined as:

$$L_s = \begin{bmatrix} L_{ls} + L_{ms} & -\frac{1}{2}L_{ms} & -\frac{1}{2}L_{ms} \\ -\frac{1}{2}L_{ms} & L_{ls} + L_{ms} & -\frac{1}{2}L_{ms} \\ -\frac{1}{2}L_{ms} & -\frac{1}{2}L_{ms} & L_{ls} + L_{ms} \end{bmatrix} \tag{26}$$

The L_{ms} is mutual inductance and L_{ls} is the stator-leakage. The translator-speed ω_{rm} related to electrical counter-torque τ_e and mechanical input torque τ_m by

$$\tau_e - \tau_m = J\frac{d}{dt}\omega_{rm} + \mathrm{D}_m\omega_{rm} \tag{27}$$

where J is translator inertia of the translator and create resistance and D_m is the mechanical-damping. The electric torque produced by linear generator is specific to the geometry of HOWWE. It is complicated by the system design such as winding distribution. By assuming the generator winding distribution as constant then the τ_e is expressed as:

$$\tau_e = \frac{p}{2}\left\{\frac{\sqrt{3}}{2}\left(i^2{}_{ys}i^2{}_{zs} - 2i_{xs}i_{ys} + 2i_{xs}i_{zs}\right) + \lambda'_m\left[\left(i_{xs} - \frac{1}{2}i_{ys} - \frac{1}{2}i_{zs}\right)\cos\theta_{re} + \frac{\sqrt{3}}{2}\left(i_{ys} - i_{zs}\right)sin\theta_{re}\right]\right\} \tag{28}$$

For the variable generator equation the self-inductance matrix (16) and voltage equation for stator (12) will remains the same while the flux linkage equation is defined as

$$\lambda_{xyzs} = \mathrm{L}_s\mathrm{i}_{xyzs} + \lambda'_m\sum_{n-1}^{\infty}k_{2n-1}\begin{bmatrix}\sin((2\mathrm{n}-1)\theta_{re})\\ \sin((2\mathrm{n}-1)(\theta_{re}-\frac{2\pi}{3}))\\ \sin((2\mathrm{n}-1)(\theta_{re}+\frac{2\pi}{3}))\end{bmatrix} \tag{29}$$

where magnitude of harmonic coefficient is k_n . So, the torque equation is become as:

$$\tau_e = \left(\frac{3}{2}\right)\left(\frac{p}{2}\right)\lambda'_m\sum_{n-1}^{\infty}k'_{2n-1}\begin{bmatrix}i_{xs} & i_{ys} & i_{zs}\end{bmatrix}\begin{bmatrix}\cos((2\mathrm{n}-1)\theta_{re})\\ \cos((2\mathrm{n}-1)(\theta_{re}-\frac{2\pi}{3}))\\ \cos((2\mathrm{n}-1)(\theta_{re}+\frac{2\pi}{3}))\end{bmatrix} \tag{30}$$

3.3.2 Translator reference frame using dq0 variables

In order to find the translator variables, the transformation of variables through translator reference-frame. The dq0 transformation has replaced standard transformation. The dq0 transformation replaced the phase variables x, y, z into d, q, 0 axes. The graphical

representation is shown in the figure where f_{xs} , f_{ys} and f_{zs} are x, y and z axes while f_{ds} and f_{qs} are d and q axis. The 0 axis will be originated from other axes and it is not shown in the figure. The main advantages for using the dq axes for the linear generator because it gives simplified direct torque. To find transformation, there is multiplication between K matrix transformation and generator variables. By taking electrical translator angle θ_{re} , so transformation matrix will become as:

$$K_s^r = \frac{2}{3}\begin{bmatrix} cos\,\theta_{re} & cos\,(\theta_{re} - \frac{2\pi}{3}) & cos\,(\theta_{re} + \frac{2\pi}{3}) \\ sin\,\theta_{re} & sin\,(\theta_{re} - \frac{2\pi}{3}) & sin\,(\theta_{re} + \frac{2\pi}{3}) \\ \frac{1}{2} & \frac{1}{2} & \frac{1}{2} \end{bmatrix} \tag{31}$$

The new translator variables in dq0 frame are generalized as:

$$f^r{}_{qdos} = \begin{bmatrix} f^r{}_{qs} \\ f^r{}_{ds} \\ f^r{}_{os} \end{bmatrix} \tag{32}$$

and

$$f^r{}_{qdos} = K_s^r f_{xyzs} \tag{33}$$

The inverse transformation matrix is applied:

$$f_{xyzs} = (K_s^r)^{-1} f^r{}_{qdos} \tag{34}$$

and

$$(K_s^r)^{-1} = \begin{bmatrix} \cos\theta_{re} & \sin\theta_{re} & 1 \\ \cos\,(\theta_{re} - \frac{2\pi}{3}) & \sin\,(\theta_{re} - \frac{2\pi}{3}) & 1 \\ \cos\,(\theta_{re} + \frac{2\pi}{3}) & \sin\,(\theta_{re} + \frac{2\pi}{3}) & 1 \end{bmatrix} \tag{35}$$

The equation (12) for voltage becomes

$$v^r{}_{qs} = \mathrm{r}_s i^r{}_{qs} + \omega_{re}\lambda^r_{ds} + \frac{d}{dt}\lambda^r_{qs} \tag{36}$$

$$v^r{}_{ds} = \mathrm{r}_s i^r{}_{ds} + \omega_{re}\lambda^r_{qs} + \frac{d}{dt}\lambda^r_{ds} \tag{37}$$

$$v^r{}_{0s} = \mathrm{r}_s i^r{}_{0s} + \frac{d}{dt}\lambda^r_{0s} \tag{38}$$

and the equation (21) becomes

$$\lambda^r_{qs} = \left(\mathrm{L}_{ls} + \frac{3}{2}\mathrm{L}_{ms}\right) i^r{}_{qs} + \lambda'_m \sum_{n-1}^{\infty}(k_{6n-1}+k_{6n+1})\sin(6\mathrm{n}\,\theta_{re}) \tag{39}$$

$$\lambda^r_{ds} = \left(\mathrm{L}_{ls} + \frac{3}{2}\mathrm{L}_{ms}\right) i^r{}_{ds} + \lambda'_m + \lambda'_m \sum_{n-1}^{\infty}(k_{6n-1}-k_{6n+1})\cos(6\mathrm{n}\,\theta_{re}) \tag{40}$$

$$\lambda^r_{0s} = (\mathrm{L}_{ls} + \frac{3}{2}\mathrm{L}_{ms}) i^r{}_{0s} + \lambda'_m \sum_{n-1}^{\infty} k_{6n-3}\sin((6\mathrm{n}-3)\,\theta_{re}) \tag{41}$$

and (22) becomes

$$\tau_e=(\tfrac{3}{2})(\tfrac{p}{2})\,\lambda'_m[i^r{}_{qs}(1 + \sum_{n-1}^{\infty}(k''{}_{6n-1}+k'{}_{6n+1})\cos(6\mathrm{n}\,\theta_{re})) +$$

$$i^r{}_{ds}\sum_{n-1}^{\infty}(k'{}_{6n-1}+k'{}_{6n+1})\sin(6\mathrm{n}\,\theta_{re}) + 2i^r{}_{0s}\sum_{n-1}^{\infty}(k'{}_{6n-3})\cos((6\mathrm{n}-3)\theta_{re})] \tag{42}$$

In equation (20), power can be calculated using xyz variables. So, using dq0 variables power can be calculated as

$$P = \frac{3}{2}(v^r{}_{qs}i^r{}_{qs} + v^r{}_{ds}i^r{}_{ds} + 2v^r{}_{0s}i^r{}_{0s}) \tag{43}$$

3.4 Hybrid system modelling

The mechanical to electrical output from offshore wind is AC. Same conversion is for wave energy. This offshore wind AC and wave energy AC power to DC power based on numerous phases and a method is called a rectification. The ideal methods for understanding a VSC with electric grid is steady-state power flow method. This method delivers understanding

about operating-points with potential-contingencies. In the case of HOWWE VSC, it is significant to know about key process features with steady-state representation.

HOWWE with VSC and VSI grounded with DC-lines, such as DC-lines and traditional AC lines are used to transferring an active power from both sources to loads as shown in Fig 3. The VSC components are used for switching high frequencies comparative to the HOWWE operating frequency. An active-power control delivered to AC-load is attained by modifiable voltage-phase-angle generated on the VSI. A reactive power of VSCs are competent to offshore wind and wave energy source reactive-power to a linked to AC load. Comparable to active- power, the reactive-power produced is manageable with comparatively rapid response times. In DC, by fixing the voltage-dynamics to no dynamics, the output voltage can be calculated as:

$$V_{Dc(\,OW)} = V_{ref} - DI_{Dc(\,OW)} \tag{44}$$

where V_{ref} is the input-signal value across offshore wind, D is the drop of DC voltage across offshore and $I_{Dc(\,OW)}$ is the DC current output across offshore wind.

The reference active power of offshore wind is defined as:

$$P^{*}_{ow(k)} = V^{*}_{ow(k)} I_{ow(k)} \tag{45}$$

where $V_{ow(k)}$the DC voltage of is offshore wind converter and $I_{ow(k)}$ is the DC side reference current. In wave energy DC, by fixing the voltage-dynamics to no dynamics, the output voltage can be calculated as:

$$V_{Dc(\,WE)} = V_{ref} - DI_{Dc(\,WE)} \tag{46}$$

where V_{ref} is the input-signal value for wave energy, D is the drop of DC voltage across wave energy and $I_{Dc(WE)}$ is the DC current output of wave energy side. Similarly, for the wave energy we have reference active power;

$$P^*_{we(k)} = V^*_{we(k)} I_{we(k)} \tag{47}$$

where $V_{we(k)}$the DC voltage of is wave energy converter and $I_{we(k)}$ is the DC side reference current.

In the AC side the input-power of DC offshore wind is equivalent to output-power of AC side of offshore wind if we adjust the power-balance dynamics.

$$P_{DC(OW)} = P_{AC(OW)} \tag{48}$$

Similarly, for wave energy is defined as;

$$P_{DC(we)} = P_{AC(we)} \tag{49}$$

To determine the 3-phase input currents at the DC side, the block first calculates the dq-axes.

The combined power can be calculated using xyz variables of both offshore wind and wave energy. So, using dq axes for the OWT output from the system is 75 % and wave energy the output power 25 %.

$$P_{hybrid} = P_{ow} + P_{we} = \frac{3}{2}(v^r{}_{qs} i^r{}_{qs} + v^r{}_{ds} i^r{}_{ds}) * 0.75 + \frac{3}{2}(v^r{}_{qs} i^r{}_{qs} + v^r{}_{ds} i^r{}_{ds}) * 0.25 \tag{50}$$

Boundary assumptions, which contain a variety of factors that define the system's performance and dependability, are crucial considerations in the design and operation of hybrid wind and wave energy systems. The aforementioned assumptions establish parameters and circumstances that promote optimal system performance. These include environmental

factors, technological limitations, economic factors, operational demands, resource accessibility, and regulatory frameworks. The operational envelope of the system is defined by environmental factors including wind, wave heights, and tidal variations, which guarantee efficient and secure operation. Technical limitations determine the maximum power production, mechanical stresses, and voltage stability of the system. These limitations include those imposed by electrical infrastructure, wave energy converters, and wind turbines. The system's financial feasibility and return on investment are influenced by economic boundaries, including capital costs, maintenance charges, and energy market pricing. Reliability and safety are ensured by operational standards such as emergency shutdown procedures and maintenance schedules. Furthermore, the system's development and integration into the energy landscape are shaped by regulatory and legislative frameworks, while resource availability considerations account for the unpredictability and predictability in wind and wave patterns. In order to ensure the efficacy, efficiency, and sustainability of hybrid wind and wave energy systems, adherence to certain boundary assumptions is crucial for their deployment and operation.

3.5 HOWWE power calculation

In the renewable energy sector, analytical methodologies for measuring HOWWE potential are critical for effective resource power evaluation, power distribution modelling and load data. Mathematical methodologies and data analysis techniques are required to make one system dominant using probability. Here are some major analytical aspects for assessing HOWWE:

3.5.1 Power distribution modelling

HOWWE systems use power distribution modelling to systematically assess the capacity and availability of offshore wind and wave energy sources for each system unit. This modelling strategy achieves a number of important goals. First of all, it makes it possible to evaluate the offshore wind and wave energy capacity of each HOWWE unit, offering insights into their future power generation capacities. Second, the model provides probabilistic evaluations of the potential for power generation by integrating probability distributions related to offshore wind and wave energy. This takes into account the possibility that various capacity levels will occur. In addition, the model helps with system optimization and effective power generation all year round by identifying seasonal fluctuations and determining which energy source is dominant during particular seasons. Additionally, the model aids in decision-making about resource allocation, system design, and operational planning by quantifying the levels of availability and capacity of each resource. This makes it easier to integrate many renewable energy sources into a single, cohesive system. Finally, the evaluation of HOWWE systems' resilience and dependability is aided by the assessment of availability and capacity levels, which makes it possible to spot weaknesses and put plans in place to strengthen system resilience. In general, power distribution modelling is essential for directing HOWWE system design, operation, and optimisation. It also facilitates the sustainable integration of offshore wind and wave energy resources and allows for informed decision-making.

The unit availability model is designed for HOWWE. This model is based on different states parameters and states levels such as for season which source is dominant. The designed model is based on C_r^{ow} and C_r^{we} of rth of HOWWE can be given by the following probability distribution:

$$C_r^{ow} = \left[\{C_{r,n}^{ow}, \quad P\left(c_{r,n}^{ow}\right)\}: \ n = 1 \ to \ NC_r^{ow} \right] \tag{51}$$

In the above equation, $P\left(c_{r,n}^{ow}\right)$ is the probability associated with offshore wind and $C_{r,n}^{ow}$ is the capacity level in the model.

Similarly, availability model of rth wave energy:

$$C_r^{we} = \left[\{C_{r,n}^{we}, \quad P\left(c_{r,n}^{we}\right)\}: \ n = 1 \ to \ NC_r^{we} \right] \tag{52}$$

In the above equation, $P\left(c_{r,n}^{we}\right)$ is the probability associated with wave energy and $C_{r,n}^{we}$ is the capacity level in the model.

$$P\left(c_{r,n}^{we}\right) = C_r^{ow} + C_r^{we} \tag{53}$$

3.5.2 Wind, wave and load data

The sea wave irradiance for the wave energy is measured as a random variable. So, we assumed Beta distribution. The wave energy irradiance w is given as:

$$f_w(we) = \left\{ \frac{\Gamma(\alpha^t+\beta^t)}{\Gamma(\alpha^t)\Gamma\beta^t)} \left(\frac{we}{we_{max}^t}\right)^{(\alpha^t-1)} \left(1 - \frac{we}{we_{max}^t}\right)^{(\beta^t-1)} \right. \tag{54}$$

with $\alpha^t \ and \ \beta^t > 0$. In the above equation $f_w(we)$ is the Beta distribution at t^{th} time frame and we_{max}^t is the maximum wave irradiance and Γ represents gamma function.

Similarly for the offshore wind, Weibull distribution is used for random speed for t^{th} time frame is given as

$$f_v(ow) = \frac{\mathrm{k}^t}{\mathrm{c}^t} \left(\frac{v}{\mathrm{c}^t}\right)^{(\mathrm{k}'-1)} e^{-\left(\frac{v}{\mathrm{c}^t}\right)} \tag{55}$$

In the above equation $\mathrm{c}^t \ and \ \mathrm{k}^t$ denotes scale and shape parameters. The combined load function form from (54) and (55):

$$L_f = = f_w(we) + f_v(ow) \tag{56}$$

The probabilistic form load data can be generated from the discrete form of offshore wind and wave equations is given as:

$$L^p = [\{l_n^t, \quad P(l_n^t)\} \quad : \quad N = 1 \quad to\ NL^p \tag{57}$$

So, $P(l_n^t)$ is given as fallow:

$$P(l_n^t) = \frac{No.of\ occurance\ of\ load\ level(l_n^t)}{Offshore\ wind\ point\ and\ wave\ point\ at\ t^{th}} \tag{58}$$

3.6 Summary

The focus of this chapter is on numerical approaches for evaluating the HOWWE. To set the scene, the chapter begins with an introduction. In this chapter, the numerical modelling of wind ECS, state equation of the system and normal form conversion from third order to the second order of the system (i.e., from three states variables to two states variables) are presented. In this context, the stability analysis of the zero dynamic term is discussed. The practical results of offshore wind are tested using MATLAB in the chapter 4. The chapter then delves into the numerical modelling of wave energy conversion using linear generator. It provides variable equations for linear generators and explores translation using the dq0 reference frame tested in chapter 5. The modelling of hybrid system is investigated, with the integration of these two renewable energy sources being emphasized and tested using MATLAB in chapter 6. Finally, the chapter offers an analytical method for calculating power from HOWWE under the condition of dominancy using probability. This section includes HOWWE power modelling and HOWWE modelling with load data. These numerical techniques are crucial in assessing the performance and economic feasibility of the HOWWE system.

Chapter 4 Design and Control Techniques for Offshore Wind

In this chapter, offshore wind design and control techniques are modelled and tested. Section 4.1 is an introduction of offshore wind energy system. Section 4.2 is the control solution of offshore wind turbine (OWT). The wind energy conversion is an important part to maximize power output of the HOWWE system; therefore, the solution set of OWT is studied with different techniques. Different controllers are implemented in this chapter by numerical modeling with their steps of implementations. PID, SMC, FBL, STA and IBRTA are implemented and presented in Section 4.3, 4.4., 4.5, 4.6 and 4.7. In the last Sections 4.8 and 4.9, different case studies are carried out using constant and practical wind speeds by applying an AI-based IBRTA technique. The models are tested and validated in the MATLAB Simulink.

4.1 Introduction

The essential idea of driving the maximum power point tracking (MPPT) in offshore-wind energy conversion system (ECS) is to adjust and manage the speed of AC generator, along with the speed of PMSG wind-turbine and coupling shaft [119]. Therefore, the implementation of a control scheme to find MPPT for finding the optimal point of operation in offshore-wind ECS is important [117]. These control schemes are in [117] and the hill climb search (HCS) is referred to use perturb and observe algorithm in [117].

For wind-turbine, a particular ratio called the optimal- tip speed ratio (TSR) is used for the extraction of power maximization. An optimum TSR value is needed for the system, which changes from system to system [126,127]. The TSR range for offshore wind energy applications is 6 to 8. This range minimizes aerodynamic losses and structural loads while optimizing energy capture. The ideal TSR range, however, may differ and may be impacted by the interplay between wind conditions in HOWWE systems. Controlling the TSR becomes essential for preserving turbine efficiency in the case when the turbine is a DFIG, particularly when there are no direct wind speed readings available. Turbine efficiency depends on TSR, hence control systems that modify the TSR in response to measurements or estimates that are available must be put into place. Generally, the optimal torque control (OTC) scheme is simple to be executed and also efficient and quick. In any case, its proficiency is less than the TSR, due to the restriction of estimating the wind speed straightforwardly [117]. However, there is no such difference between OTC and TSR schemes [128].

Unlike TSR, the power signal feedback (PSF) control technique does not require the measurement of a particular wind speed but it does require prior information of the wind turbine curve. which is obtained either through tests or simulations for single wind turbine.

This way it makes the implementation of PSF control technique costly [129]. Unlike TSR, HCS control technique requires no such prior knowledge of the OWT MPPs. By selecting a suitable step size is a difficult task, because a greater step size gives a faster convergence, although improving efficiency, gives a slower convergence [117].

Most of the complications concerned with these methods can be solved by applying artificial intelligence schemes and also some hybrid control schemes. The FLC (fuzzy logic control) contributes to parameters insensitivity to variation and better convergence [130].

The combination of two different control techniques constitutes a hybrid technique, which utilizes the benefits of first technique to mitigate the problems of the second technique. For example, a hybrid technique was proposed in [128] by merging OT with HCS to mitigate the problems rendered by HCS: wrong direction under rapid wind speed variations and speed-efficiency trade-off. Similarly, PSF control technique was merged with HCS to develop a flexible and sensor-less technique that applies to all wind system [117]. The testing of algorithm on offshore wind is followed by characterizing surface which called as switching surface. This switching surface is in terms of errors such as the mismatches between two states. The following states are actual and desired. There is a designed control law in the switching-manifold which execute sliding mode alongside with the characterized surfaces. Subsequently, the framework directions are coordinated towards their individual sliding manifolds.

4.2 Control solution to offshore wind turbine

The more ideal controllers for offshore wind turbine (OWT) such as STA and IBRTA are studied, implemented and tested in MATLAB Simulink. The PID is considered for the

offshore wind turbine because of simplicity and versatility. This technique is considered as more ideal for the OWT due to its tunability. The PID is more ideal for fast response. FBL is also better for OWT due model based control strategy and the tracking accuracy of OWT tracks its set point. SMC is ideal in the case of the control saturation handling but produce chattering. The chattering of OWT can be minimize by using STA. The concept behind STA is the reachability law. Furthermore, AI have increased the controllability for controller using variable wind speed applied to the system as shown in Fig. 4.1. The more ideal controller under practical applications is the IBRTA technique and it will be presented in the results section.

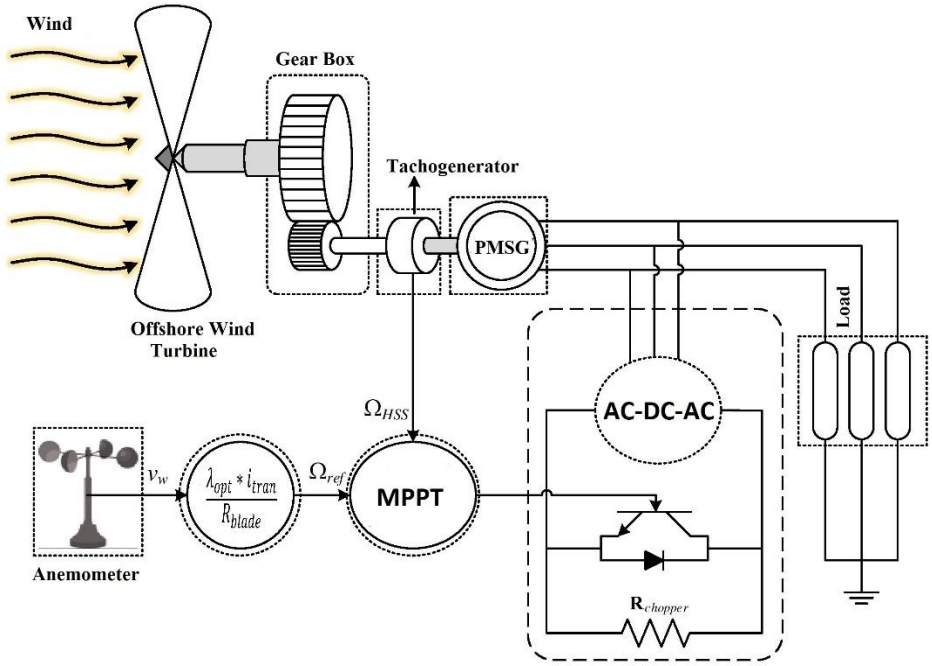

Figure 4.1 Variable wind speed PMSG for offshore wind

Wind energy has emerged as a prominent solution to address the increasing demand for clean and sustainable energy sources. With its limitless supply and environmentally friendly attributes, wind energy has surpassed other forms of renewable energy. Technological

advancements have significantly contributed to its rise, making it the most cost-effective and efficient option available. Unlike traditional energy sources, wind power generation produces no harmful emissions, resulting in a reduced carbon footprint. Additionally, wind energy systems boast low operational costs and a high energy yield, making them economically viable. Given these advantages, wind energy is poised to play a pivotal role in meeting the ever-expanding global energy needs.

The efficiency of an offshore wind ECS depends on the wind speed and the system's operating point. To achieve maximum power extraction, an effective MPPT control scheme is essential. Previous research studies have emphasized the significance of employing an MPPT control strategy to determine the optimal operating point for a WECS [131].

An AI methodology has helped mitigate various issues encountered in previous control systems. The FLC method, for instance, offers benefits such as insensitivity to parameter fluctuation, faster convergence, and the ability to handle noisy and imperfect signals [132]. Additionally, neural network-based schemes leveraging an inverse-turbine model have been employed to address challenges related to wind speed measurement or estimation. This approach utilizes the model as a virtual anemometer, estimating wind speed based on actual torque and speed measurements [133].

To overcome the challenges previously mentioned, this study introduces the utilization of observer-based SMC and reaching STA as effective solutions for achieving fast and accurate MPPT in offshore wind ECS. Among these techniques, the STA is recognized as the most straightforward twisting scheme, as highlighted by [134]. The proposed control schemes are designed to ensure asymptotic convergence to a desired equilibrium point while effectively mitigating disturbances, showcasing a high level of robustness against variations in system

parameters and external disturbances. Additionally, in the case of STA, the control schemes exhibit effective suppression of chattering, further enhancing their performance.

4.3 PID controller

A PID controller is based on the feedback control process and it is used to manage variables output with accuracy and stability. A PID-controller is also used to implement MPPT for an OWT. MPPT is a technique used to extract the MPP from an OWT by regulating the blade-pitch-angle and rotor speed with power conversion in different conditions. The feedback concept in PID can minimize the error in the desired value and calculated value. Initializing the PID parameters, which include the derivative, integral, and proportional gains (Kp, Ki, and Kd), is the first step in the PID control process. After that, a setpoint is established, which stands for the process variable's intended target value. After measuring the process variable's current value, the error is computed as the difference between the measured value and the setpoint. On the basis of the error, the proportional, integral, and derivative control components are then calculated. These elements are then combined to determine the control output. The actuators or inputs of the system are adjusted using this output. The process variables are measured once more and the system's performance is assessed following the application of the control output. To enhance performance, the PID parameters are changed as needed. The PID controller used as proportional, integral and derivative control for MPPT for OWT. The PID proportional-component regulates the blade-pitch-angle customized on the change between the OWT output and the MPPT output that can be attained. The controller maximized the pitch-angle or MPPT power conversion if the calculated output is lower than MPP, and cuts it if the output is more than its MPP. The quantity of change is proportional to the variance between the output measured power and the MPP. The PID integral-

component regulates the rotor speed based on the gathered error over time. If the turbine has been steadily making minimized power than the MPP, the integral-component will progressively rise the rotor-speed to manage output. The PID derivative-component controller regulates the pitch-angle grounded on the rate of alteration of the output power. If the output power is quickly growing, the derivative-component will rise the rotor-speed to sustain the MPP. With the combination of these three components, the system maintains the pitch-angle or rotor-speed of the OWT in real-time to handle the MPP. The parameters can be tuned to maximize controller efficiency. A PID algorithm is a generally used for industrial applications such as robotics and MPPT control for OWT. PID algorithm's purpose to curtail the variance between the actual and desired output by regulating a control-signal. In perspective of MPPT for OWT, the PID can be used to control the turbine's operating parameters, such as rotor speed or blade pitch angle, to maintain MPP output. Measure the OWT speed and generated output power: The initial phase is to calculate OWT speed and the OWT output power. This method is used to find the error among the actual and desired output-power. In algorithm the signal is measured in addition of three quantities: the proportional, integral and the derivative. It is significant to regulate the PID parameters to confirm optimal performance of OWT and environment.

4.4 Feedback linearization

FBL is nonlinear method that changes a nonlinear system into a linear with feedback. It can be implemented by describing the system dynamics: This comprises the aerodynamic performance of the OWT blades, the mechanical performance of the PMSG, and the power conversion performance of the system. The second step is the selection of the input-output variables: The controller variable called as input variables and controller will operate in

directive to attain the wanted output variable. The third step is the design to stop out the nonlinearities, likely to use linear control methods. This includes choosing a feedback gain that will change the nonlinear to linear system. Generally, feedback linearization can be further difficult to implement because it simplifies control design by transforming the nonlinear systems into linear ones, practical implementation can be challenging due to system complexity and sensitivity to the modeling errors.

4.5 Sliding mode control

A SMC is a robust controller and used for MPPT in OWT. The key benefit of SMC is to manage uncertainties with disturbances in the system, which usually comes in OWT due to fluctuations in speed and environment. There are following steps to implement SMC on OWT: By stating the sliding surface: The sliding surface is a function of the error between the measured wind turbine power output and the reference power output. The sliding surface should be designed to ensure that the error converges to zero asymptotically. The first step is the function that enable the OWT sliding-surface and tune it. The control-law is planned to guarantee that the OWT functions in the sliding-mode. Generally, an SMC is a real control approach for MPPT in OWT.

The SMC algorithm is a vigorous control method that can grip system doubts, turbulences, and variations. It mechanism is forming a sliding surface that gives instruction to the controller towards a preferred optimal point to calculate the MPP of the OWT.

4.5.1 Steps to implement SMC controller

There are following points to instruct the SMC algorithm to OWT: such as by defining the system-dynamics, sliding surface, controller and tuning of tune under different circumstances.

The dynamics are based on the aerodynamic performance of the OWT blades, the performance of the PMSG generator, and the power conversion performance of the system.

The sliding surface is the main part of the algorithm. It tracks the MPP of an OWT. One main method is measuring the output variance between the actual and MPP power as the sliding-variable. The SMC controller at OWT is verified and tuned to confirm its operation properly and to get the preferred outcomes. In general, the algorithm can offer vigorous and correct MPPT for OWT in the existence of disturbances.

4.5.2 Design and implementation of SMC

The design model is followed by characterizing surface which called as switching surface. This switching surface is in terms of errors such as the mismatches between two states. The following states are actual and desired. There is a designed control law in the switching-manifold which execute sliding mode alongside with the characterized surfaces. Subsequently, the framework directions are coordinated towards their individual sliding manifolds. The reference tracking, can be carried out by defining the tracking error, $e(t)$, as follows:

$$e_r(t) = G_1 - G_{ref} \tag{59}$$

where $G_{1ref} = \omega_{ref}(t)$. Taking the derivative of (59) we have

$$\dot{e_r}(t) = \dot{G_1} - \dot{G_{1ref}} \tag{60}$$

In the above equation, the value of $\dot{G_1} = G_2$. So, equation (60) can be written as

$$\dot{e_r}(t) = \dot{G_2} - \dot{G_{1ref}} \tag{61}$$

Differentiating (61) along (14) and (15), it becomes

$$\ddot{e_r}(t) = L_A^2 h(x) + L_B L_A h(x) u \tag{62}$$

A proportional integrated (PI) based sliding surface or manifold can then be designed as:

$$S_m = G_2 - \dot{G_{1ref}} + k_1 G_1 - G_{1ref} + k_2 \int_0^t \left(G_1 - G_{1ref}\right) d\tau \tag{63}$$

where k_1 and k_2 are gains. Furthermore, the derivative of manifold along (14) and (15) can be expressed as:

$$\dot{s_m} = G_2 \ddot{G_{1ref}} + k_1 G_2 - k_1 \dot{G_{1ref}} + k_2 G_1 - k_2 G_{1ref} \tag{64}$$

In this way, a reachability law of the following form is adopted.

$$\dot{s_m} = u_{dis} = -k_3 s_m - k_4 sign(s_m) \tag{65}$$

Now, the overall control law by comparing (64) and (65) can be expressed:

$$\dot{G_2} - \ddot{G_{1ref}} + k_1 G_2 - k_1 \dot{G_{1ref}} + k_2 G_1 - k_2 G_{1ref} = -k_3 s_m - k_4 sign(s_m) \tag{66}$$

By replacing $\dot{G_2}$ from (14), we have

$$u = \frac{1}{L_B L_A h(x)} \Big(\ddot{G_{1ref}} - k_1 G_2 - k_2 G_1 + k_1 \dot{G_{1ref}} + k_2 \dot{G_{1ref}} + L_A^2 h(x) - k_3 s_m - k_4 sign(s_m) \Big) \tag{67}$$

where k terms are the gain parameters displayed in Table 4.1 from equation (67). In order to get rid of chattering, a super-twisting based algorithm is subsequently proposed.

4.6 Super twisting based algorithm

A STA is a nonlinear controller is use to get MPP in power electronics of OWT. It is utilized to improve the efficiency and consistency of the offshore wind turbine (OWT) output. A STA is a feedback control system that is based on robust control method to attain MPP of OWT. It is measured to provide robust-control in the occurrence of disturbances. The STA attains this by producing a signal that is relational to the error. In the situation of MPPT for OWT, it regulates the OWT parameters. This supports to guarantee that the OWT works at the MPP. It can benefit to recover energy efficiency, decrease system costs, and improve overall system consistency and strength. Here are the phases based in applying the STA algorithm: Measure the OWT speed: In this step the wind speed is measured by actual and desired output. Second step is the calculation of the sliding variable: This step is measured by comparing the error and the product of a gain parameter. Third step is based on the generation of the signal, this is taken by sliding variable derivative and multiple it by a gain parameter. Fourth step is the modifying the OWT parameters by modifying OWT parameters and the list of parameters is presented in Table 4.1 [123].

4.6.1 Design and implementation of STA

As the sliding mode design can produce vibrations around the switching-surface which are not desirable in a practical scenario. Consequently, such vibrations or chattering can be mitigated by adopting the following reachability law:

$$\dot{s_m} = -p_1|s_m|^2 sign(s_m) - p_2 \int sign(s_m)\, dt \tag{68}$$

where p_1 and p_2 are constants.

Table 4.1 Details of Parameters [123]

Type	Name of Parameters	Magnitude
Turbine	Air-density(ρ) Blade-radius, R_b Gear-Transmission ratio, q	1.25 kg/m^3 2.5 m 7
PMSG	Stator-resistance, R_{stator} Stator-Inductance along d-axis L_d Stator-Inductance along q-axis, L_q Equivalent load inductance, $L_{chopper}$ Flux, φ Pole number, p Shaft inertia, J	3.3 Ω 0.0416 H 0.0416 H 0.08 H 0.04382 Wb 3 0.0552 kg/m^2
Controller	Constant,(K_1) Constant, (K_2) Constant, (K_3) Constant, (K_4) Constant, (p_1) Constant, (p_2)	60 20000 0.8 200 150 0.08

The OWT system, PMSG, and controller have all been rigorously modelled and analyzed; parameters in Table 4.1 have been chosen and justified accordingly [123]. The reachability law in (68) has two terms; the first term indicates about the chattering reduction while the second term indicates a low pass filter which eliminates the vibrations.

By comparing Eq. 64 and Eq. 68, the following control algorithm can be formed.

$$u = \frac{1}{L_B L_A h(x)}\Big(\ddot{G}_{1ref} - k_1 G_2 - k_2 G_1 + k_1 \dot{G}_{1ref} + k_2 \dot{G}_{1ref} + L_f^2 h(x) - p_1 |s_m|^{0.5} sign(s_m) - p_2 \int sign(s_m)\, dt\Big) \quad (69)$$

where the gain parameters are listed in Table 4.1. The selection of Table 4.1 parameters are tested in existing research based on PID, FBL and SMC algorithms. These constant values are tested by tuning these parameters of wind turbine.

4.7 Integral back-stepping-based real-twisting algorithm

The study proposes three different control algorithms, namely SMC, IBRTA and FBL controller, to optimize the power output of a fixed-pitch WECS equipped with a variable speed, 3 kW, PMSG. In practical applications, acquiring accurate nonlinear terms and aerodynamic forces for control algorithms may be impractical. To enhance the robustness of the control algorithms, an offline artificial feed-forward neural network (FFNN) based on the back propagation algorithm is employed to approximate the nonlinearity in the drift and control input pathways. This approach enables the control algorithms to adapt to varying conditions and uncertainties. The results provide insights into the performance of each control algorithm and its suitability for wind energy systems. The findings contribute to the development of sophisticated MPPT control strategies that can optimize power extraction from wind energy systems under various operating conditions.

4.7.1 Feed forward neural networks with back propagation for nonlinear functions-estimation

Lie-derivatives estimation via feed forward neural networks with back propagation which is commonly used for estimation tasks, where the objective is to estimate a target variable based on input data. The feed forward process involves propagating the input data through the network, while back propagation is used to update the network's weights and biases to minimize the estimation error as shown in Fig. 4.2 and the list of parameters is presented in Table 4.2.

Let's denote the input data as X€R$^{n\times d}$, where n is the number of data points and d is the dimensionality of the input, so input is (i.e., X=[z_1, z_2, z_3, V_{wind}]). The target variable we want to estimate is Y€R$^{n\times m}$, where m is the dimensionality of the target. So, the output is (i.e., y=$L_f^2 h(x)$, and $l_g, l_f, h(x)$ respectively.

In a feed forward neural network, the estimation process can be represented as follows: $h^{(1)} = g\left(W^{(1)}X + b^{(1)}\right)$; $h^{(2)} = g\left(W^{(2)}h^{(1)} + b^{(2)}\right)$. So,

$$y = g\left(W^{(L)}h^{(L-1)} + b^{(L)}\right) \tag{70}$$

where $h^{(l)}$ represents the activations of the neurons in the l^{th} hidden layer, $W^{(L)}$ and $b^{(L)}$ are the weight matrix and bias vector, respectively, for the l^{th} layer, and g (.) is the activation function applied element-wise to the weighted sum of inputs.

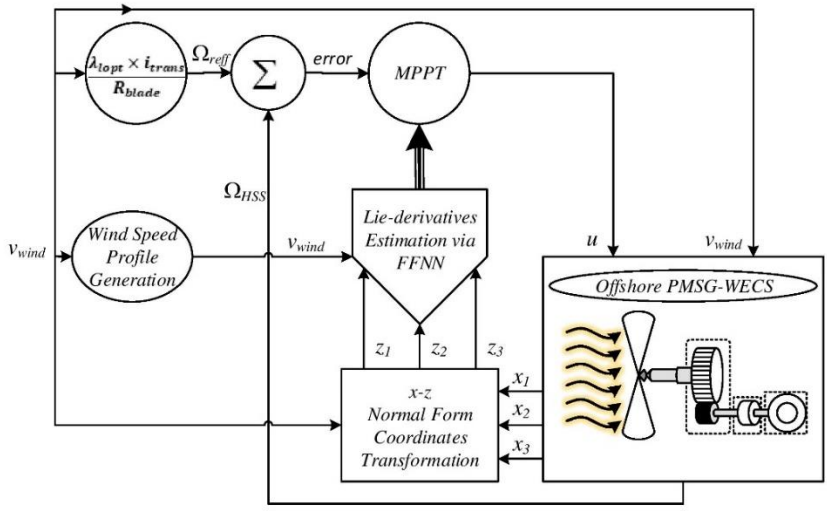

Figure 4.2 Estimation error calculation of offshore wind turbine

The back propagation algorithm is then used to update the weights and biases in order to minimize the estimation error. This can be summarized as follows:

$$\Delta W^L = -\eta \frac{\partial L}{\partial W^L} \tag{71}$$

$$\Delta b^L = -\eta \frac{\partial L}{\partial b^L} \tag{72}$$

So, we have

$$\Delta W^1 = -\eta \frac{\partial L}{\partial W^1} \tag{73}$$

$$\Delta b^1 = -\eta \frac{\partial L}{\partial b^1} \tag{74}$$

where η is the learning rate, L is the loss function that quantifies the difference between the estimated output y and the true target Y, and ΔW^L and Δb^L are the updates to the weight matrix and bias vector, respectively, for the l^{th} layer. The gradients are computed using the chain rule and propagated backward through the layers. The exact form of the gradients depends on the specific loss function used. By iteratively performing the feed forward and back propagation steps on the training data, the network's weights and biases are adjusted to minimize the estimation error, leading to improved accuracy in estimating the target variable.

Lie-derivatives are connected to the observed and predicted outcomes depicted in Fig. 4.3 and Fig. 4.4, illustrating the training outcomes.

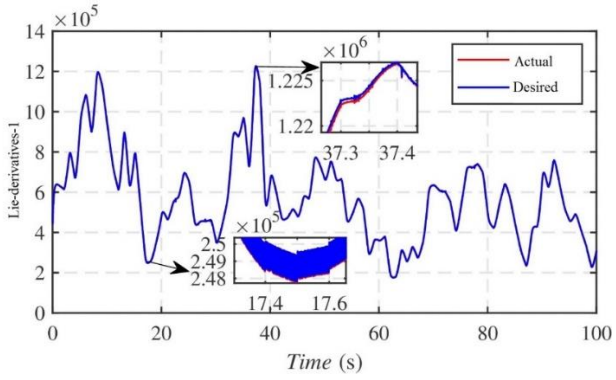

Figure 4.3 Actual and estimated $Lie - derivative - 1\ L_f^2 h(x)$

Table 4.2 Various parameters for the stated training of IBRTA

S. No	Parameters	Description
1	No. of inputs ANN	4
2	No. of outputs ANN	1
3	Training-algorithm	Back propagation
4	Number of hidden-layers	2
5	Number of hidden-neurons	2
6	Number of validation-check	0-6
7	Number of iterations	100

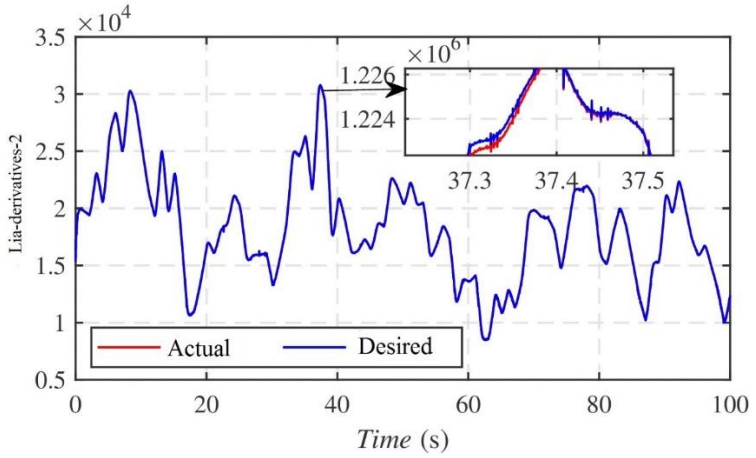

Figure 4.4 Actual and estimated $Lie - derivatives - 2\ l_g l_f h(x)$

4.7.2 Designing the MPPT control strategy based on IBRTA

The IBRTA-based MPPT approach is specifically developed to enhance the performance of WECS by improving their tracking capability of the maximum power point.

The following steps outline the design of the IBRTA algorithm [135]:

S. 1: Utilize the tracking error and its derivative under the following assumptions

$$er_1 = er \tag{75}$$

$$er_2 = er \tag{76}$$

S. 2: The proposed control law, IBRTA (Integral-Based RTA), incorporating the standard ISMC (Integral Sliding Mode Control) approach [135]:

$$u=u_{ideal}+u_{discountinous} \tag{77}$$

In this context, u_{ideal} represents the ideal or optimal control that can be achieved by employing a linear-feedback control law. On the other hand, $u_{discountinous}$refers to the discontinuous control that is obtained through the application of a back-stepping design approach. The following expression illustrates how u_{ideal} can be designed using the linear feedback control law:

$$u_{ideal} = -l_5(er_1) - l_6(er_2) \tag{78}$$

In this equation, l_5 and l_6 are the respective gains, and er_1 and er_2 denote the error terms.

S. 3: To design $u_{discountinous}$ using the backstepping approach, we need to select a Lyapunov function candidate $V_1(er_1)$ that satisfies three conditions: it must be positive definite. A suitable definition for $V_1(er_1)$ is as follows:

$$V_1(er_1) = \frac{1}{2}(er_1)^2 \tag{79}$$

By taking the time derivative of V_1, we obtain the following expressions:

$$\dot{V_1} = er_1\dot{er_1} = er_1(\dot{Z_1} - \dot{Z_{Reference}}) = er_1(Z_2 - \dot{Z_{Reference}}) \tag{80}$$

If we consider Z_2 in equation (80), so we have:

$$\dot{Z_2} = -l_7 er_1 + \dot{Z_{Reference}} \tag{81}$$

Yields:

The time derivative of V_1 , denoted as $\dot{V}_1$ can be expressed as $-l_g e{r_1}^2 < 0$, indicating global asymptotic stability.

S. 4: Provide the description of the ISMC sliding surface, including the integral term Z_i as referenced in [136][137].

$$s_1 = z_2 + l_g e r_1 - \dot{Z_{Reference}} + Z_i \tag{82}$$

Taking the derivative of equation (82) and simplifying it using the system's equation (77) leads to

$$\dot{s_1} = {L_f}^2 h(x) + L_g L_f h(x)(u_{ideal} + u_{discontinous}) + l_g \dot{e r_1} \tag{83}$$

Now, selecting

$$\dot{z_\iota} = -L_g L_f h(x) u_i + \ddot{z}_{reference} \tag{84}$$

By substituting equation (84) into equation (82) along with equation (83), we obtain:

$$\dot{s_1} = {L_f}^2 h(x) + L_g L_f h(x)(u_{discontinous}) + l_g \dot{e r_1} \tag{85}$$

S. 5: The following equation defines a potential composite Lyapunov function candidate, represented as:

$$V_2(e r_1, s_1) = \frac{1}{2}({e r_1}^2 + {s_1}^2) \tag{86}$$

Upon differentiating equation (86) and simplifying equation (80), the result is as follows:

$$\dot{V_2} = (e r_1 \dot{e r_1} + s_1 \dot{s_1}) = \dot{V_1} + s_1 \dot{s_1} \tag{87}$$

In this context, we consider a string reachability law in the form presented in [138].

$$\dot{s_1} = (-l_9 s_1 - l_{10} sign\,(s_1)) \tag{88}$$

Substituting Equation (88) for Equation (87) yields the following outcome:

$$\dot{V}_2=\dot{V}_1 + s_1(-l_9 s_1 - l_{10} sign\,(s_1)) \tag{89}$$

Upon comparing Equation (85) and Equation (88), the following relationship can be established:

$$u_{discontinous} = \frac{-1}{L_g L_f h(x)}[{L_f}^2 h(x) + l_g \dot{er}_1 + l_9 s_1 + l_{10} sign\,(s_1)] \tag{90}$$

To complete the process, we substitute u_{ideal} from Equation (25) and $u_{discontinuous}$ from Equation (90)) into Equation (77), resulting in the final formulation of the proposed IBRTA law presented below:

$$u_{IBRTA} = \frac{-1}{L_g L_f h(x)}[{L_f}^2 h(x) + l_g \dot{er}_1 + l_9 s_1 + l_{10} sign\,(s_1)] - l_{11} sign\,(er_1) - l_{12} sign\,(\dot{er}_1) \tag{91}$$

Table 4.3 The gain of IBRTA

Gain-1	l_8	0.1
Gain-2	l_9	100
Gain-3	l_{10}	0.001
Gain-4	l_{11}	2
Gain-5	l_{12}	700

The implementation of the algorithm is illustrated through the computational flow chart depicted in Fig. 4.5 while Table 4.3 and 4.4 provide gain and a list of the parameters associated with the IBRTA law.

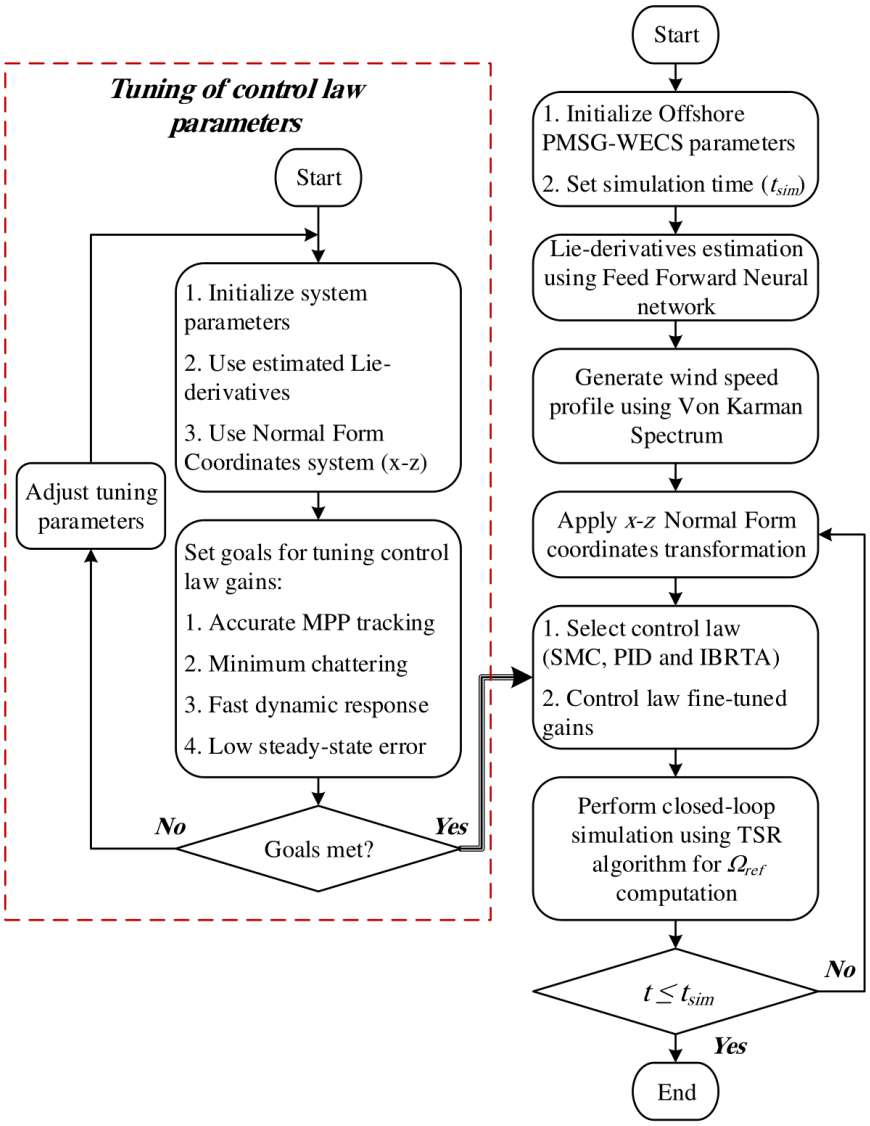

Figure 4.5 Flowchart depicting the computational steps of the entire system

These parameters are used to test wind turbine and PMSG under practical application of IBRTA. These parameters have been proposed and improved to provide optimal values in complex designs to capture and transform wind energy into power. Various criteria are employed in wind turbine design and operation to ensure optimal performance.

Table 4.4 List of the parameters associated with the IBRTA

Name	Quantity	Value
Wind Turbine	Density of air mass, ρ_{air} Radius of turbine blade, R_{blade} TSR, λ_{lopt} Transmission or gear ratio, $i_{transmission}$ Power coefficient, $C_{pr\ (max)}$ Wind speed average value, v_{wind}	1.25000 kg/m^3 2.5000 m 7.000 7.000 0.476000 7.000
PMSG	Stator-resistance, R_{stator} Inductance, $L_{chopper}$ Flux-constant, $\phi_{constant}$ Pole pairs number, p_{pole} Stator d=q-axis inductance, $L_d = L_q$ Shaft-inertia, J_{HS}	3.300 Ω 0.008 00 H 438.200 mWb 3.000 41.560 00 mH 0.055200 kgm^2

4.8 Results and comparisons

4.8.1 PID, FBL, SMC AND STA controllers

The wind turbine ECS alongside the planned proposed control techniques are simulated in MATLAB Simulink. In the simulations, the wind-speed (i.e., average speed) is assumed as 7m/s. In Fig. 3.1. The optimum TPR λ_{opt} = 7 and a maximum coefficient of power C_{prmax}= 47.6. To affirm the viability of the control schemes, the designed simulations are performed for a time frame of 100 sec. Initially, the simulations are carried out for conventional based PID and SMC, and then the superiority of proposed STA control-scheme is showed to empower the maximum extraction of the output power. The comparison is made among the designed schemes and standard FBL technique [117]. To ensure the maximum power-extraction, the ECS should be operated at optimal tip speed radio (i.e. λ_{opt}) in all the designed controller cases by controlling the shaft speed ω_h . By comparing the reference-tracking of PMSG shaft speed, the PID and FBL display oscillatory behavior (i.e. chattering) with significant steady-state errors. The SMC additionally goes through oscillatory tracking

around the reference, with a moderately lower amplitude (lower chattering) as compared to the other two techniques. The STA notices an absolute minimum steady state error as compared to the PID, SMC and FBL schemes as depicted in Fig. 4.6. In Fig. 4.6, the range of (32.81 to 32.84) shows the optimal area closest to the reference line. To obtain the maximum wind power, and operate the wind turbine ECS at the MPPT, the speed of shaft should be controlled in such a manner to ensure the TPR at its optimum value λ_{opt} =7, and power-oefficient C_{pr} closed to 47.6.

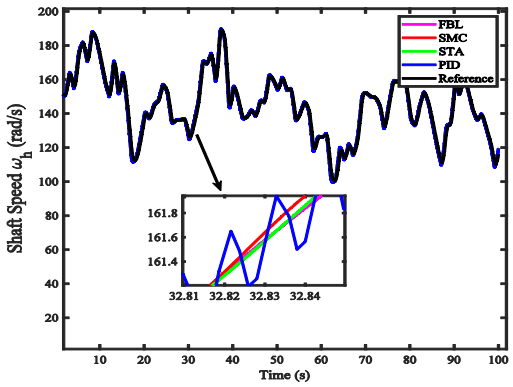

Figure 4.6 Reference speed tracking of shaft

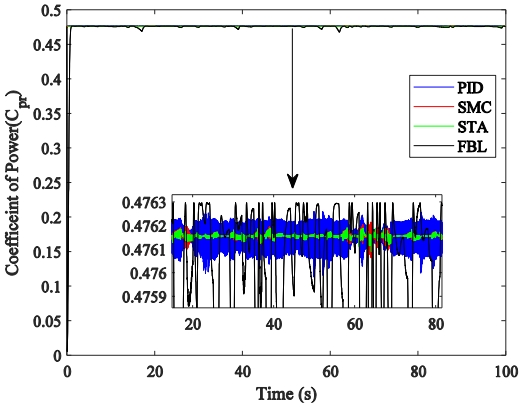

Figure 4.7 Coefficient of power

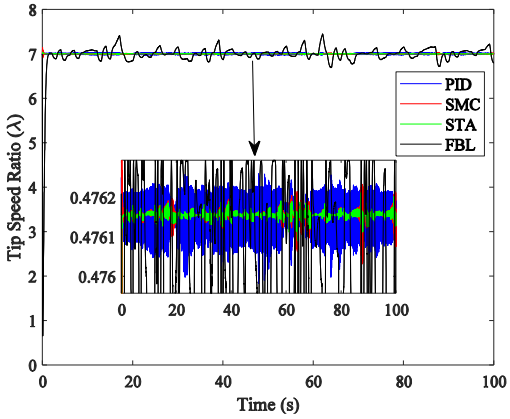

Figure 4.8 Tip speed ratios

Figure 1. One can see that in the case of STA, the TPR is very close to its optimum value and smoothly retains its behaviour for the whole simulation period while other techniques show statistic errors and disturbances which can lower the power extractionas depicted in the zoomed portion of Fig. 4.6 . Due to the stochastic nature of wind, there are abrupt variations in the convergence of power coefficients in the cases of PID, FBL and SMC while no such changes can be observed in the STA case which ensures the maximum extraction of wind power. This can be demonstarted by the tracking of Cpr in the zoom sections of Fig. 4.7. In Fig. 4.7, zoomed part from (20-80) shows the optimise operation and closest to the reference line. To tackle the maximum power from wind and decrease chattering, it is important that turbine should be run around ORC (i.e., Optimal Regime Characteristics) of the torque and power. ORC system for a wind turbine describes the operating circumstances in which the ORC system, when integrated with the wind turbine, achieves optimal efficiency and performance. Therefore, it can be seen in the zoomed parts of Fig. 4.8 and Fig. 4.9, the STA guarantees the smooth ORC tracking which in turn ensures the reduction of chattering and clearly visible in the range 0-100 of Fig. 4.8 and (6.95-7.05). In Fig. 4.9 the STA shows better results than PID, FBL and SMC. Fig. 4.10 shows lots of variations that depict the presence of chattering. In Fig. 4.10, there are black lines represent FBL due to chattering and the most smooth output is STA that is represented by straight green line and optimal range shows in between (21-21.4).

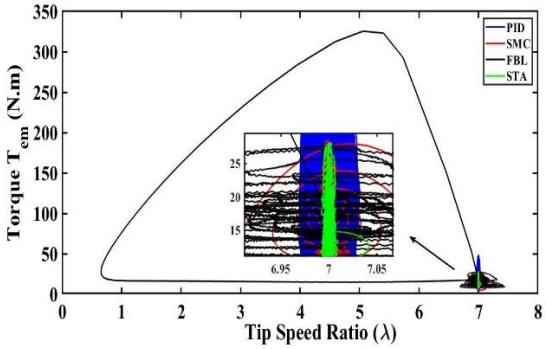

Figure 4.9 Tip speed ratios vs torque

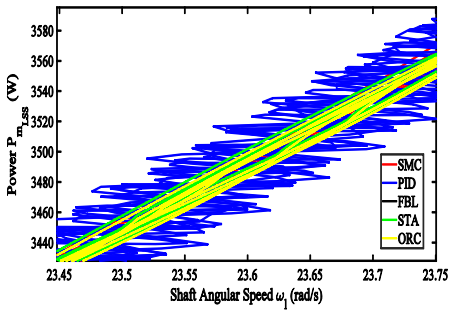

Figure 4.10 Shaft angular speed vs power

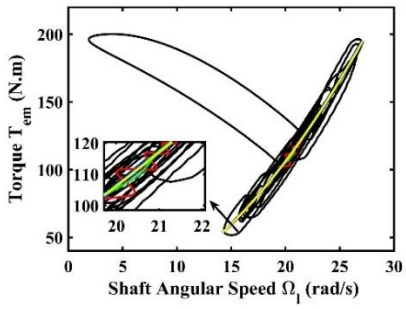

Figure 4.11 Shaft angular speed vs torque

Variations in TPR's Vs torque and the power are given in Fig. 4.9 and 4.12, the TPR keeps its optimum value in the STA case. The Fig. 4.11 shows the shaft speed vs torque in which STA ensures the MPP as shown in zoomed part in range between (20-22) and for Fig. 4.12 with optimal range (6.9-7.1), while the other schemes show variations in their tip speed ratios (one can say that MPP is not guaranteed). As can be seen from the errors in Fig. 4.13 in term of shaft speed versus reference speed for the four competitors, STA is more appealing than the other three methods.

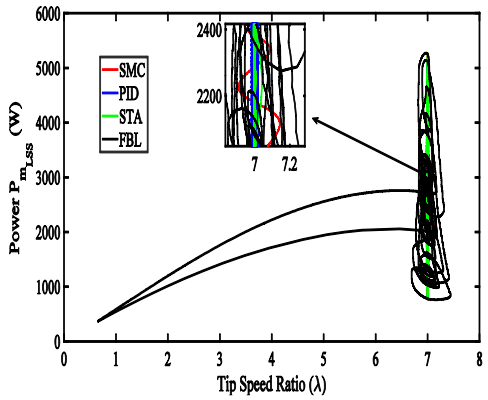

Figure 4.12 Tip speed ratio vs power

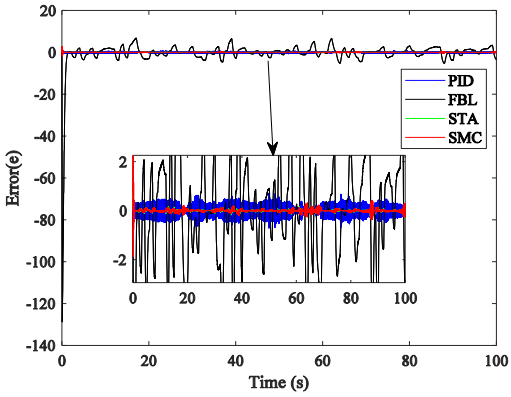

Figure 4.13 Errors in term of shaft vs ref speed

There are distinct advantages and disadvantages to PID, FBL, SMC, and STA controllers. PID controllers can be difficult to use with highly nonlinear or time-varying dynamics, but they are easy to build and effective for stabilising systems with low to moderate nonlinearities. By converting nonlinear systems into linear ones, FBL provides flexibility and robustness and makes it possible to use linear control schemes. However, in order to achieve optimal performance, substantial mathematical study and tuning are necessary. SMC has quick transient reaction and is resilient to uncertainties and disturbances, but it may have chattering and difficult controller design and tuning. Although STA provides reliable tracking and finite-time convergence, it comes with implementation complexity and parameter adjustment difficulties. The performance and dynamics of the system determine which controller is best.

4.8.2 STA and AI based back stepping controllers

AI-based back-stepping and STA are both innovative controllers. Both are ideal having their individual specification and advanced features. The more appropriate selection between these control techniques for offshore wind turbine depends on the specific requirements to

achieve the desired objectives. A comparative analysis of STA and IBRTA control techniques are presented in the Table 4.3. In summary, AI-based back-stepping is advantageous for complex and nonlinear wind turbine systems because of its adaptability, robustness, and performance optimization. STA offers strong disturbance rejection, quick reaction times, and chattering suppression. Depending on the particular needs of the wind turbine application, such as the necessary amount of flexibility, disturbance rejection capacity and response speed.

Table 4.3 An analysis of super twisting algorithm and integral based real twisting controller

Super twisting Algorithm	Integral based real twisting controller
Robustness to Disturbances: STA is a robust control method that excels at handling disturbances. Due to the existence of turbulent wind conditions, it offers high disturbance rejection properties, which are essential in wind turbine control.	Robustness: By integrating the AI technology into the system, back-stepping can increase output power from wind turbine. It offers better tracking and regulatory performance by properly capturing external disturbances and uncertainty.
Quick Response time: STA has quick convergence and response times, making it possible to track set points or references quickly. This is helpful for wind turbines since they frequently need to react quickly to shifting wind conditions.	Non-linear: IBRTA is especially effective for nonlinear systems, such as offshore wind turbines, which have intricate dynamics. It can manage the system's innate nonlinearities and uncertainties.
Minimizing chattering: STA has the ability to reduce or suppress chattering, which is the term for high-frequency oscillations in control signals. This may be crucial for reducing mechanical deterioration of the wind turbine parts.	Machine-learning: It is frequently used in AI-based backstepping controllers in order to adaptively learn the properties of the system and modify the controller parameters accordingly. Performance Optimization: IBRTA can progress the control method to accomplish specific performance goals, such increasing power generation or reducing fatigue loads.

4.9 Case studies on AI based back stepping controller

The current objective is to optimize power extraction from wind by implementing an appropriate control algorithm capable of operating the plant at its MPP. To accomplish this goal, two control strategies have been designed: SMC, IBRTA. Figure 4.1 provides a comprehensive overview of the entire WECS and the associated control schemes proposed in this research, enabling an evaluation of its findings. Conversely, Figure 4.2 depicts the offshore PMSG based WECS specifically considered in this study. It highlights important parameters such as a maximum power coefficient of $C_{pr(\max)}$=0.47600 and an optimal TSR of I_{opt}=7. The simulations were conducted using an average wind speed of 7 m/s, as indicated in Fig. 4.1. The simulation results were divided into two distinct cases: 1. Variation in wind speed profile for a nominal scenario, and 2. Deterministic offshore wind speed profile, including a comparison between the IBRTA, FLB, and SMC controllers.

In the first case, the research evaluates the performance of the proposed MPP tracking algorithm in the presence of a stochastic wind speed profile. This implies that the wind speed undergoes random variations over time, requiring the algorithms to adapt and optimize the wind turbine's power output accordingly. The simulations are conducted for a duration of 100 seconds.

In the second case, the study assesses the robustness of the proposed control techniques when confronted with abrupt variations in the offshore wind speed profile. These variations involve sudden and rapid changes in wind speed, posing a challenge to the control system. The objective of this analysis is to determine how effectively the proposed control techniques can respond to these sudden changes and maximize the wind turbine's power output.

Both in case 1 and case 2, a comparison is made between the proposed controllers, namely SMC, IBRTA, and FBL, to determine their relative performance.

4.9.1 Case 1: Wind speed profile with variations

To maximize power extraction through the evaluation of three distinct control algorithms: SMC, IBRTA, and FBL. The objective is to operate the wind turbine at its optimal TSR, represented by I_{opt}, which ensures the highest power coefficient value, $C_{pr(\max)}$. The comparison depicted in Fig. 4.14 reveals distinct characteristics in terms of reference tracking among the different control algorithms. Specifically, the control performed by FBL exhibits oscillatory behavior accompanied by a notable steady-state error. The SMC algorithm demonstrates oscillatory tracking around the reference; however, it introduces chattering, which is not observed in the case of FBL. IBRTA exhibits an exceptionally small steady-state error, surpassing both SMC and FBL in performance. Additionally, the convergence-time is significantly faster for IBRTA, as evidenced in the zoomed section of Figure 4.14. Here, the STA achieves convergence at 0 seconds, IBRTA at 0.01 seconds, and SMC at 0.1 seconds. Moreover, the results displayed in Fig. 4.15 and Fig. 4.16 highlight that the IBRTA control algorithm yields more favorable outcomes in terms of the power coefficient C_{pr} and TSR compared to SMC and FBL. This indicates that MPPT is more effectively achieved using IBRTA. Additionally, when examining the mechanical power of the shaft within the optimal range, as illustrated in Fig. 4.17, both IBRTA and SMC outperform FBL, thereby corroborating the elimination of chattering. These observations can be clearly observed in the zoomed sections of the reference tracking, TSR, power coefficient C_{pr} and mechanical powers in the respective figures. In summary, the results demonstrate that IBRTA serves as the superior controller, by minimizing chattering at optimal point.

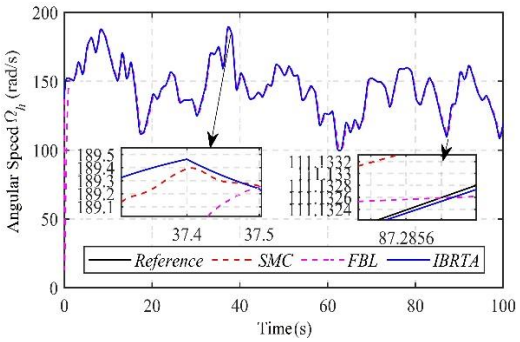

Figure 4.14 Desired and actual angular speed

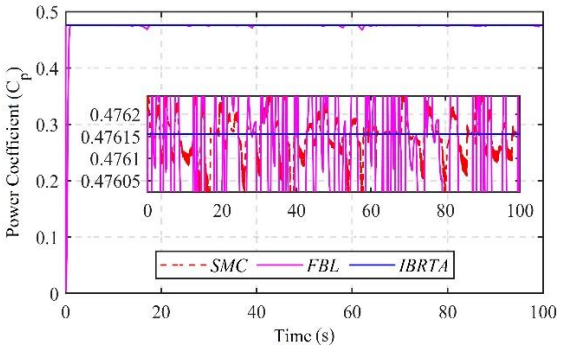

Figure 4.15 Coefficient of turbine power vs. time

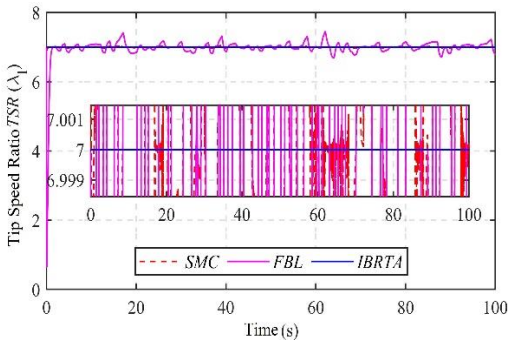

Figure 4.16 Tip speed ratio vs. time plot

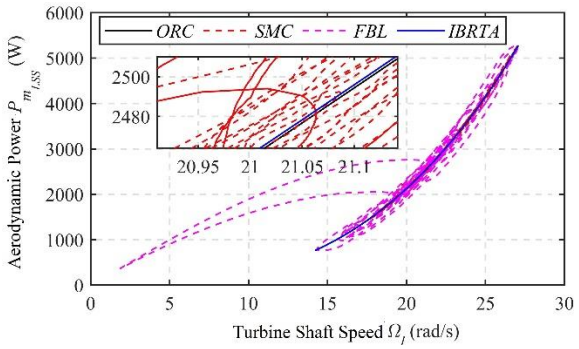

Figure 4.17 Turbine shaft speed vs. aerodynamic power

The graphical representation of the analysis results can be observed in Fig. 4.18, depicting the relationship between electromagnetic torque Γ_{em} and TSR λ_l. The findings clearly indicate that IBRTA exhibits superior performance compared to both SMC and FBL controllers and clearly shown in the optimal zoomed part in (6.9-7). As a result, it is recommended for power engineers to prioritize the utilization of the model-based IBRTA controller over SMC and FBL alternatives, as it offers enhanced overall performance in the context of the studied wind energy conversion system.

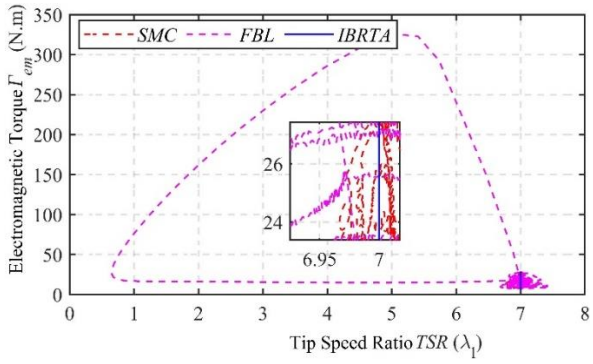

Figure 4.18 TSR versus electromagnetic torque

4.9.2 Case 2: Deterministic offshore wind speed profile

A deterministic wind speed profile is a predictable wind speed time series profile that follows a precise valued of IBRTA model. Offshore wind harvest wind energy efficiently require knowledge of wind speed fluctuations. So, the deterministic profiles aid in the design of turbines and systems for specific wind conditions by using IBRTA. The primary focus of Fig. 4.19 is to assess the system's capability to withstand sudden shifts in wind speed. In this deterministic scenario, the wind speed experiences abrupt and drastic changes, necessitating the system to operate at its maximum power coefficient $C_{pr(\max)}$ during these fluctuations. The graph presented in Fig. 4.19 demonstrates that the SMC and FBL controllers exhibit spikes or irregularities in response to these rapid variations.

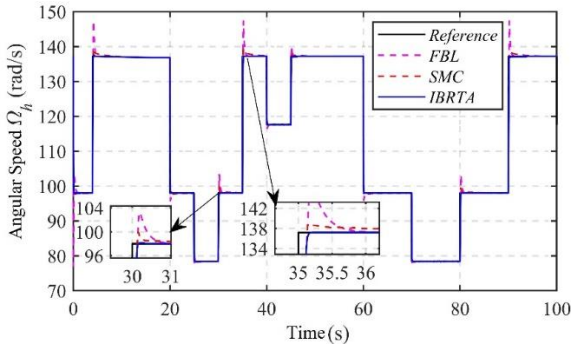

Figure 4.19 Deterministic speed profile desired and actual

While there may be some temporary disturbances observed in the power coefficient, TPR and HSS angular speed. Fig. 4.20 and 4.21 further demonstrate the stability and effectiveness of the control scheme under these challenging conditions, reaffirming its performance. Fig. 4.22 and 4.23 indicate the output power of generator and output power of turbine.

Initially, the model comprises three states, which are later transformed into a simplified and output-oriented two-state normal form. To enhance the controller's robustness, the simplified model is further improved with SMC, enabling efficient wind speed tracking in various scenarios, including the nominal case and a deterministic offshore wind speed profile case.

In practical scenarios, accessing nonlinear terms and aerodynamic forces may pose challenges. To tackle this, the study introduces an offline feed forward neural network scheme specifically designed to estimate the nonlinear drift components, such as $L_f{}^2 h(x)$ and $l_g, l_f, h(x)$. Through extensive simulations in MATLAB/Simulink, it is observed that the proposed MPPT strategy, namely Improved IBRTA, outperforms other benchmark techniques, including SMC and FBL. The IBRTA strategy demonstrates remarkable attributes such as accurate MPPT, low steady-state error, fast dynamic response, and minimal chattering.

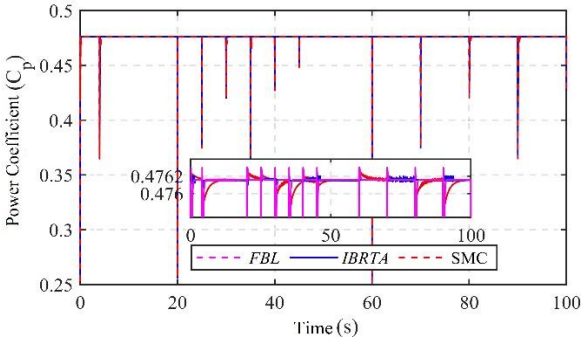

Figure 4.20 Power coefficient vs. time

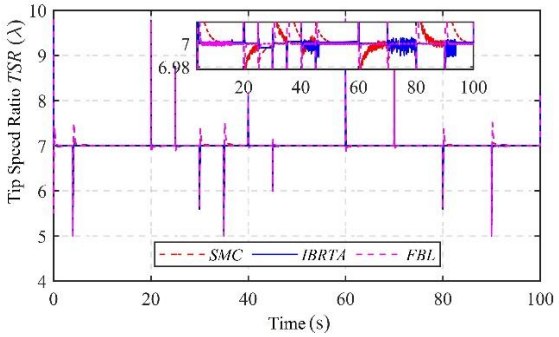

Figure 4.21 TSR vs. time for deterministic profile

The simulation results validate the effectiveness of the proposed strategy under both stochastic and deterministic wind speed profiles. The stability analysis of the closed-loop system, employing Lyapunov stability theory, further confirms the reliability of the IBRTA-based approach. Overall, the study concludes that the IBRTA strategy presents the best MPPT performance among the examined candidates and holds significant promise for enhancing the performance of offshore PMSG-WECS systems.

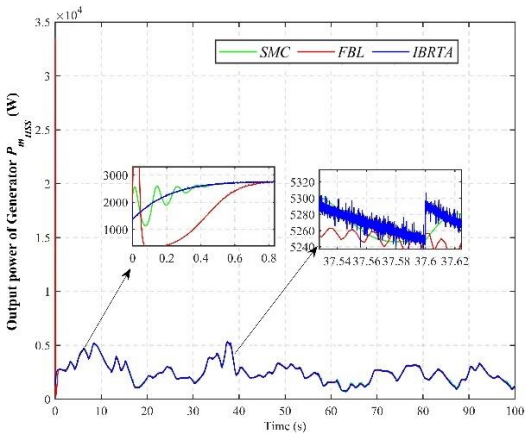

Figure 4.22 Output power of generator

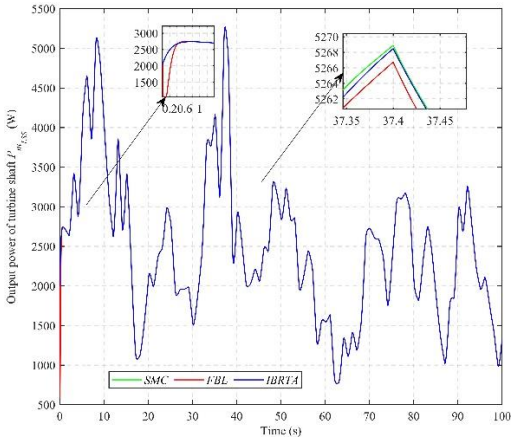

Figure 4.23 Output power of turbine

4.10 Summary

In this chapter, PMSG OWT is modelled and tested using SMC, STA and IBRTA controllers. The modelled OWT with three state variables is transformed into two states as a normal form model to simplify the system. PID and SMC are equipped with normal state form for the tracking of wind speed in a nominal wind speed profile for evaluation of the controllers. During the simulations, it is demonstarted that PID and SMC are showing oscillatory behaviors (chattering) with some steady state errors that can be improved by the discontinuous control component of STA. However, the switching frequency is constrained by the sampling frequency, leading to system chattering. The proposed STA scheme assures MPPT while mitigating chattering issues and ensuring rapid convergence. Finally, this chapter navigates through a wide range of control approaches, from traditional PID to cutting-edge IBRTA controller. Furthermore, improved performance and efficiency of offshore wind controllers is observed under different case studies.

Chapter 5 Design and Control Techniques for Wave Energy

In this chapter, different design techniques for wave energy are presented and compared. The selection of the generator for wave energy perceptibly depends on several factors, including climate, sea tides, sizing, structure, location, and working principles. The interaction of a single buoy with a linear generator is commonly used with the semisubmersible platform to integrate with the offshore wind. There are the following arising contributions from the chapter. Section 5.2 is on a SPA with subsections of dynamic and reactive control. Section 5.3 is a new innovative approach to wave energy using MPA with a subsection array of generators, three-point generation, wave catcher and trijunction design. Section 5.4 presents the solution set of wave energy using real time data. Section 5.5 covers the power take off technique from wave energy. In Section 5.6, SPA and MPA case studies are presented using real time data.

5.1 Introduction

The array of single buoys using linear generators interacting or jointly linked with the platform is the most suitable option. In this way, the same buoy interacts with the energy from every point and is also structural-wise better than a normal SPA. This chapter unfolds through a series of distinct sections, encompassing a variety of absorber methodologies. This chapter, commences with a detailed investigation of single-point absorbers, exploring both their dynamic and reactive control mechanisms. Further, the transition to an extensive examination of multipoint absorbers, subdivided into further subsections focused on three-point generation, wave catchers, tri-junction designs, linear generators, and multipoint harvesting. The final segments of the chapter delve into solution sets and power takeoff. The proposed techniques for both single-point and multipoint absorbers are validated using real-time data within MATLAB. Finally, a comparison of the derived output of MPA from nine generators is evaluated.

5.2 Single point absorber (SPA)

The simple point absorber for wave energy includes one generator and a buoy. The wave energy converter incorporates with floater, linked to the sea bed by a type of device – called PTO. The part of the PTO system in the whole HOWWE system is to offer two functionalities. In the wave energy, the PTO system provides the control to the device and therefore is used to improve the performance to produce energy gathered from the incident waves to the wave energy. Secondly, the PTO system converts the mechanical energy from the buoy-floater to electrical energy as shown in Fig. 5.1. The linear generator model is linked with the offshore wind offshore base. The sea waves interact with the buoy with sinusoidal motions as shown in Fig. 5.1. Due to the linear-motion of the buoy model, the force is acting

on the translator part of the linear generator. Thus, mechanical energy produces electrical energy. The primary operating mechanism includes the interaction of a magnet and a wire coil to generate an electric current. The lower end stop spring offers resistance and support at the generator's bottom end. It prevents the translator (the moving part of the generator) from travelling too far below and absorbs energy when the translator reaches its lower limit. The retracting spring is in charge of returning the translator to its original position after it has been moved. When squeezed, this spring stores potential energy and releases it to drive the translator upward when the external force is removed. The stator is a stationary component that is located around the translator. It is typically made out of wire coils twisted around a core. When the translator moves, the changing magnetic field between the stator and the translator causes an electric current to flow through the stator coils. The translator is the moving part comprises with magnetic element.

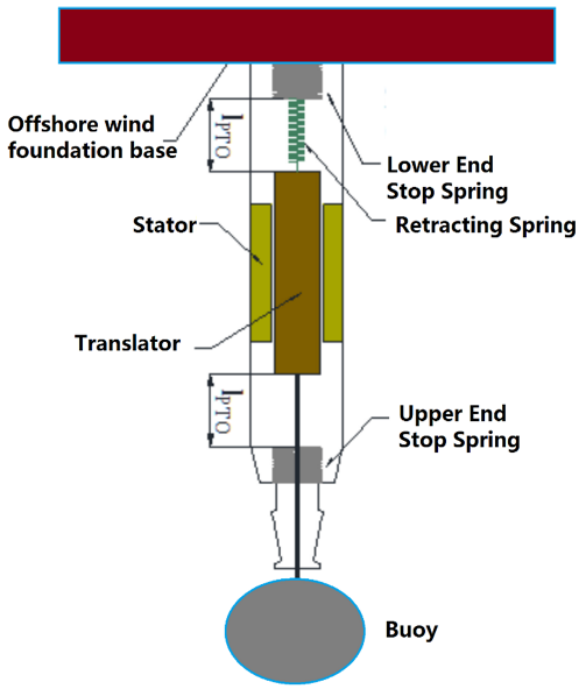

Figure 5.1 Single point absorber for wave energy

As it moves along a linear route, it creates a change in the magnetic field within the stator, creating an electromotive force (EMF) in the stator coils. The upper end stop spring, like the lower end stop spring, offers resistance and support at the linear generator's upper end. It prevents the translator from moving too far upward and absorbs energy when the translator reaches its limit as shown in Fig. 5.1.

5.2.1 Dynamic control

To enhance the power generation from the sea waves, the control of the HOWWE is key. The simplest technique used is a second-order model, it is enough to describe the control of control strategies on the PTO system. In Fig. 5.2, the second order electrical-analogue model for a point absorber is described.

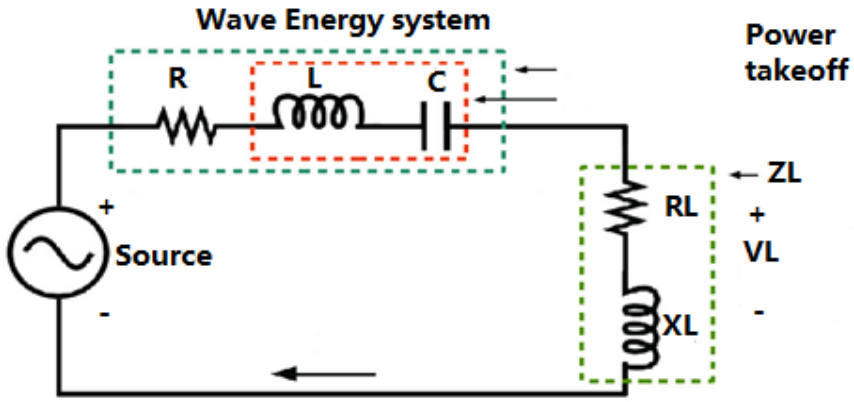

Figure 5.2 Electric analogue of a point absorber WEC

The mechanical analogue is based on spring, mass, force, mass and damper. The output power is maximized with the PTO by matching with the wave excitation force frequency and Eigen frequency of the system. The natural damping of wave energy is equal to PTO damping (R = RL in Fig. 5.2). This method to control a wave energy converter is characterized as reactive control or conjugate complex control.

5.2.2 Reactive Control

A reactive control, in order to maximize the single output provides: The PTO overturned power flow in the wave cycles. Secondly, large displacements between the buoy and the PTO system. Finally, in the PTO system the enormously high peak forces. The second control technique, called linear damping is often projected. The technique is to remove XL in Fig. 5.2, prominent to a passive behavior of the PTO system. Optimistic features of this approach are: No overturned power flow is necessary, reduced displacements of the buoy, minimized peak forces, minimum peak to mean ratio.

5.3 Multi point absorber (MPA)

The multipoint absorber represents a cutting-edge technique, integrated with offshore wind turbines. The distinctiveness of this method stems from its incorporation of multiple linear generators, which can either be independently connected in an array to the base of an offshore wind turbine or leveraged using a wave catcher method.

5.3.1 Array of linear generators

An array of linear generators is affixed to the semisubmersible platform of the offshore wind turbine, as illustrated in Fig. 5.3. The resulting output power from the system is contingent upon the number of linear generators deployed. Conveniently, all power output is gathered via the same cables within the existing structure.

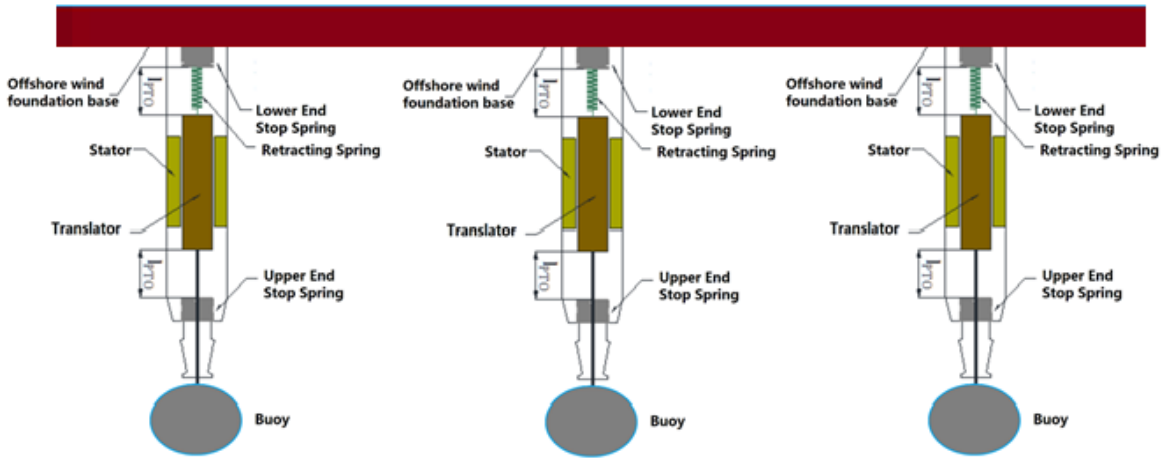

Figure 5.3 Array of linear generator attached to offshore wind base

5.3.2 Three points generation

In this section, three-point energy generation for HOWWE is explained vs. most present designs such as single-point energy generation. With 3-points energy generation this device is capable of generating energy from every movement of a buoyant structure and thus can harvest 3-4 folds more energy from comparable single-point energy harvesting systems using a same structure with HOWWE as shown in Fig. 5.4.

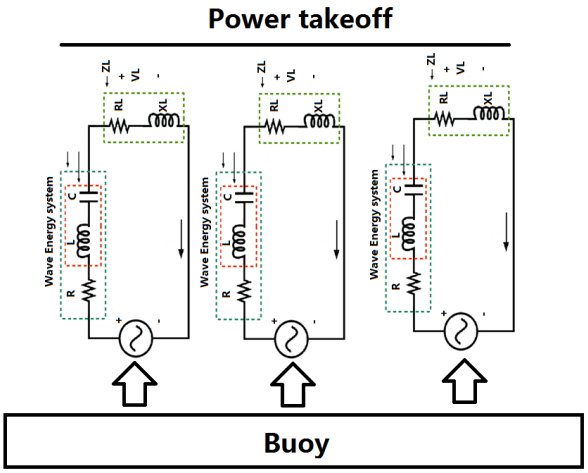

Figure 5.4 Three-point energy generation device

Fig. 5.4, shows the combination of the power takeoff from three generators using the same structure. Three points will move independently from each other without putting any stress on the frame on HOWWE.

5.3.3 Wave-catchers

Wave catchers help to intercept a larger section of moving water under a floating wind turbine thus harvesting more energy vs. most present designs utilize a harvesting method which has a limited potential of harvesting energy from HOWWE. The wave catcher size depends on the floating structure base such as the tripod or monopole structure. Also, hybrid wave catchers can work efficiently in changing wave patterns. The system being afloat below the water surface is being protected from the storms; also eliminates any requirement for a mechanism to cope with the constantly changing water level surface.

5.3.4 Tri-junction design

The tri-junction design eliminates any movement of the lower end of each wave energy harvesting (WEH) device thus any movement of the buoyant tri-angle structure will result in an energy harvesting vs. most present system's buoy with a linear generator that does not harvest energy if the entire unit slides side to side which results in lower efficiency of energy generation.

5.3.5 Linear generator

The linear generator is an innovative gearing set-up that converts linear reciprocating movements of the linear shaft into a one-directional rotational motion for minimum energy loss compared to a system that changes the direction of rotation with each reciprocating movement. The linear permanent magnet generator (LPMG) is used in our case and it is more popular choice for wave energy applications than linear induction generators and linear

synchronous generators. The selection of LPMG is determined by considerations of different factors such as efficiency, maintenance requirements, and wave environment characteristics. The LPMG structure is discussed in the Section 5.1. The LPMG is an efficient and revolutionary system for converting ocean wave energy into electrical power. The LPMG is a sophisticated working principle that consists of a translator as the moving component, a fixed stator, and a magnet system. The translator, which is frequently attached to a buoyant structure that responds to wave motion, moves linearly down a track or within a housing. This coordinated motion causes a dynamic interaction between the magnets positioned on the translator and the wire coils within the stator. The resulting shifting magnetic field creates an electromotive force (EMF) in the stator coils, resulting in the creation of continuous electric current. Importantly, the translator's linear motion is tightly linked to the undulating motion of ocean waves. When the buoyant structure is placed in motion by waves, the translator exactly duplicates this movement, and the LPMG expertly converts it into a sustainable source of electrical power. This marriage of cutting-edge technology and the rhythmic force of nature shows the LPMG's promise in creating sustainable energy solutions.

The linear generator, a critical component in the field of renewable energy, is defined by a set of important factors that optimize its efficiency and operational characteristics. Among these parameters, the number of coil turns (N) has a significant impact on electromagnetic induction and voltage output, whilst the physical length of the coil (L) within the generator is critical in determining the spatial distribution of the magnetic field. Magnetic field strength (B) and magnetic flux (u), the products of which influence induced voltage, are critical factors to consider. The velocity (V) of the linear generator in the magnetic field and the cross-sectional area (A) further govern the rate of change of magnetic flux and the effective area

through which flux flows. The electrical characteristics and efficiency are influenced by the material properties and resistance of the conductor, load resistance external to the generator, and inductance. Furthermore, the back-electromotive force constant, force exerted on the generator, and overall efficiency provides insight into the link between induced EMF and velocity, external mechanical forces, and kinetic energy conversion into electrical energy, respectively. These characteristics serve as the foundation for building and optimizing linear generators for use in HOWWE systems. To maximize efficiency, key practical components of a linear generator in wave energy conversion include optimizing design parameters such as coil length, number of turns, and magnetic field strength. Furthermore, concerns for the generator's resilience in hostile marine settings, maintenance requirements, and overall cost-effectiveness of the system are critical.

The linear generator is deployed in real-world situations, such as offshore wave energy test locations, for practical testing and validation. Data on the linear generator's electrical output, efficiency, and overall performance are collected and analyzed in order to optimize the design and improve its reliability. Furthermore, advanced control systems and monitoring tools are essential for optimizing generator performance and adjusting it to changing wave circumstances.

To ensure effective and reliable power generation, the technical characteristics of a linear generator incorporated into a wave energy conversion system require careful consideration of numerous aspects. The coil arrangement, which includes the number of turns and the length of the coil, is critical for optimizing electromagnetic induction efficiency and voltage output. The magnetic system, which is controlled by the magnetic field strength and total magnetic flux, is critical in defining the generator's overall power output capability. The wave energy

converter's motion mechanism, which converts ocean wave motion into linear movement, necessitates rigorous engineering for flawless integration. The induced voltage and power generating capacity are affected by the velocity and frequency of this linear motion. The selection of conductor materials, as well as their resistance, is critical to improving overall system efficiency. To optimize power output under varied wave conditions, load resistance and control systems are linked. Efficiency is a vital measure that represents the ratio of useable electrical power to mechanical power input. Longevity in offshore conditions is ensured by environmental concerns such as corrosion resistance and maintenance requirements. Real-world testing at real-world wave energy installations, together with monitoring systems, gives critical data for continual optimization. The integration of the linear generator with power conditioning and grid connection technologies completes the comprehensive technical framework, matching it with practical and sustainable wave energy conversion applications.

5.4 Solution set of wave energy

5.4.1 Single point absorber

A single-point wave energy generation configuration usually has a buoyant structure set up to float freely with moving ocean water. The buoyant structure is tethered in the center to an anchor at the ocean bed with a cable and a WEH mechanism in between. The buoyant structure floats below the water's surface and moves around with moving water. This design can harvest energy only when the center of the buoyant structure (where the WEH is attached to) moves further away from the anchor it's been tethered to. Most wave energy harvesting technologies use a hydraulic cylinder to harvest energy. The hydraulic cylinder gets actuated from the movements away from the anchor and results in a pressurized hydraulic fluid. The

pressurized fluid is then transferred to a shore station with underwater hoses where the pressurized hydraulic fluid spins a turbine generator where the hydraulic fluid pressure is converted into electricity. A buoyant structure has a single-point wave energy harvesting mechanism (hydraulic cylinder) which gets pulled or pushed as the buoyant structure moves upward-downward. This set-up is able to generate electricity only when the water level of the entire surrounding buoy area to the buoy rises upward. This system is unable to generate electricity if the water level rises on one side and drops on another side as shown using green arrows and red arrows. The water in the surrounding area shown in the green must rise at the same time in order to lift the buoyant structure upward. This configuration is also unable to harvest any energy from side-to-side moving water waves shown in yellow and blue arrows. Also, the structure itself is very heavy to be lifted very easily with water thus buoyant movements are not as efficient as they would be with a lighter inertia design with minimum components moving during energy harvesting.

5.4.2 MPA

This multi-point wave energy harvesting mechanism will have a triangle frame with three of one float attached near each of the three corners. Each corner of the triangle frame will be tethered to the top end of the WEH device (one WEH device for each corner) and the bottom end of the WEH will be attached to three distinctly separated anchors at the tripod offshore wind which will create a tri-junction at the bottom of each of three linear generators connected to the triangle frame. The tri-junction will eliminate any side-to-side and/or upward movements of the bottom end of each of the three linear generators; thus any movements of the triangle frame will result in the actuation of one or more linear generators. A triangle frame is chosen because three distinct buoys can float and move independently

from each other without stressing the frame. With a three-point design and tri-junction anchoring set-up, that minimizes movements of the bottom end of each of three linear generators; any side-to-side or upward or rocky-boat-like movements of the triangle frame will result in the actuation of one or more linear generators.

As shown in Fig. 5.5, above, a triangle platform with one buoy in each corner is tethered to 3 anchors that are secured at the ocean bed with the help of cables and one linear generator in between. As shown in the Fig. 5.5; each linear generator's bottom end is connected to a tri-junction to eliminate side-to-side movements. The round disc which is marked as wave-catcher intercepts a larger cross-section of moving ocean water and moves around thus harvesting energy from even slow-moving waves. The electricity generated from this system will be transferred to a cost by running underwater electricity cables in a large scale commercial application.

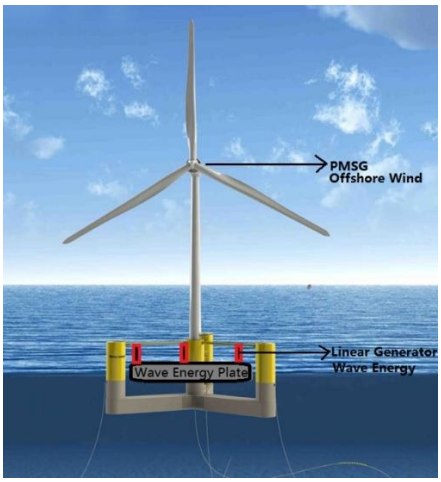

Figure 5.5 Multi-point wave energy harvesting technology's configuration

If the entire platform rises upward with the help of moving ocean waters being intercepted by the wave catcher at an angle; all three linear generators will be actuated with offshore wind. The above movement of the triangle structure is very unlikely to occur because most

of the waves are moving at and around the horizontal plane. Most present wave energy harvesting technologies are unable to harvest moving waters at an angle because they are designed to have only vertical movements but this multi-point set-up will be able to harvest energy from a tri-angle structure's movement in any direction as shown in Fig. 5.6.

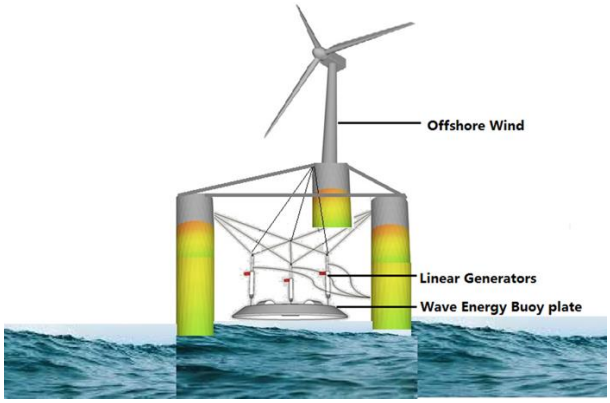

Figure 5.6 Anticipated movements with moving ocean waters

These movements result in the actuation of all three wave harvesting units as shown in above Fig. 5.6. The angle of the wave catcher's plane will determine the angle at where the entire set-up will be pushed at.

The platform will be moving in a boat-like rocky manner most of the time as ocean waves pass by from one side of this system to another. During rocky movements, one or more units will be actuated together or another as shown in the above figure. With the use of 3-points; the overall stress can be distributed around the structure thus a lighter structure can be used which will result in more efficiency due to lesser inertia mass moving around and also will reduce the cost of the overall system drastically.

In reality, the movements will be any combination of Fig. 5.5 and 5.6. The solution set of wave energy is analyzed using real-time data and the explanation is mentioned under different

conditions from time 0.05 to 0.5 considering wave amplitude and displacement. Table 5.1 explains the wave amplitude and displacement in three directions x axis, y axis and z axis with force acting on buoy.

Table 5.1 Real Time wave energy displacement analytics

T(s)	WAVE(m)	X1(m)	X3(m)	X5(rad)
0.05	-0.15492	0.000301	9.20E-05	3.68E-05
0.1	-0.12245	0.001209	0.000382	0.000147
0.15	-0.09041	0.002729	0.000896	0.000333
0.2	-0.05783	0.004865	0.001657	0.000592
0.25	-0.02523	0.00762	0.002688	0.000926
0.3	0.005256	0.010993	0.00401	0.001334
0.35	0.031947	0.014982	0.005638	0.001814
0.4	0.05502	0.019584	0.007591	0.002365
0.45	0.07659	0.024793	0.00988	0.002986
0.5	0.099377	0.0306	0.012518	0.003673

5.5 Power take off (PTO)

5.5.1 Wave harvesting unit

Any movement of the floating structure will be harvested into electrical energy by wave energy harvesters. WHU is consists of the following components: A geared shaft that moves in a reciprocating manner and linear generator. Each wave-harvesting unit is basically a linear generator.

The body holds the generator with the gearbox in place and allows the geared linear shaft to move in a reciprocating manner. With the help of a few gears and one-way clutch packs; this linear motion can be converted into one-directional-rotational motion. By keeping the generator with the gear box's rotational direction in one direction; a significantly lighter-duty gearbox also can be used.

5.5.2 Parts of PTO

A PTO is composed of three parts: The oscillator, three wave energy converting devices and wires. The PTO uses the motion of the buoy to drive its oscillator. The oscillator in turn is connected to two energy converter devices using a cog wheel-based gear. One energy converter harnesses the up movement of the oscillator, whereas the other is used during the oscillators down motion. Hence when one converter is in use, the others also generate energy.

5.5.3 Mechanism of PTO

The energy converter can be split into two main components – a buoy/flywheel and a generator. The role of the flywheel is to store energy. A generator is required to extract all the stored energy from the flywheel – most can be obtained during the free state of an energy converter.

The upper and lower reservoirs of a PTO are filled with gas to protect it from large forces. The so-called gas-spring acts a pre-tension force to put the initial position of the oscillator at the midpoint. PTO can be modelled as a sum of the following forces acting on the oscillator:

$$F_{PTO} = k.F_g + F_{buoy} + 3F_{LG} \tag{92}$$

where $F_g =$ force of gravity, $F_{buoy} =$ force on the buoy, $F_{lg} =$ force on the linear generator and K=1 when energy from the device is engaged and 0 otherwise.

The structural diagram of the multipoint generator using nine linear generators for wave energy and one PMSG for offshore wind is presented in Fig. 5.7.

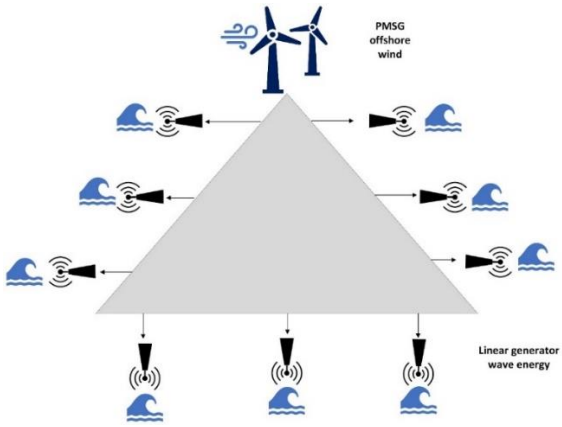

Figure 5.7 Structural diagram of the multipoint generator

5.6 Results and discussions

Wave energy is a one of the ideal source of renewable energy. The conversion of energy from ocean waves into electricity is tested and implemented. There is significant unpredictability, wave patterns can be anticipated to some extent using characteristics such as wind speed, direction, and shoreline geography. This predictability helps with wave energy system planning and optimization.

The maximum displacement or distance that a wave rises above or falls below its equilibrium (resting) position is defined as its amplitude. In other terms, it assesses the power or intensity of a wave. Amplitude is frequently depicted on a graph by the height of the wave. It is the distance from the crest (peak) or trough (lowest point) to the equilibrium position of a transverse wave.

The energy carried by a wave is proportional to its amplitude. Higher amplitudes indicate greater energy transfer. Amplitude is connected with the perceived loudness of a sound or the brightness of light in the case of sound waves and light waves, respectively. A bigger amplitude sound wave, for example, produces a louder sound. For mechanical waves, such

as water waves, amplitude is measured in metres, while for electrical waves, it is measured in volts. The frequency of a wave is the number of complete cycles that occur in a unit of time. It is measured in hertz (Hz), with one hertz equaling one cycle per second.

A cycle is a complete oscillation of a wave from its starting point to its maximum displacement in one direction, back to its starting point, and through its maximum displacement in the other direction. The period is the amount of time required to complete one cycle. The reciprocal of period is frequency. The number of cycles per second is a common way to represent frequency. A frequency of 10 Hz, for example, means that 10 full cycles occur in one second.

A wave's energy is precisely proportional to its frequency. In general, higher-frequency waves carry greater energy. In conclusion, wave amplitude and frequency are important variables that help characterize and differentiate distinct types of waves, providing information about their energy content, intensity, and perceptual aspects. Different case studies analysis is presented below:

5.6.1 Bench mark SPA technique to implement linear generator

In Fig. 5.8, "power-complex" plots show the complex model's power as a function of time, whereas the "power-complex-Zoom" plots focus on a specific time span. These charts provide a visual depiction of the complex model's dynamic behavior and provide specific insights based on the underlying parameters and attributes. Similarly, Fig. 5.9 shows the output power in zoom view.

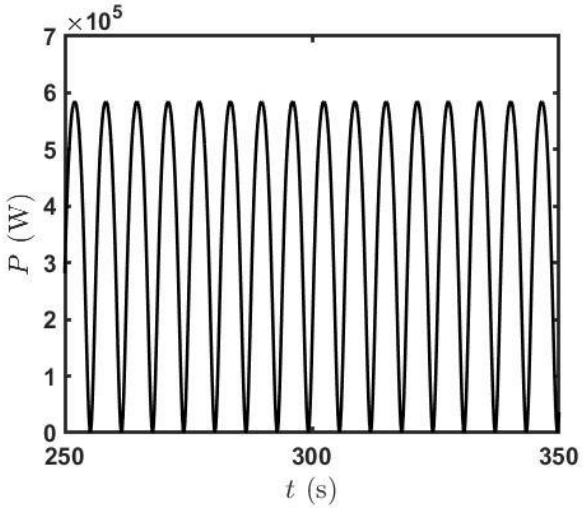

Fig. 5.8 Power of SPA linear generator

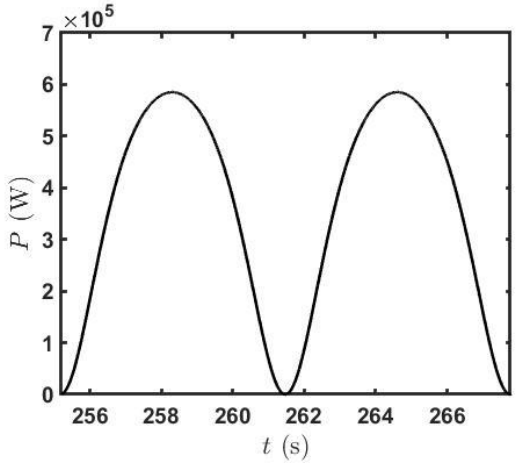

Fig. 5.9 SPA zoomed output power

5.6.2 Implementation of MPA for practical applications

In Fig. 5.10, each subplot shows the power generated by a specific linear generator in the system. The x-axis represents time, and the y-axis represents the power created by each linear generator. Each subplot's title reveals which generator it relates to (Generator 1 through Generator 9). The power of each generator is computed as the product of its current and voltage. These diagrams show the dynamic response of each linear generator to the input wave and how it contributes to overall power generation. When opposed to a single point

source, distributing energy extraction across numerous sites on the semi-submersible platform may have a lower impact on the marine environment. This can be useful in reducing ecological problems.

Power variations between all generators due to reaction of input sea waves and other system characteristics. Several things can influence mechanical qualities behavior such as damping, inertia, and torque constants, may differ. These variances can cause variations in the response to the input force acting on buoy. By evaluating these subplots, it becomes evident that a multipoint absorber interacting with multiple generators generates more output power than a SPA, hence enhancing system efficiency.

This efficiency can further be boosted by using an array of linear generators interfacing with the base of offshore wind or by employing a three-point generation concept. The combined output power curves of all linear generator shown in Fig. 5.11. It is clearly seen that all different linear generator have different response due to the interaction of sea waves. Assuming generator 1 is interacting the sea waves firstly as compared to other generators. As clearly observed in Fig. 5.11, high amplitude sea waves have more force on buoy and the resultant will be more output power from linear generator.

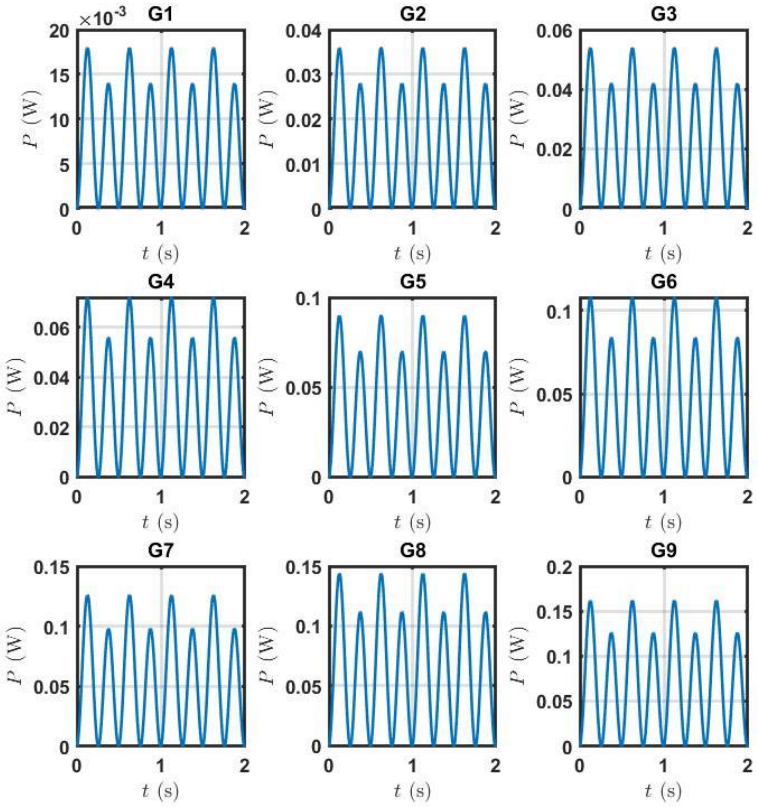

Fig. 5.10 Output power behavior of MPA

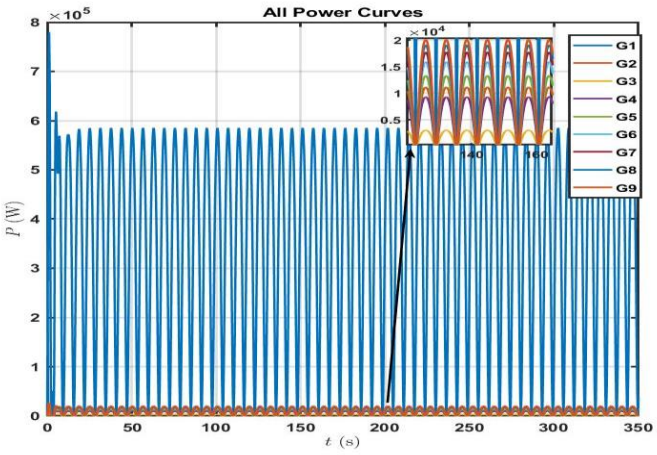

Fig. 5.11 Combined output power curves of MPA

5.6.3 Case study 3: SPA testing using real time data

Fig. 5.12 presents a series of subplots that delineate various parameters over time for a single-point absorber, providing valuable insights into its performance and operation. The first subplot illustrates the wave amplitude over time. This representation helps elucidate the magnitude of the sea wave's energy, offering a glimpse into the energy available for absorption. The second subplot depicts the displacement in the X1 direction.

This graph effectively illustrates the absorber's motion induced by the energy of the sea waves. The third and fourth graphs elaborate on the displacements in the X3 and X5 directions, respectively. X3 represents vertical displacement, while X5 signifies angular motion—both of which are the direct consequences of the sea wave's energy. In the fifth graph, we present the force exerted in the X direction over time.

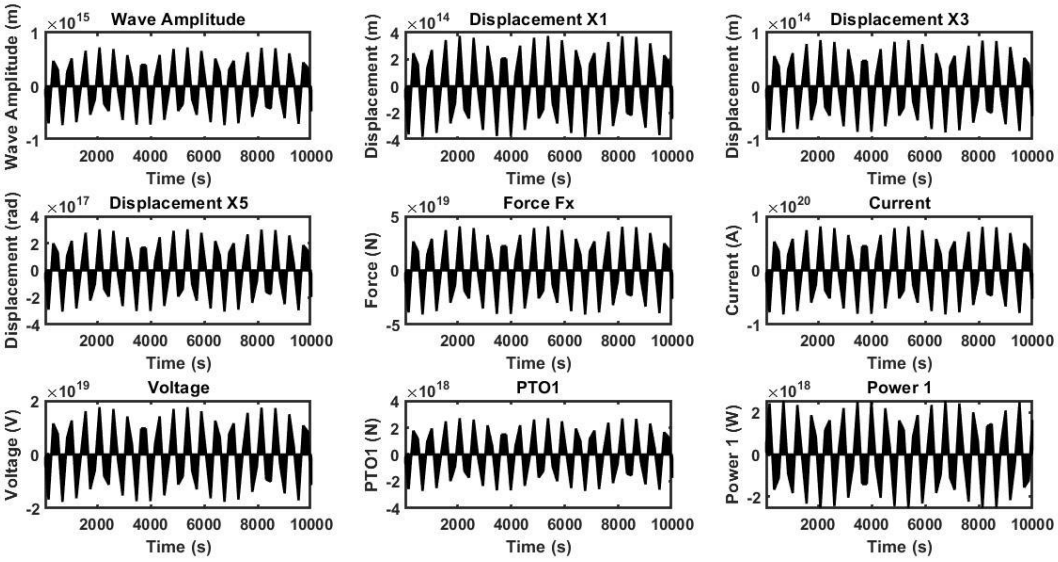

Figure 5.12 Output results of SPA with real time data

This force, acting on the absorber, signifies the extent of energy transfer from the sea wave to the absorber. The sixth and seventh subplots demonstrate the current and voltage respectively, providing insights into the electrical aspects of energy transformation. Lastly, the eighth and ninth subplots showcase the PTO1 and the output power generated from the wave energy system respectively. These final plots complete the depiction of the energy transfer process, from initial sea wave to usable electric power.

5.6.4 Case study 4: MPA testing using real time data

For HOWWE, there are a number of possible benefits to using nine linear generators with a semi-submersible platform as opposed to one linear generator with a mono-pole design. Here are a few main benefits: The possibility of producing more power is the main benefit. Simultaneous HOWWE harvesting is made possible by the nine linear generators. When compared to a single linear generator, this may lead to a larger total power generation capacity. Having redundant generators is a good idea.

The other generators can keep running even if one needs repair or has problems, providing a more dependable and constant power supply. Having numerous generators enables the system to adjust to varying environmental circumstances, as wind and wave conditions might vary. An energy system that is more flexible and adaptive may result from the fact that some generators work better under particular wave or wind conditions.

Energy harvesting efficiency can be maximized by optimizing different generators for different situations. Certain generators, for instance, might be more effective at capturing wave energy, while others might be better at capturing wind energy. It is possible for this specialization to improve overall efficiency. By distributing the load among numerous generators, the mechanical stress on each unit is reduced. This can help individual

components last longer and lessen the probability of equipment failure. A system with numerous generators is modular, it is easy to scale up or down based on energy demand or site-specific requirements. Additional generators can be installed as needed to improve capacity. Fig. 5.13, each subplot illustrates a specific linear generator's response (displacement) to the applied wave and input signal. The x-axis represents time, and the y-axis represents the output power of the corresponding linear generator. Each subplot's title reveals which generator it relates to (Generator 1 through Generator 9).

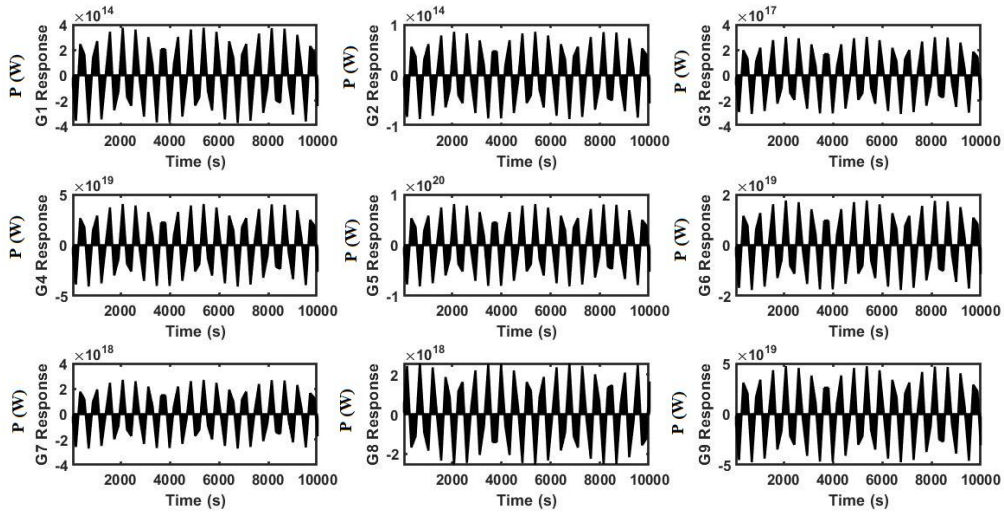

Figure 5.13 Output results of MPA using real time data

In the real world, the number of linear generators required for a linked offshore wind system bottom base will vary depending on the system's specific design, intended capacity, local environmental circumstances, and energy needs.

MPA also enhanced energy production for HOWWE in comparison to standalone single-point absorbers, an array of linear generators might improve the overall energy production potential depending on the site and resource availability.

5.7 Summary

This chapter conducts a comprehensive analysis of both SPA and MPA, with a particular focus on the maximum output power achievable through these techniques. Additionally, it introduces and discusses a novel MPA technique, offering new perspectives in this domain. MPA harvesting mechanism for maximum energy harvesting from every movement using an array of linear generators. By keeping the entire set up below water surface level; it is protected from storms and hurricanes. Below water surface set-up allows this unit to be less rigid thus lightweight and low-cost. Structurally a least complicated configuration that uses off the shelf components and overall uses minimum components to keep the cost lowest possible. Harvesting most movements of the triangle structure and reducing the stress on the frame. Furthermore, different case studies are conducted using real-time data of SPA and MPA techniques.

Chapter 6 Design and Control Techniques for HOWWE

In this chapter, HOWWE integration is carried out using offshore wind-coupled VSC and wave energy coupled VSC using multi-terminal transmission systems to connect with the AC load. In Section 6.2 and 6.3, the VSC model for HOWWE is examined. The HOWWE integration is examined using MATLAB simulations in Section 6.4. MATLAB results show different waveforms by changing the wind speed and wave input. Furthermore, integrated results of HOWWE using different case studies are presented in 6.5. In Section 6.6, the HOWWE system is tested under real-world application of Northwest, Greenwich Lightship and Silverstone Lightship United Kingdom.

6.1 Introduction

The MPPT techniques are established via a VSC to attain power from PMSG wind turbine. To obtain the maximum power from wave energy the best choice is the use of a linear generator with the VSC. HOWWE system is coupled with an offshore wind source on the top and wave energy at the bottom of the semisubmersible platform. The integrated model for HOWWE using VSC and VSI presents three terminals: the first one for offshore wind, the second for wave energy source and the third is the AC grid supply. The integrated HOWWE system with VSC injects the power generated in each hybrid farm into the grid; however, the VSI injects the power from the DC grid into the AC side grid. Clearly, the VSC and VSI can supply a stable fed AC voltage to the AC-grid.

Fig. 6.1 represents a feasible arrangement of a conversion framework with an OWT and a WEC conversion. This arrangement presents conversion (AC-DC) and inversion (DC-AC) with reference to wind-wave energy generation. The power conversion is carried out by VSC and power inversion is carried out by VSI. This topology improves the system's efficiency of the system in relation to output power and co-generation cost. VSI based on a phase-locked loop (PLL) is a sophisticated control paradigm that is frequently used in power electronic systems that requires perfect synchronization with an external reference signal, such as the grid voltage. The PLL is the control technique, constantly comparing the phase of the VSI output with that of the reference signal, which is commonly taken from the grid. The technology provides perfect synchronization by dynamically altering the frequency and phase of the VSI output, which is crucial in applications such as grid-tied inverters for renewable energy. This synchronization not only allows for seamless grid connectivity, but it also

improves system stability and efficiency. PLL-based control is well-suited for handling variations in grid conditions and load fluctuations due to its robust and adaptive nature.

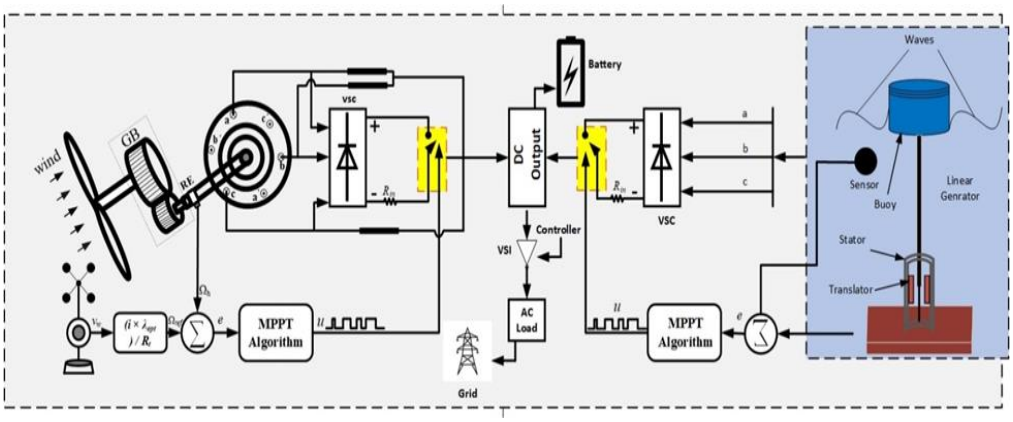

Figure 6.1 HOWWE with VSC and PLL-based VSI

6.2 HOWWE model operation principles

The integration method seeks to harness the power of both wind and ocean waves, utilizing their complementary nature as explained in Fig. 6.2. The first stage, like with any renewable energy project, is to examine the local wind and wave resources such as wind speed and wave height. This information is critical for calculating the potential for energy generation. The hybrid system is designed by using appropriate wind turbines and wave energy converters. In this research, VSC is implemented and tested on both sources. Other components such as system generators, power electronics, and load connection are also considered in the design. Offshore wind and wave energy VSC are combined in one system using VSI. HOWWE systems are linked to the AC power after combined DC. Excess energy can be supplied to storage bank such as using battery bank. It also maintains a consistent power supply by taking electricity from the battery bank when renewable sources are insufficient.

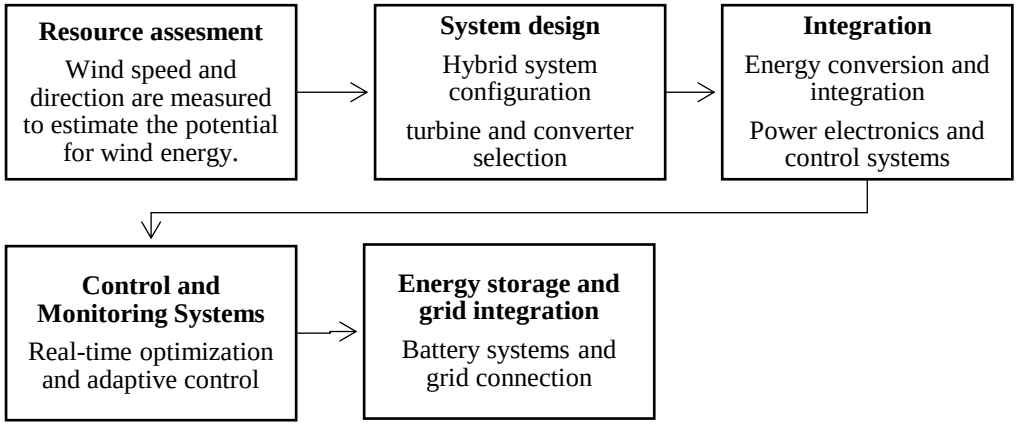

Figure 6.2 HOWWE model operational aspects

6.3 VSC model for HOWWE

The integration of HOWWE transmission systems is established on current-fed VSC converters. This innovative converter technique minimizes the priced for HOWWE system based on VSC-VSI using fast-switching semiconductors. The VSC and VSI configuration is presented in Fig. 6.3.

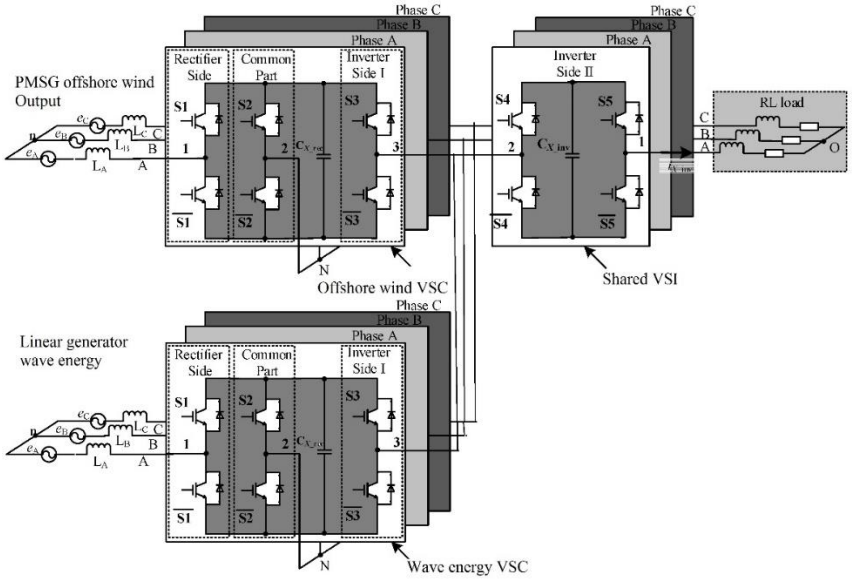

Figure 6.3 VSC configuration for HOWWE

There are the following advantages for VSC-VSI such as fast switching and the capability to autonomously control both active-reactive powers.

6.3.1 Converter bridge

Insulated-gate bipolar transistor (IGBTs) is used in the converter bridge of HOWWE-VSCs. At the transmitting end called a rectifier, power is converted to DC, the receiving end called as an inverter. The function of inverter is to convert DC output to AC output. A voltage is delivered to the gate of the IGBT. There are three terminals in the IGBT and it is called a power semiconductor device. It permits electricity flow while it is ON and inhibits it when it is OFF. The converter obstructive voltage competency is increased by connecting a lot of IGBT cells in series. The converter bridge's DC capacitors reduce ripple in the DC voltage, store energy and allow power flow to be controlled. The VSC using a level IGBT diode is shown in Fig. 6.4.

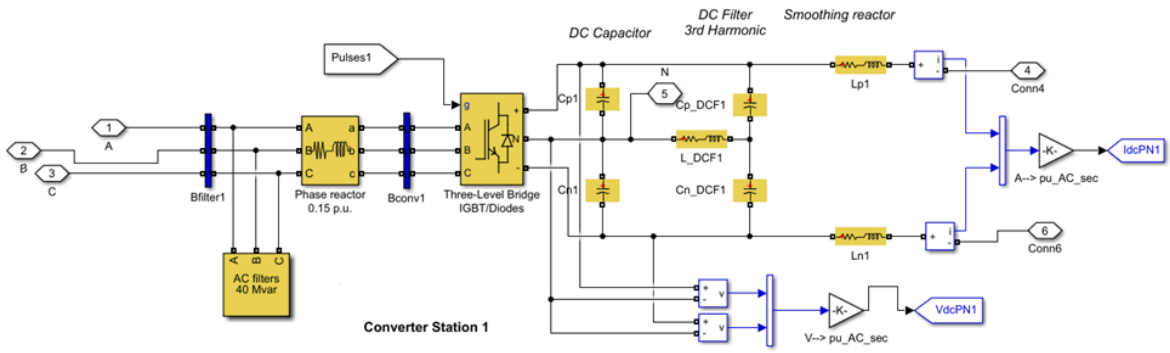

Figure 6.4 VSC for offshore wind (same technique applied to wave energy)

6.3.2 Phase reactor

Phase reactor is used to link the converter and offshore wind system in series. Similarly, in the case of wave energy separate phase reactor is used to link the converter in series. It generates a difference in the voltage of the converter bridges and the AC output. The active-

reactive power of the VSCs is managed by the alternating current that passes through the phase reactors. Phase reactor also lessen the alternating current's high-frequency harmonic components.

6.3.3 AC filters

VSCs produce high-frequency harmonic components in output voltage. The value is around 1 kHz or more. In output voltage to remove the high-frequency, filters are required to link in parallel with the system.

6.4 Operating characteristics of VSC for HOWWE

VSC exchanges active-reactive power while producing an output voltage waveform at their output. The V_{out} is produced by a VSC at the sending end, while the V_{ac} presents the voltage across AC and it is at the receiver side. If there are no power losses so the active power (P) moves through the VSC. At the sending end there is reactive power (Q) and the apparent power (S) of the offshore wind VSC and defined as:

$$P_{ow} = \frac{V_{out} \sin \delta}{X_L} V_{ac\ (ow)} \tag{94}$$

$$Q_{ow} = \frac{V_{ac} - V_{out} \cos \delta}{X_L} V_{ac\ (ow)} \tag{95}$$

$$S = \sqrt{{P_{ow}}^2 + {Q_{ow}}^2} \tag{96}$$

Similarly for wave energy:

$$P_{we} = \frac{V_{out} \sin \delta}{X_L} V_{ac\ (we)} \tag{97}$$

$$Q_{we} = \frac{V_{ac} - V_{out} \cos \delta}{X_L} V_{ac\ (we)} \tag{98}$$

$$S = \sqrt{{P_{we}}^2 + {Q_{we}}^2} \tag{99}$$

6.5 Results and discussions

6.5.1 Case study 5: HOWWE integration using multi-terminals AC

The connection of HOWWE offshore wind and wave energy can be achieved with a shared AC-DC based converter on a multi-terminal grid. The integrated model for HOWWE using VSC and VSI as shown in Fig. 6.5. The HOWWE-VSC injects the power generated in each hybrid farm into the grid, however, the VSI inject the power into the AC side grid. The physical structure of VSC for HOWWE is based on transformers, phase reactors, converter bridges, and AC filters that make up the majority of the VSC system's parts.

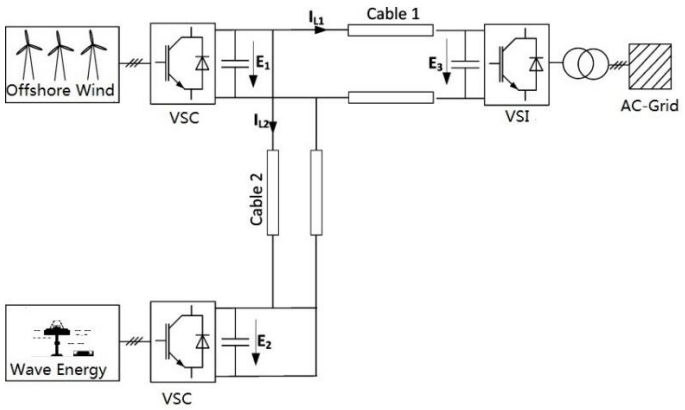

Figure 6.5 Multi-terminal VSC for HOWWE

An OWT and wave energy modelling are simulated in MATLAB. The VSC is used to improve the overall system reliability and reduce the cost and size of offshore wind system and wave energy systems. The wind speed is supposed as 12m/s and wave energy is supposed by taking wave height using MPA real time data. The comparison and simulation of both energy sources are made among the designed schemes separately. In the case of OWT, the extraction of maximum output should be guaranteed. To find energy conversion from wave

energy by modelling linear generator using MPA. The results in MATLAB also show a steady output power flow by adding both energy sources. Fig. 6.6 and Fig. 6.7 show the control signal of DC parts for wind and wave devices respectively. Changing the modulation index in power electronics applications allows for control of the output voltage amplitude and harmonic content. Higher modulation indices result in higher voltage output and lower harmonic distortion in general, but they can also result in higher switching losses and increased pressures on power electronic components.

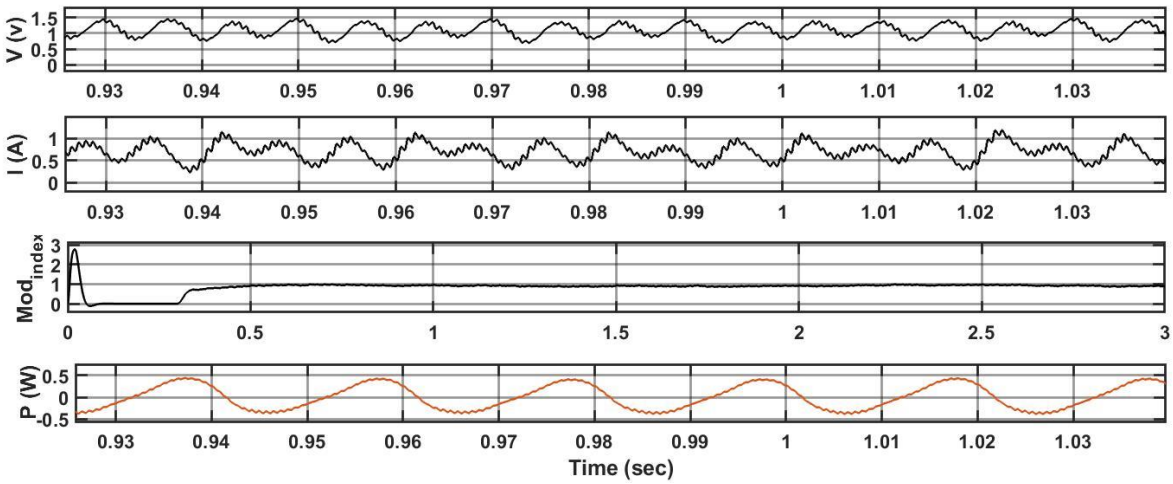

Figure 6.6 Control signals across the DC offshore wind

The filter bus is applied sequentially on both wind and wave energy sections and the results of voltages across time are shown in Fig. 6.8 and Fig. 6.9.

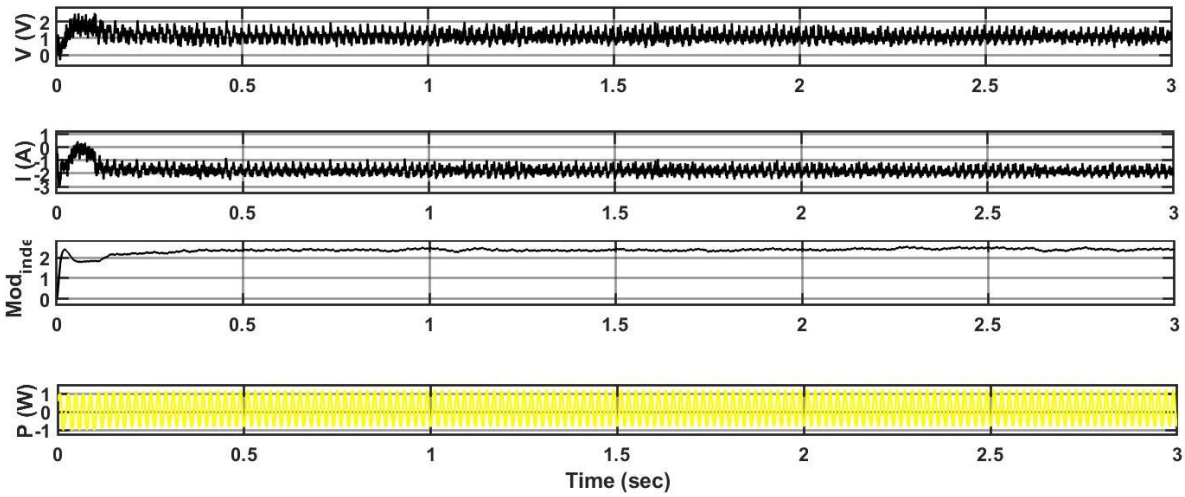

Figure 6.7 Control signals across DC wave energy device

The control signals across the DC offshore wind system in Fig. 6.6 show that using the PMSG in conjunction with the VSC converter results in greater performance.

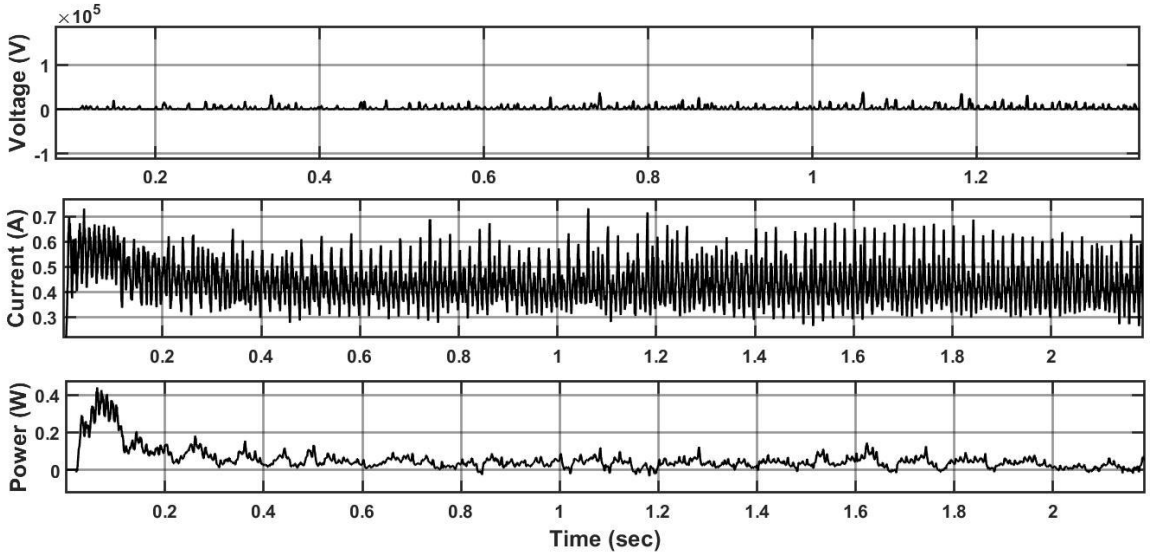

Figure 6.8 Filter bus of offshore wind

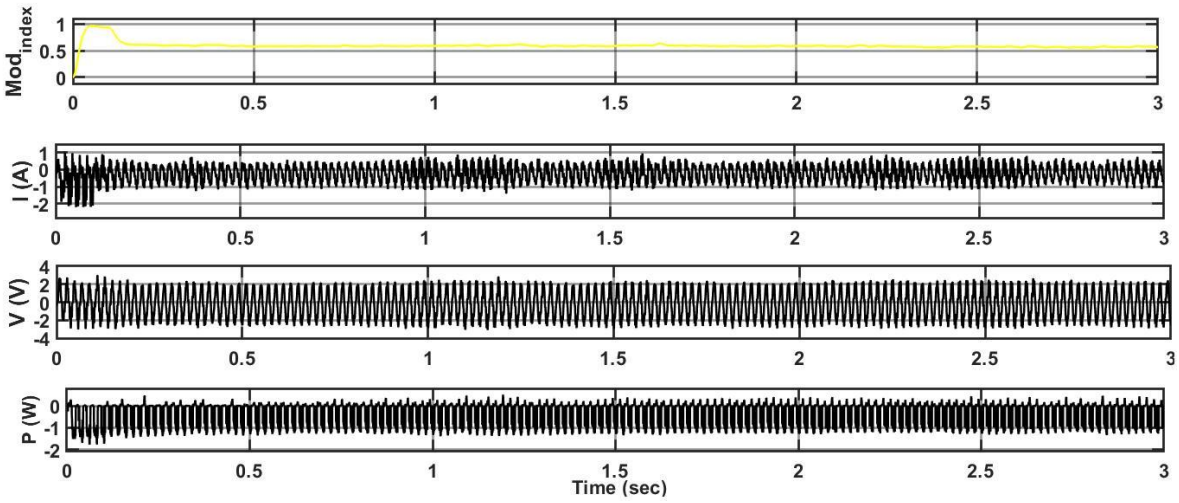

Figure 6.9 Filter bus of wave energy device

The use of a PMSG in an offshore wind setup improves the control system's efficiency. In this context, the VSC converter is critical in regulating and optimising the control signals, providing smoother operation and improved overall performance. The combination of these technologies enables more precise and effective control of the DC offshore wind system, resulting in higher stability, fewer fluctuations, and increased energy output. The results shown in Fig. 6.6 and 6.7 highlight the benefits of using PMSG VSC converter designs to optimise control signals for improved performance in HOWWE. Fig. 6.6, PMSG VSC converter design in the DC offshore wind system is validated by a complete examination of essential parameters. Notably, PMSG's intrinsic stability helps to maintain more consistent power output, lowering the need for extra stabilization methods and improving grid integration. The VSC's improved control capabilities provide faster response times and finer control precision, which is critical for reacting to changeable wind conditions. Furthermore, the system's capacity to minimise voltage and frequency variations assures a consistent and steady power production, alleviating concerns about grid disruptions. The PMSG and linear generator VSC converter configuration's total efficiency advantages into higher energy

yields, making the system economically competitive. Furthermore, the ease of use and dependability of PMSG systems contribute to decreased maintenance requirements, resulting in improved availability and less downtime. The findings in Figure 6.8 and 6.9, in summary, highlight the superiority of the PMSG VSC converter arrangement, emphasising greater stability, control accuracy, efficiency, and dependability in the context of HOWWE generation, exceeding previous systems.

6.5.2 Case Study 6: Power optimization using shared VSI

The control arrangement is based on two phases. The first phase is the current control of each VSC. The second phase is the voltage regulation of DC which is attained by the control approach. The current control is achieved by tuning the voltage provided by the converters. In the VSC scenario, a continuous 3-phase voltage is applied to deliver the voltage of the offshore wind and wave energy. Hence, the current passing from VSC into the VSI is dependent on the offshore wind and wave energy injected power.

The VSI current control is attained by depending on the current control system which delivers independent control of active-reactive. The input loop of current is the supposed or reference value of the power provided to the grid as shown in Fig. 6.10.

The grid-tied VSI is needed to provide the generated power of the HOWWE systems to the power grid. This is essential to comply with electrical quantities on the grid side such as frequency, voltage magnitude, phase angle and sequence.

The main control purpose of the VSI is to maintain the DC bus voltage by regulating the DC micro-grid active power supplied to or gained from the AC grid. The grid-tied VSI needs the generated power of the HOWWE systems to the power-grid. This is essential to comply

electrical quantities on the grid side such as frequency, voltage magnitude, and phase angle and phase sequence.

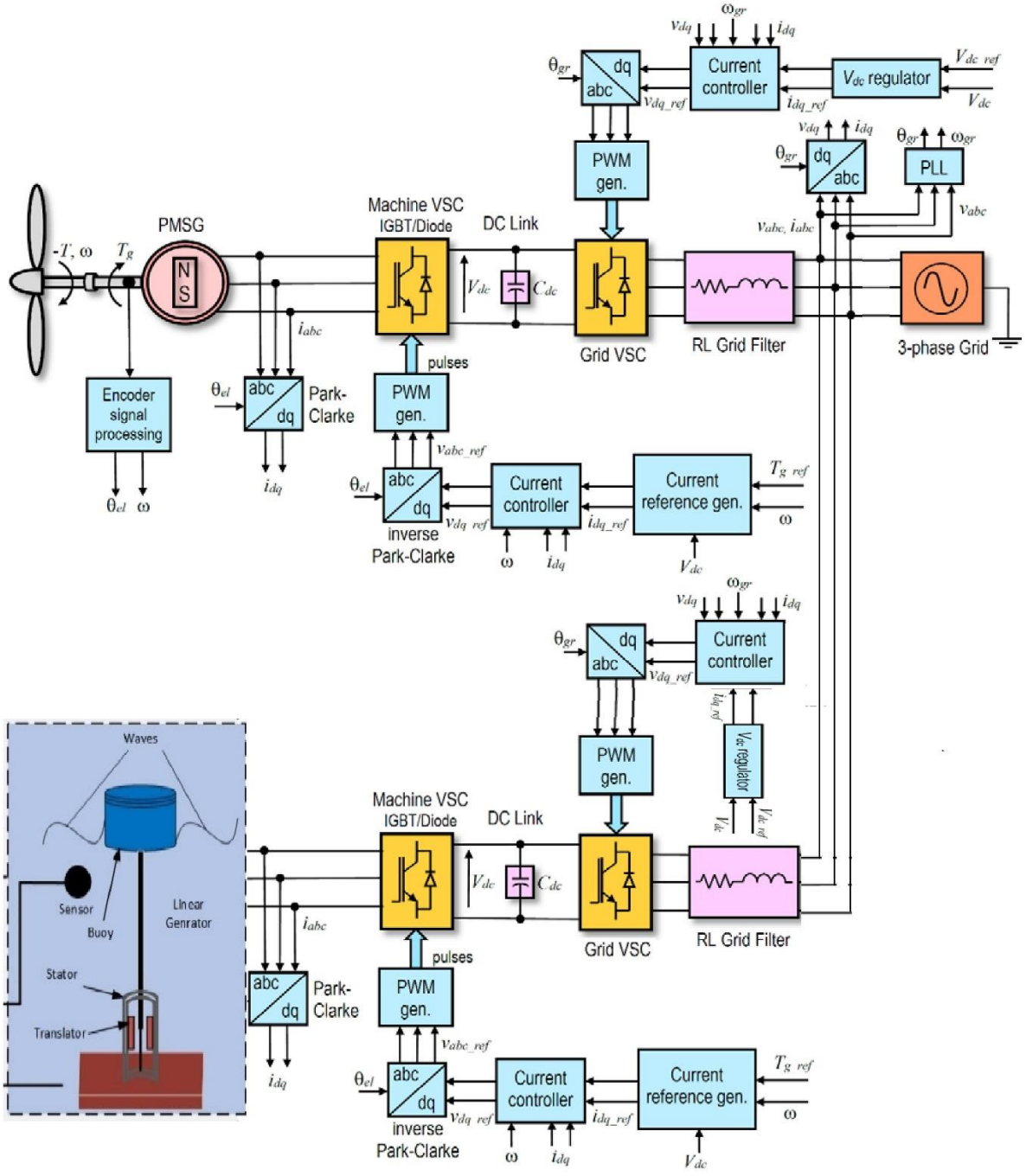

Figure 6.10 Control Diagram of HO WWE with VSC and PLL-based VSI

A stable inverted power is achieved and output power of the inverter is shown in Fig. 6.11. The overall combined output power from HOWWE is presented in Fig. 6.11.

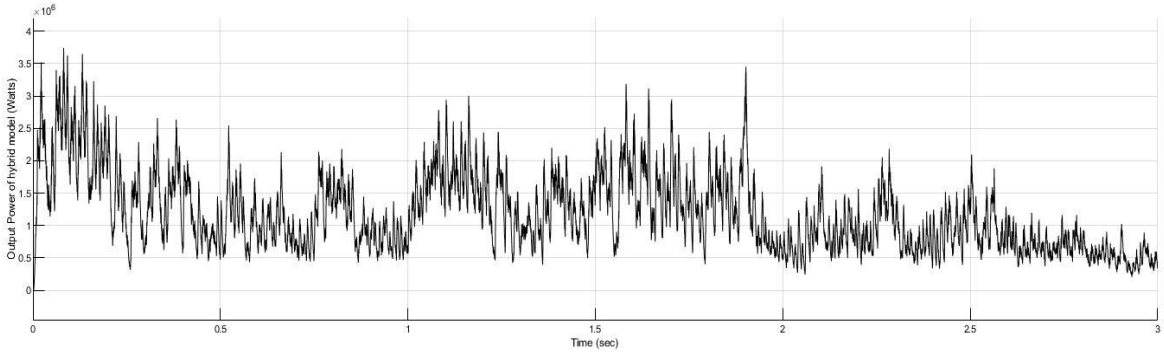

Figure 6.11 Combined output power from HOWWE

The Fig. 6.11 shared VSI provides a single control and coordination system for both offshore wind and wave energy outputs, providing optimal power flow and efficient energy conversion. In contrast, the current system, which relies on separate inverters, may struggle to balance the various energy sources, potentially resulting in inferior performance. The shared VSI arrangement streamlines the entire system architecture, lowering complexity and increasing dependability while also saving money on manufacturing, installation, and maintenance. Furthermore, the shared VSI's centralised control enhances efficiency and grid integration, assuring stable power delivery. The HOWWE system's resilience to changing weather conditions is a significant strength, allowing it to dynamically change energy production in real-time. This comparison highlights the clear benefits of the shared VSI in the HOWWE system, emphasizing its potential to outperform existing separate wind-wave systems and contribute to the growth of integrated offshore wind and wave generation technology.

6.6 Complementary operations using Perturb and Observe

Perturb and observe is used in VSI to maximize the power production from HOWWE systems. It's vital to keep in mind that a VSI is often used in applications where it creates or controls AC voltage, and the control target may be different from that of a HOWWE system.

Here is a general description of how the P&O algorithm might be modified for a VSI-based system. To optimize certain performance criteria, the P&O algorithm for a VSI may modify the VSI output voltage or frequency. The following steps are used to implement the P&O algorithm. Firstly, we need to measure the performance of the parameter: It depends on the HOWWE DC-AC, the output voltage magnitude and frequency of HOWWE need to be measured for optimization. Secondly, continuously monitoring of HOWWE variables. Thirdly, initialization of the duty cycle. PWM controls are set accordingly initial duty cycle. The average voltage or frequency output of the VSI is determined by the duty cycle. The duty cycle should be slightly altered (increased or decreased). Based on the rate at which the performance parameter changes, the magnitude of the perturbation can either be predetermined or dynamically modified. Finally, measure the impact of the perturbation on the performance parameter by observing the effect. The duty cycle should be adjusted in a way that enhances the performance parameter in light of the observation made in step 4 of the process. Continue perturbing in the same direction if the parameter increases; if it declines, alter the direction of the perturbation. Finally iterate the process, constantly going through steps 3 through 5 again. The perturb and observe algorithm's performance depends on adjusting a number of parameters, including the perturbation step size, the dead band width, and the response time. Although this approach offers a HOWWE place to start for optimization, it might need to be modified for your specific use case. Additionally, stability and safety issues must be taken into by perturb and observe control algorithms for HOWWE power systems.

6.6.1 Case study 7: Complementary operations at Northwest England when wave is dominant

The efficiency and dependability of HOWWE output can be increased by complementarily integrating both energy sources. In order to work together in real world effectively, their energy capture must be optimized based on each type of system's advantages. The following are some ways they can enhance one another such as seasonal variability.

Depending on the season and the weather, HOWWE is frequently accessible. Wave energy tends to be more predictable during particular seasons or in particular geographical places, although offshore wind energy is frequently more consistent and reliable. The consistent and continuous energy supply by combining these sources is adjusted by taking one source more dominant than other. HOWWE systems can be created to work in harmony with one another throughout the year. In some places, for instance, wave energy more available in the winter while wind energy is more prevalent in the summer. To maximize energy production throughout the year, each system's functioning should be adjusted correspondingly. In Table 6.1 term ‘Dir’ means, the direction the ocean current is flowing toward 0-360 degrees, 360 is due north, 0 means no measurable current [139]. Similarly, ‘Obs’ represents the observation in between 0-360 degree. VSC-VSI that can efficiently capture both offshore wind-wave energy. Depending on the circumstances, these converters can flip between modes. For example, during calm seas, a device could function as an offshore wind and then switch to wave energy capture during storms. By adding energy storage, such as batteries, can be used to store excess energy created by one source for use when the other source is less active. This helps to smooth out the energy supply and ensures that the power output remains constant. The designed approach and MPPT-based power conversion technique decrease infrastructure

costs and increase resource sharing, consider putting offshore wind-wave energy systems on the same platform or structure. The site of North West of England is tested by taking data from National Data Buoy Center [139] and the data is presented in Table 6.1.

Table 6.1 Real-Time data of average wind speed and average sea waves of Northwest United Kingdom

Date (UTC)	Average Wind Dir (True)	Average Wind Speed m/s	Wind Obs	Average Seas meters	Wave Obs
2023-09-06 1200Z	35	1.543	6	1.829	6
2023-09-06 0600Z	10	2.0576	6	1.829	6
2023-09-06 0000Z	63	2.5728	6	1.829	6
2023-09-05 1800Z	65	5.6636	6	1.829	6
2023-09-05 1200Z	80	7.216	1	0.3048	1
2023-09-05 0600Z	70	8.2296	1	0.3048	1
2023-09-05 0000Z	50	9.144	1	0.3048	1
2023-09-04 1800Z	60	10.668	1	0.3048	1
2023-09-04 1200Z	50	9.7224	1	0.3048	1
2023-09-04 0600Z	70	7.216	1	0.3048	1
2023-09-04 0000Z	60	6.7056	1	0.3048	1
2023-09-03 1800Z	60	9.7224	1	0.3048	1
2023-09-03 1200Z	50	6.7056	1	0.3048	1
2023-09-03 0600Z	60	5.144	1	0.3048	1
2023-09-03 0000Z	50	8.2296	2	0.6096	2
2023-09-02 1800Z	60	8.2296	1	0.3048	1
2023-09-02 1200Z	60	6.7056	1	0.3048	1

The average wind-wave data is plotted to check the response with PMSG and linear generator as shown in Fig. 6.13. The offered data generates a plot of the alternating current power output

over a simulated time period for HOWWE is shown in Fig. 6.12. The x-axis indicates time in seconds, while the y-axis represents alternating current power output in watts (W).

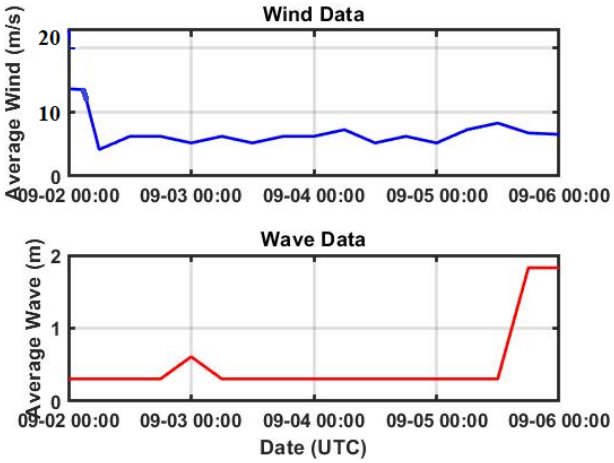

Figure 6.12 Average wind-wave data of Northwest United Kingdom

The Fig. 6.13 depicts how the hybrid energy system's AC power output varies over time. Offshore wind and wave conditions are monitored, as well as the efficiency of the energy conversion and inverter systems, all have an impact on the AC power production. The Fig. 6.13 also depicts how the system responds to changes in wind speed and wave height, as these are the key elements influencing power generation.

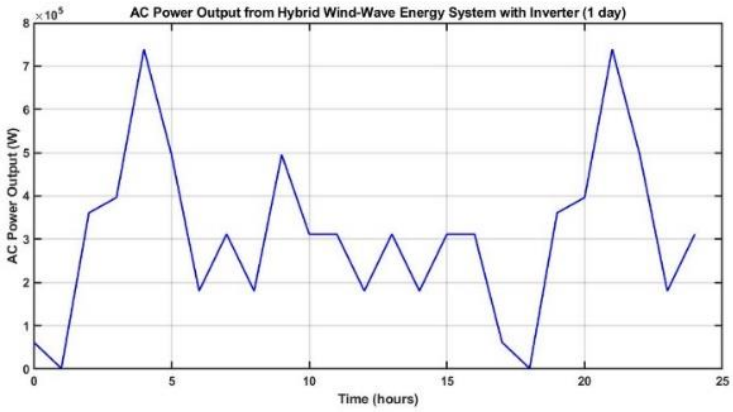

Figure 6.13 PMSG and single linear generator output with data from Northwest United Kingdom

In order to evaluate the total output of PMSG and single linear generator within the Northwest region of the United Kingdom, normally first take wind wave energy patterns and the power output is represented in Fig. 6.13. Fig. 6.13 also highlights the unstable power output behavior, notably depicting a significant power drop within the system. This occurrence is attributed to the presence of both a single linear generator and a single PMSG, clearly discernible in the data. Fig. 6.14, combined plot results show the following information from the HOWWE system, which includes both wind and wave energy sources. These charts provide information about how the hybrid system works under changing wind and wave conditions. The output of the PMSG is affected by wind speed m/s that is low, whereas the output of the linear generators is affected by wave height and other factors and wave energy is dominant in this case as shown in Fig. 6.14.

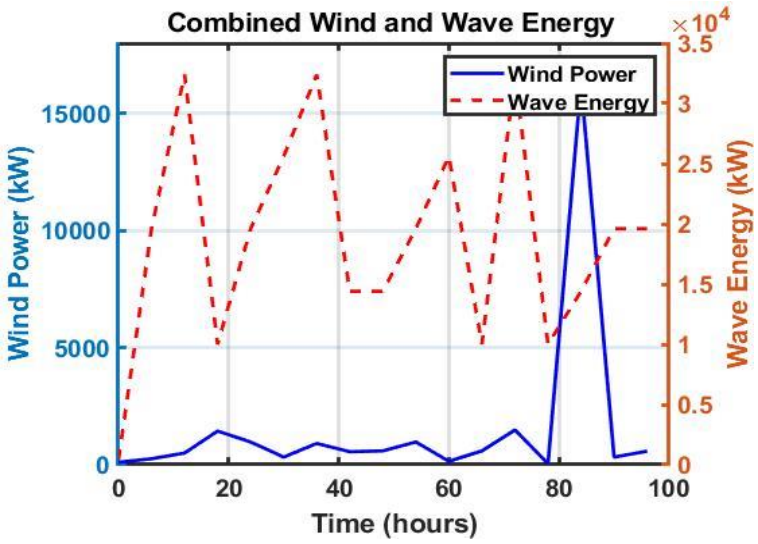

Figure 6.14 HOWWE at Northwest England using MPA

6.6.2 Case study 8: Complementary operations at Greenwich Lightship England when wind is dominant

The initial data includes arrays representing wind speeds in m/s and wave heights in meters at different time points. In Fig. 6.15 the algorithm generates a two-subplot after extracting pertinent data, including the date formatted in UTC and the numerical values for wind speed and wave height. The first subplot shows how wind speed varies over time, and the second subplot shows how wave height changes. Both subplots' y-axes display wave height in meters and wind speed in meters per second, while the x-axis displays dates in UTC format.

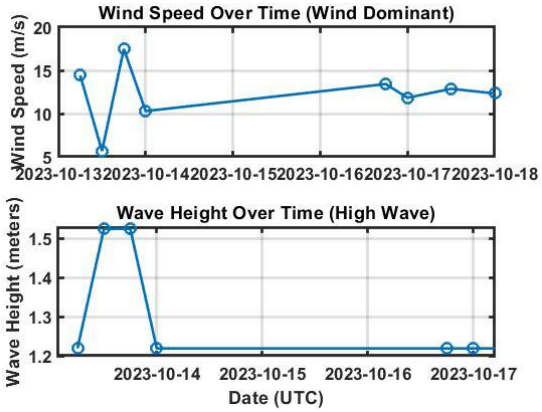

Figure 6.15 Average wind-wave data of Greenwich lightship United Kingdom

To calculate wind power using standard formulas considering air density, swept area, and a typical power coefficient for a wind turbine. Based on the data provided of Greenwich lightship in Table 6.2, the algorithm calculates wind speed and wave energy. Here is what we learn from the findings: The blue line in the plot depicts the wind speed in m/s at various time.

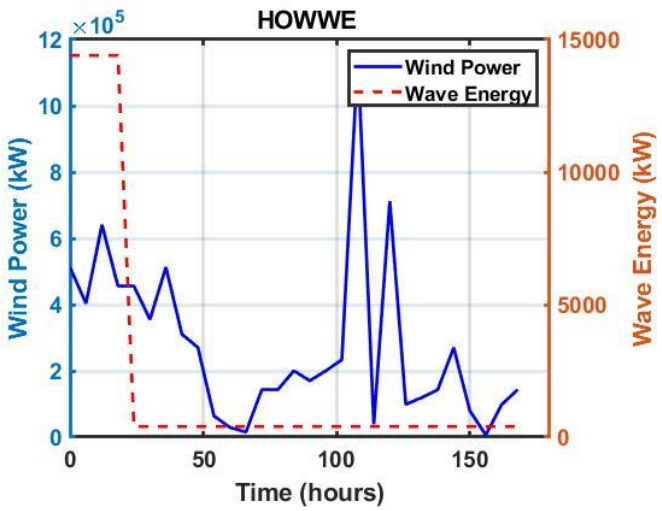

Figure 6.16 HOWWE at Greenwich Lightship England

Based on the data presented, the wind speed changes over time. Based on the provided wave height data, the red dashed line indicates the calculated wave energy in watts (W). Wave energy increases as wave height increases. The Fig. 6.16 depicts the wind speed and wave energy as they change over time. The wind speed is calculated directly from the input wind speed data. The Fig. 6.16 shows the dominancy of wind speed as compared to wave data. Wind speed and wave height at various time intervals are supplied. Using MPA system, following output of system presented in Fig. 6.16. The data and Fig. 6.16 shows wind power's supremacy in the energy generation scenario. Wind power, measured in kilowatts (kW), outperforms wave energy greatly. Wind speed variety, constancy of wind power generation, and established infrastructure for wind energy conversion all contribute to this supremacy. Although wave energy is present, it is comparably weaker and less varied throughout the observed time periods.

6.6.3 Case Study 9: Complementary operations at Silverstone Lightship England when both sources are dominant

In this case study, the data of Silverstone Lightship is tested and plotted using P&O when both sources are dominant. These characteristics are critical for calculating the power output of offshore wind turbines and wave energy converters. Based on the supplied data, the Figure 6.17 creates two useful plots to graphically depict the temporal patterns of wave height and wind speed. Using the "average wind speed" data, the first plot shows the fluctuation in wind speed over time. A continuous line connecting circular markers creates a clear depiction of the variations in wind speed. The y-axis shows wave height in meters, and the x-axis shows dates in UTC, much like in the first plot.

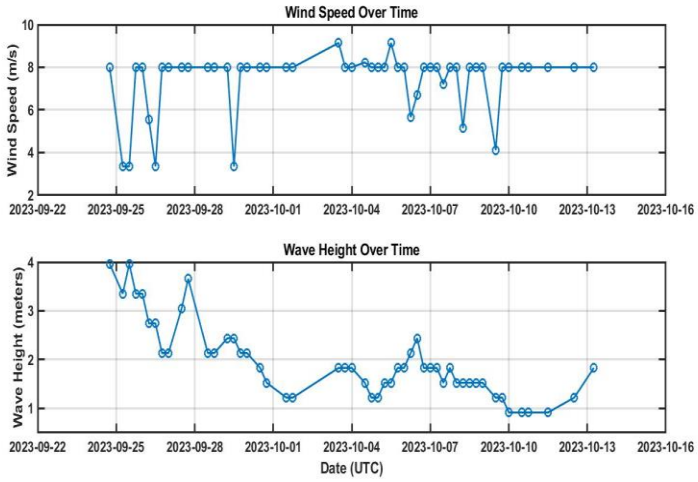

Figure 6.17 Average wind-wave data of Silverstone Lightship United Kingdom

The wind output is derived using a simplified model that assumes a PMSG wind turbine. Similarly, wave power is computed using a MPA model that assumes a linear relationship between wave height and square. Offshore wind and wave power statistics are shown across time, with the x-axis representing time in hours and the y-axes reflecting power values in

watts. Fig. 6.18 plots HOWWE power on a single graph with dual y-axis, wind power in blue and wave power in red.

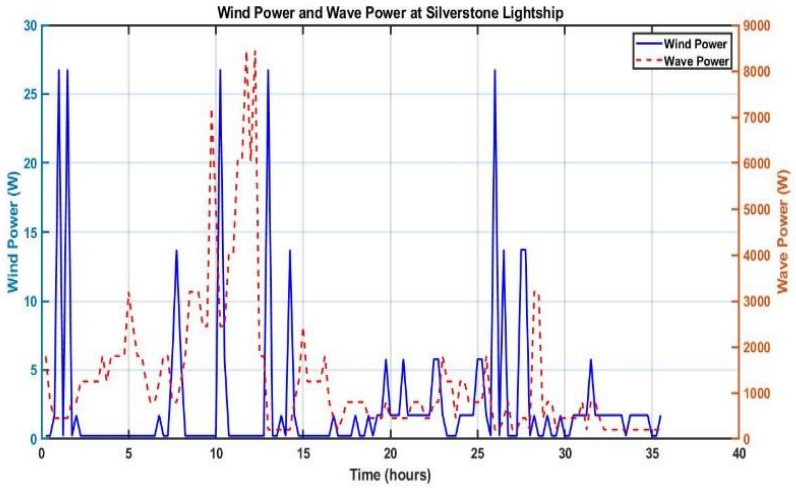

Figure 6.18 HOWWE at Silverstone Lightship England

Under the assumption of the provided data from Table 6.3 and power conversion models, the output shows the depicting how wind and wave power vary over time in Fig. 6.18. It is clearly visible that both wind and wave sources are dominant.

6.7 Summary

In this chapter, an integration of HOWWE using PMSG and linear generator has been proposed. The PMSG-based offshore wind turbine ECS is modelled with three state variables which are then transformed into two states or normal form model to simplify the system. The wave energy numerical and simulated modelling is presented and the integration of both sources is carried out using the voltage source inverter. During the simulations, it is demonstrated that offshore wind and wave energy are modelled separately and then their AC power is integrated via VSC. The power inversion is carried out for the AC grid connectivity. Finally, the proportional simulated and measured results of offshore wind and wave energy under load switching have been performed, and it illustrates the system with the proposed techniques functioned steadily under different conditions. In the last section, complementary operations and real-world application of proposed techniques are tested using real-time data from the NorthWest, Silverstone Lightship and Greenwich Lightship of England.

6.7 Summary

In this chapter, an integration of HOWWE using PMSG and linear generator has been proposed. The PMSG-based offshore wind turbine ECS is modelled with three state variables which are then transformed into two states or normal form model to simplify the system. The wave energy numerical and simulated modelling is presented and the integration of both sources is carried out using the voltage source inverter. During the simulations, it is demonstrated that offshore wind and wave energy are modelled separately and then their AC power is integrated via VSC. The power inversion is carried out for the AC grid connectivity. Finally, the proportional simulated and measured results of offshore wind and wave energy under load switching have been performed, and it illustrates the system with the proposed techniques functioned steadily under different conditions. In the last section, complementary operations and real-world application of proposed techniques are tested using real-time data from the NorthWest, Silverstone Lightship and Greenwich Lightship of England.

Chapter 7 Conclusion and Future Work

7.1 Conclusion

This thorough thesis has successfully met its stated goals. We have learned a great deal about the selection criteria for generators and power conversion for HOWWE farms by carefully analyzing the current WEC and OWT technologies. We have created a reliable hybrid system model by modelling and simulating wind turbines with linear generators for wave power generation and PMSG. Additionally, thorough insights into the effectiveness of various control strategies for OWT applications have been provided by the implementation and comparative analysis of these strategies, which include PID, FBL, SMC, STA, and an AI-based IBRTA. Following that, the investigation looks into substructures such as floating barges, spars, and tension leg platforms. This deepens the design considerations, providing useful insights into platform selection and optimization for the HOWWE systems. The research within HOWWE farms is broad, with bottom-fixed wind turbines, wave energy converters, and hybrid configurations all being investigated. Each configuration is examined using real time data. Revealing both sources particular benefits and challenges connected with their deployment in offshore contexts.

Our understanding of HOWWE systems is further enhanced by the testing of wave energy conversion using SPA and MPA approaches, as well as the investigation of power conversion and inversion techniques using VSC and VSI. Using real-time data from multiple locations, such as the Northwest of England, Silverstone, and the Greenwich Lightship in England, we have illustrated in detailed case studies the performance and practical application of HOWWE systems in a range of environmental circumstances. All things considered, the accomplishment of these goals highlights the extensive scope and importance of our research

efforts in promoting sustainable offshore energy solutions. For both offshore wind and wave energy systems, these strategies are investigated in conjunction with P&O. The goal is to minimize the complexities of converting harvested energy into usable forms, thereby contributing to the development of efficient and dependable power systems suited for integration into existing electrical grids or freestanding applications. These case studies not only corroborate theoretical findings, but also offer essential insights into the flexibility and performance of the HOWWE system in a variety of environmental circumstances.

This research, which spans numerous chapters, gives a full overview of the HOWWE system research findings. In Chapter 2, there is an in-depth examination of wind-wave control concepts emphasizes the importance of collocated systems, which combine OWT arrays with WEC arrays. For maximizing energy output, the analysis of power conversion, advanced control coupling, and site selection emphasizes the necessity of efficient control design, power conversion, and dependable grid integration.

Chapter 3 emphasized on numerical methodologies for analyzing HOWWE. The numerical modelling, stability analysis, and integration of wind and wave energy sources demonstrate how important these techniques are in assessing system performance and economic feasibility.

Chapter 4 is the modelling of SMC, IBRTA and STA for offshore wind generation using a PMSG. The findings illustrate the limitations of standard controllers as well as the enhanced performance gained by innovative control systems such as STA and IBRTA which address issues such as chattering and ensure MPPT.

Chapter 5 includes wave energy harvesting systems, including both single-point and multipoint absorbers. The introduction of a revolutionary multipoint approach reveals advances in optimising energy harvesting while also delivering cost-effective and structurally simplified solutions. Real-time case studies support the efficacy of various harvesting systems.

In Chapter 6, the integration of offshore wind and wave energy is proposed using a shared VSI. A holistic approach is demonstrated by the numerical and virtual modelling of PMSG-based offshore wind turbines and linear based wave energy converters, followed by the integration of their AC power via VSI. The complimentary operations and real-world applications demonstrated the viability and stability of the offered methodologies using data from specific places.

7.2 Limitation of work

HOWWE has great potential as a renewable energy source, but it confronts severe obstacles. Because of the high initial expenses of installation, maintenance, and operation, as well as the exposure to extreme marine conditions, specialized engineering and materials for robustness are required. Technical challenges, such as building foundations that can endure dynamic waves and guaranteeing dependable grid connections, hinder implementation even further. Environmental considerations, such as potential repercussions on wildlife habitats and marine ecosystems, add to the challenges. Legal constraints, aesthetic problems, and a scarcity of suitable areas all impede widespread implementation. To fully realize HOWWE's potential, limitations in conversion must be overcome. Because wind and wave energies are unpredictable, specialized power conversion equipment are required to assure consistent production. Integrating renewable energy into current systems raises concerns about power

quality and grid reliability, particularly during peak periods. Operational thresholds, turbine start-up and cut-in rates all contribute to intermittent power generation, which has an impact on efficiency and durability. Losses in the multi-stage conversion process diminish overall energy conversion efficiency even more. Due to the demanding working conditions, maintenance becomes a key problem, potentially affecting dependability and uptime. Despite these obstacles, continued research and development is improving power electronics, control systems, and grid synchronization. These developments are paving the road for wind energy to cement its vital role in the worldwide renewable energy system.

7.3 Future work

The energy performance of the hybrid system can be improved by incorporating storage system. There are many benefits to incorporating a battery storage system into a hybrid energy arrangement, like a HOWWE system. First of all, by storing extra energy produced during times of strong wind or wave activity and releasing it during times of low or fluctuating energy production, it helps to balance out the system's energy output. This enhances the hybrid system's overall predictability and dependability. Batteries also improve grid stability by serving as a buffer against abrupt changes in energy supply and demand, guaranteeing a steadier flow of electricity. Furthermore, battery storage systems improve grid flexibility by allowing energy to be stored and dispatched as needed, which makes it easier to integrate intermittent renewable energy sources into the system. In order to maximize efficiency and revenue creation, complex control algorithms can also optimize energy management inside the hybrid system. These algorithms can schedule charging and discharging cycles based on variables like energy consumption, market prices, and weather forecasts. Additionally, battery storage ensures service continuity and improves system

resilience by offering a dependable backup power source in the event of equipment failures or grid outages. Finally, battery storage systems assist in lowering energy costs for end users and grid operators by storing excess energy and discharging it at times of high electrical demand or peak demand. The energy system of hybrid system can also be improved by adding a third source of energy generation such as the wind-wave-hydrogen system. This is an innovative approach that will enhance the reliability of the system. Energy generated by the offshore wind and wave combined together using the same approach VSC and VSI. The third source will be passed with an electrolyze process.

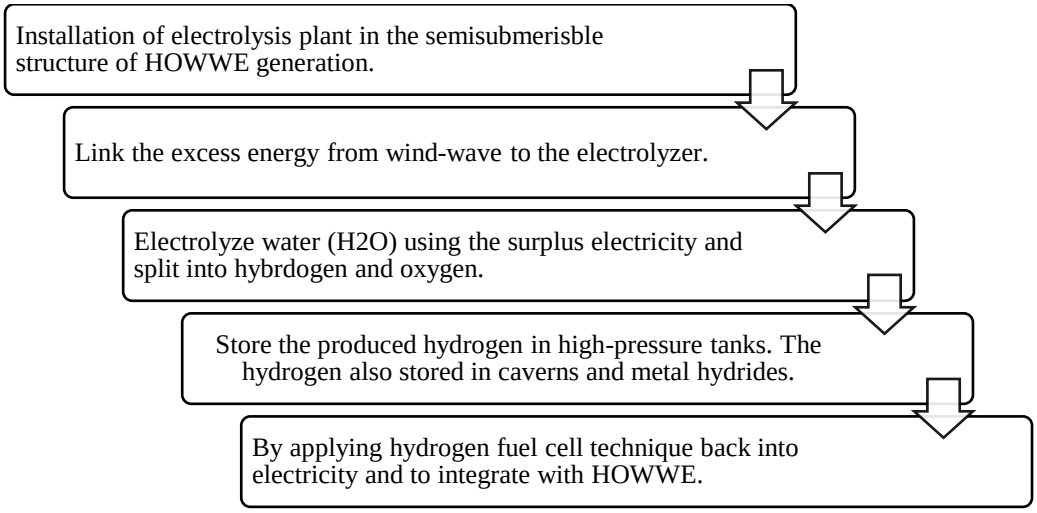

Figure 7.1 Electrolysis for hydrogen production combined with HOWWE

In the hydrogen source, the main process is the electrolysis water splits into hydrogen H_2 and oxygen O_2. Install an energy system that organizes the hydrogen-based backup power when HOWWE generation is insufficient. The process of installation and integration of the three sources are mentioned in Fig. 7.1.

Reference

1. N. Abas, A. R. Kalair, and N. Khan, "Review of fossil fuels and future energy technologies," Futures, vol. 69, pp. 31-49, 2015.
2. Astariz, S. and Iglesias, G. "Enhancing wave energy competitiveness through co-located wind and wave energy farms". A review on the shadow effect. Energies, 8, pp.7344-7366, 2015.
3. P. Higgins and A. Foley, "The evolution of offshore wind power in the United Kingdom," Renew Sustain Energy Rev, vol. 37, pp. 599-612, 2014.
4. A. S. Bahaj, "Generating electricity from the oceans," Renew Sustain Energy Rev, vol. 15, pp. 3399-416, 2011.
5. S. Astariz and G. Iglesias, " G. Enhancing marine energy competitiveness: Co-located offshore wind and wave energy farms," Coast Eng Proc, vol. 1, p. waves.4, 2017.
6. P. Contestabile, E. Di Lauro, P. Galli, C. Corselli, and D. Vicinanza, "Offshore Wind and Wave Energy Assessment around Malè and Magoodhoo Island (Maldives)," Sustainability, vol. 9, 2017.
7. C. V. C. Weiss, R. Guanche, B. Ondiviela, O. F. Castellanos, and J. Juanes, "Marine renewable energy potential: A global perspective for offshore wind and wave exploitation," Energy Convers Manag, vol. 177, pp. 43-54, 2018.
8. C. Pérez-Collazo, D. M. Greaves, and G. Iglesias, "A review of combined wave and offshore wind energy," Renew Sustain Energy Rev, vol. 42, pp. 141-53, 2015.
9. C. G. Soares, J. Bhattacharjee, and D. Karmakar, "Overview and prospects for development of wave and offshore wind energy," 2014.

10. Z. Chen, J. M. Guerrero, and F. Blaabjerg, "A Review of the State of the Art of Power Electronics for Wind Turbines," IEEE Trans Power Electron, vol. 24, pp. 1859-75, 2009.
11. J. Li, G. Wang, Z. Li, S. Yang, W. T. Chong, and X. Xiang, "A review on development of offshore wind energy conversion system," Int J Energy Res, vol. 44, pp. 9283-97, 2020.
12. R. Perveen, N. Kishor, and S. R. Mohanty, "Off-shore wind farm development: Present status and challenges," Renew Sustain Energy Rev, vol. 29, pp. 780-92, 2014.
13. N. Ertugrul and D. Abbott, "DC is the Future [Point of View]," Proc IEEE, vol. 108, pp. 615-24, 2020.
14. R. Cardenas, R. Pena, S. Alepuz, and G. Asher, "Overview of Control Systems for the Operation of DFIGs in Wind Energy Applications," IEEE Trans Ind Electron, vol. 60, pp. 2776-98, 2013.
15. A. Fernández-Guillamón, K. Das, N. A. Cutululis, and Á. Molina-García, "Offshore Wind Power Integration into Future Power Systems: Overview and Trends," J Mar Sci Eng, vol. 7, 2019.
16. S. M. Tripathi, A. N. Tiwari, and D. Singh, "Grid-integrated permanent magnet synchronous generator based wind energy conversion systems: A technology review," Renew Sustain Energy Rev, vol. 51, pp. 1288-305, 2015.
17. P. Tavner, "Offshore Wind Turbines: Reliability, availability and maintenance," Institution of Engineering and Technology, 2012.
18. López, J. Andreu, S. Ceballos, I. M. de Alegría, and I. Kortabarria, "Review of wave energy technologies and the necessary power-equipment," Renew. Sustain. Energy Rev., vol. 27, pp. 413-434, 2013.

19. D. Magagna and A. Uihlein, "Ocean energy development in Europe: Current status and future perspectives," Int J Mar Energy, vol. 11, pp. 84-104, 2015.
20. W. Sheng, R. Alcorn, and A. Lewis, "On thermodynamics in the primary power conversion of oscillating water column wave energy converters," J Renew Sustain Energy, vol. 5, p. 23105, 2013.
21. D. O'Sullivan, D. Mollaghan, A. Blavette, and R. Alcorn, "Dynamic Characteristics of Wave and Tidal Energy Converters & a Recommended Structure for Development of a Generic Model for Grid Connection," 2010.
22. C. A. Rodríguez, P. Rosa-Santos, and F. Taveira-Pinto, "Assessment of the power conversion of wave energy converters based on experimental tests," Energy Convers Manag, vol. 173, pp. 692-703, 2018.
23. B. McGilton, A. A. Almoraya, R. Raihan, R. Crozier, N. J. Baker, and M. Mueller, "Investigation into linear generators with integrated magnetic gear for wave energy power take off," J Eng, vol. 2019, pp. 5069-72.
24. M. Li and X. Jing, "A bistable X-structured electromagnetic wave energy converter with a novel mechanical-motion-rectifier: Design, analysis, and experimental tests," Energy Convers Manag, vol. 244, p. 114466, 2021.
25. M. Karimirad, "Offshore Energy Structures: For Wind Power, Wave Energy and Hybrid Marine Platforms," 1st ed., Springer Cham.
26. W. Chen, F. Gao, X. Meng, B. Chen, and A. Ren, "W2P: A high-power integrated generation unit for offshore wind power and ocean wave energy," Ocean Eng, vol. 128, pp. 41-7, 2016.

27. M. Karimirad and K. Koushan, "WindWEC: Combining wind and wave energy inspired by hywind and wavestar," 2016 IEEE Int. Conf. Renew. Energy Res. Appl., 2016, pp. 96-101.
28. L. Marquis, M. B. Kramer, J. V. Kringelum, J. F. Chozas, and N. E. Helstrup, "Introduction Of Wavestar Wave Energy Converters At The Danish Offshore Wind Power Plant Horns Rev 2," 2012.
29. E. D. Stoutenburg, N. Jenkins, and M. Z. Jacobson, "Power output variations of co-located offshore wind turbines and wave energy converters in California," Renew Energy, vol. 35, pp. 2781-91, 2010.
30. L. Wang, C.-Y. Lin, H.-Y. Wu, and A. V. Prokhorov, "Stability Analysis of a Microgrid System with a Hybrid Offshore Wind and Ocean Energy Farm Fed to a Power Grid Through an HVDC Link," IEEE Trans Ind Appl, vol. 54, pp. 2012-22, 2018.
31. S. Lu, L. Wang, T.-M. Lo, and A. V. Prokhorov, "Integration of Wind Power and Wave Power Generation Systems Using a DC Microgrid," IEEE Trans Ind Appl, vol. 51, pp. 2753-61, 2015.
32. Nehrir, M. H., Wang, C., Strunz, K., Aki, H., Ramakumar, R., Bing, J., & Salameh, Z. "A review of hybrid renewable/alternative energy systems for electric power generation: Configurations, control, and applications. IEEE transactions on sustainable energy", 2(4), pp 392-403, 2011.
33. F. Nejabatkhah and Y. W. Li, "Overview of Power Management Strategies of Hybrid AC/DC Microgrid," IEEE Trans Power Electron, vol. 30, pp. 7072-89, 2015.
34. A. Chauhan and R. P. Saini, "A review on Integrated Renewable Energy System based power generation for stand-alone applications: Configurations, storage

options, sizing methodologies and control," Renew Sustain Energy Rev, vol. 38, pp. 99-120, 2014.

35. A. H. Fathima and K. Palanisamy, "Optimization in microgrids with hybrid energy systems – A review," Renew Sustain Energy Rev, vol. 45, pp. 431-46, 2015.
36. M. F. Zia, E. Elbouchikhi, and M. Benbouzid, "Microgrids energy management systems: A critical review on methods, solutions, and prospects," Appl Energy, vol. 222, pp. 1033-55, 2018.
37. Kalogeri, C., Galanis, G., Spyrou, C., Diamantis, D., Baladima, F., Koukoula, M. and Kallos, G. "Assessing the European offshore wind and wave energy resource for combined exploitation". Renewable energy, 101, pp.244-264, 2017.
38. S. Astariz and G. Iglesias, "Output power smoothing and reduced downtime period by combined wind and wave energy farms," Energy, vol. 97, pp. 69-81, 2016.
39. Y. Wen, B. Kamranzad, and P. Lin, "Joint exploitation potential of offshore wind and wave energy along the south and southeast coasts of China," Energy, vol. 249, p. 123710, 2022.
40. K. L. McTiernan and K. T. Sharman, "Review of Hybrid Offshore Wind and Wave Energy Systems," J Phys Conf Ser, vol. 1452, p. 12016, 2020.
41. L. Wu, M. Shao, and E. Sahlée, "Impact of Air–Wave–Sea Coupling on the Simulation of Offshore Wind and Wave Energy Potentials," Atmosphere (Basel), vol. 11, 2020.
42. S. Astariz and G. Iglesias, "Enhancing Wave Energy Competitiveness through Co-Located Wind and Wave Energy Farms. A Review on the Shadow Effect," Energies, vol. 8, pp. 7344-66, 2015.

43. M. Borg, M. Collu, and F.P. Brennan, "Use of a wave energy converter as a motion suppression device for floating wind turbines," Energy Procedia, vol. 35, pp. 223-233, 2013.
44. E.E. Bachynski, V. Chabaud, and T. Sauder, "Real-time hybrid model testing of floating wind turbines: Sensitivity to limited actuation," Energy Procedia, vol. 80, pp. 2-12, 2015.
45. O. El Beshbichi, Y. Xing, and M.C. Ong, "An object-oriented method for fully coupled analysis of floating offshore wind turbines through mapping of aerodynamic coefficients," Mar. Struct., vol. 78, article 102979, 2021.
46. L. Xu, C. Zhang, and X. Zhu, "Decoupling control of a dual-stator linear and rotary permanent magnet generator for offshore joint wind and wave energy conversion system," IET Electr Power Appl, vol. 14, pp. 561-9, 2020.
47. C. Perez-Collazo, D. Greaves, and G. Iglesias, "Hydrodynamic response of the WEC sub-system of a novel hybrid wind-wave energy converter," Energy Convers Manag, vol. 171, pp. 307-25, 2018.
48. Y. Wang, L. Zhang, C. Michailides, L. Wan, and W. Shi, "Hydrodynamic Response of a Combined Wind–Wave Marine Energy Structure," J Mar Sci Eng, vol. 8, 2020.
49. Y. Zhou, D. Ning, W. Shi, L. Johanning, and D. Liang, "Hydrodynamic investigation on an OWC wave energy converter integrated into an offshore wind turbine monopile," Coast Eng, vol. 162, p. 103731, 2020.
50. Y. Si, J. Liu, S. Wang, L. Li, L. Li, "The influence of power-take-off control on the dynamic response and power output of combined semi-submersible floating wind turbine and point-absorber wave energy converters," Ocean Eng, vol. 227, p. 108835, 2021.

51. Y. Wang, C. Yang, X. Li, X. Zhang, "WEC shape effect on the motion response and power performance of a combined wind-wave energy converter," Ocean Eng, vol. 250, p. 111038, 2022.
52. J. S. Rony and D. Karmakar, "Coupled Dynamic Analysis of Hybrid Offshore Wind Turbine and Wave Energy Converter," J Offshore Mech Arct Eng, vol. 144, 2021.
53. Muliawan, M.J., Karimirad, M., Gao, Z. and Moan, T., "Extreme responses of a combined spar-type floating wind turbine and floating wave energy converter (STC) system with survival modes," Ocean Eng, vol. 65, pp. 71-82, 2013.
54. L. Wan, Z. Gao, and T. Moan, "Experimental and numerical study of hydrodynamic responses of a combined wind and wave energy converter concept in survival modes," Coast Eng, vol. 104, pp. 151-69, 2015.
55. D.N. Konispoliatis, D.I. Manolas, S.G. Voutsinas, S.A. Mavrakos, "Coupled Dynamic Response of an Offshore Multi-Purpose Floating Structure Suitable for Wind and Wave Energy Exploitation," Front. Energy Res., vol. 6, p. 786, 2022.
56. J.F. Gaspar, M. Kamarlouei, F. Thiebaut, C.G. Soares, "Compensation of a hybrid platform dynamics using wave energy converters in different sea state conditions," Renew. Energy, vol. 177, pp. 871–883, 2021.
57. M. Chen, P. Xiao, Z. Zhang, L. Sun, F. Li, "Effects of the end-stop mechanism on the nonlinear dynamics and power generation of a point absorber in regular waves," Ocean. Eng., vol. 242, p. 110123, 2021.
58. M. Chen, P. Xiao, H. Zhou, C.B. Li, X. Zhang, "Fully Coupled Analysis of an Integrated Floating Wind-Wave Power Generation Platform in Operational Sea-states," Front. Energy Res., vol. 10, p. 819, 2022.

59. K. Sun, Y. Yi, X. Zheng, L. Cui, C. Zhao, M. Liu, X. Rao, "Experimental investigation of semi-submersible platform combined with point-absorber array," Energy Convers. Manag., vol. 245, p. 114623, 2021.
60. Hu, J., Zhou, B., Vogel, C., Liu, P., Willden, R., Sun, K., ... & Collu, M., "Optimal design and performance analysis of a hybrid system combing a floating wind platform and wave energy converters," Appl. Energy, vol. 269, p. 114998, 2020.
61. L. Wan, M. Greco, C. Lugni, Z. Gao, T. Moan, "A combined wind and wave energy-converter concept in survival mode: Numerical and experimental study in regular waves with a focus on water entry and exit," Appl. Ocean Res., vol. 63, pp. 200–216, 2017.
62. H. Lee, Y.H. Bae, I.-H. Cho, "One-way Coupled Response Analysis between Floating Wind-Wave Hybrid Platform and Wave Energy Converters," J. Ocean Eng. Technol., vol. 30, pp. 84–90, 2016.
63. Z. Gao, T. Moan, L. Wan, C. Michailides, "Comparative numerical and experimental study of two combined wind and wave energy concepts," J. Ocean Eng. Sci., vol. 1, pp. 36–51, 2016.
64. N. Ren, Z. Gao, T. Moan, L. Wan, "Long-term performance estimation of the Spar–Torus-Combination (STC) system with different survival modes," Ocean. Eng., vol. 108, pp. 716–728, 2015.
65. M.J. Muliawan, M. Karimirad, T. Moan, Z. Gao, "STC (Spar-Torus Combination): A Combined Spar-Type Floating Wind Turbine and Large Point Absorber Floating Wave Energy Converter—Promising and Challenging," in Proc. ASME 2012 31st Int. Conf. Ocean, Offshore and Arctic Engineering, Rio de Janeiro, Brazil, 1–6 July 2012, vol. 7, pp. 667–676.

66. S. Ding, S. Yan, D. Han, Q. Ma, "Overview on Hybrid Wind-Wave Energy Systems," in Proc. 2015 Int. Conf. Appl. Sci. Eng. Innovation, Jinan, China, 30–31 August 2015, pp. 502–527.
67. A. Peiffer, D. Roddier, A. Aubault, "Design of a Point Absorber Inside the WindFloat Structure," in Proc. ASME 2011 30th Int. Conf. Ocean, Offshore and Arctic Engineering, Rotterdam, The Netherlands, 19–24 June 2011, vol. 5, pp. 247–255.
68. Hasselmann, K., Barnett, T.P., Bouws, E., Carlson, H., Cartwright, D.E., Enke, K., Ewing, J.A., Gienapp, A., Hasselmann, D.E., Kruseman, P. and Meerburg, A., "Measurements of wind-wave growth and swell decay during the Joint North Sea Wave Project (JONSWAP)," Ergaenzungsheft Dtsch. Hydrogr. Z. Reihe A, 1973.
69. E. Homayoun, H. Ghassemi, H. Ghafari, "Power Performance of the Combined Monopile Wind Turbine and Floating Buoy with Heave-type Wave Energy Converter," Pol. Marit. Res., vol. 26, pp. 107–114, 2019.
70. H.R. Martin, R.W. Kimball, A.M. Viselli, A.J. Goupee, "Methodology for Wind/Wave Basin Testing of Floating Offshore Wind Turbines," J. Offshore Mech. Arct. Eng., vol. 136, p. 20905, 2012.
71. P. L. C. Der Valk, "Coupled Simulations of Wind Turbines and Offshore Support Structures: Strategies Based on the Dynamic Substructuring Paradigm," Wöhrmann Print Service: Zutphen, The Netherlands, 2014.
72. S. Astariz and G. Iglesias, "Selecting optimum locations for co-located wave and wind energy farms. Part II: A case study," Energy Convers. Manag., vol. 122, pp. 599–608, 2016.
73. Quevedo, E., Cartón, M., Delory, E., Castro, A., Hernández, J., Llinás, O., De Lara, J., Papandroulakis, N., Anastasiadis, P., Bard, J. and Jeffrey, H., "Multi-use offshore

platform configurations in the scope of the FP7 TROPOS Project," in Proceedings of the 2013 MTS/IEEE Oceans, Bergen, Norway, 10–14 June 2013, pp. 1–7.

74. S. Y. Boo, K.-H. Kim, K. Lee, S. Park, J.-S. Choi, K. Hong, "Design challenges of a Hybrid Platform with multiple wind turbines and wave energy converters," in Proceedings of the SNAME 21st Offshore Symposium, Houston, TX, USA, 16 February 2016.
75. T. Salic, J.F. Charpentier, M. Benbouzid, M. Le Boulluec, "Control strategies for floating offshore wind turbine: Challenges and trends," Electronics, vol. 8, p. 1185, 2019.
76. "IEC 61400-3-1:2019; Turbines—Part 3: Design Requirements for Offshore Wind Turbines," International Organization for Standardization: Geneva, Switzerland, 2019.
77. B. Skaare, T. D. Hanson, and F. G. Nielsen, "Importance of control strategies on fatigue life of floating wind turbines," Int. Conf. Offshore Mech. Arct. Eng., 2007, pp. 493–500.
78. A. Pecher and J. P. Kofoed, "Handbook of Ocean Wave Energy," Springer Nature: Berlin, Germany, 2017.
79. J. Abanades, D. Greaves, and G. Iglesias, "Wave farm impact on the beach profile: A case study," Coast. Eng., vol. 86, pp. 36–44, 2014.
80. R. Carballo and G. Iglesias, "Wave farm impact based on realistic wave-WEC interaction," Energy, vol. 51, pp. 216–229, 2013.
81. Q. Gao, N. Ertugrul, B. Ding, M. Negnevitsky, "Offshore wind, wave and integrated energy conversion systems: A review and future," in Proceedings of the 2020

Australasian Universities Power Engineering Conference, Hobart, Australia, 29 November–2 December 2020, pp. 1–6.

82. M. Ayub and X. Ma, "Non-linear supertwisting speed control PMSG based Higher Order Sliding Mode Control," in Proceedings of the 2021 26th International Conference on Automation and Computing (ICAC), Portsmouth, UK, 2–4 September 2021.
83. E. Rusu and V. Venugopal, "Offshore Renewable Energy: Ocean Waves, Tides and Offshore Wind," Energies, vol. 12, p. 182, 2019.
84. K. M. Exo, O. Huppop, and S. Garthe, "Birds and offshore wind farms: A hot topic in marine ecology," Bull. Wader Study Group, vol. 100, pp. 50–53, 2003.
85. A. L. Drewitt and R. H. W. Langston, "Assessing the impacts of wind farms on birds," Ibis, vol. 148, pp. 29–42, 2006.
86. A. H. Fayram and A. de Risi, "The potential compatibility of offshore wind power and fisheries: An example using bluefin tuna in the Adriatic Sea," Ocean Coast. Manag., vol. 50, pp. 597–605, 2007.
87. A. Azzellino, V. Ferrante, J.P. Kofoed, C. Lanfredi, D. Vicinanza, "Optimal siting of offshore wind-power combined with wave energy through a marine spatial planning approach," Int. J. Mar. Energy, vol. 3, pp. e11–e25, 2013.
88. E. Petracca, E. Faraggiana, A. Ghigo, M. Sirigu, G. Bracco, G. Mattiazzo, "Design and Techno-Economic Analysis of a Novel Hybrid Offshore Wind and Wave Energy System," Energies, vol. 15, p. 2739, 2022.
89. Abhinav, K.A., Collu, M., Benjamins, S., Cai, H., Hughes, A., Jiang, B., Jude, S., Leithead, W., Lin, C., Liu, H. and Recalde-Camacho, L., "Offshore multi-purpose

platforms for a Blue Growth: A technological, environmental and socio-economic review," Sci. Total Environ., vol. 734, p. 138256, 2020.

90. Dalton, G., Bardócz, T., Blanch, M., Campbell, D., Johnson, K., Lawrence, G., Lilas, T., Friis-Madsen, E., Neumann, F., Nikitas, N. and Ortega, S.T., "Feasibility of investment in Blue Growth multiple-use of space and multi-use platform projects; results of a novel assessment approach and case studies," Renew. Sustain. Energy Rev., vol. 107, pp. 338–359, 2019.
91. I. Legorburu, K.R. Johnson, S.A. Kerr, "Multi-use maritime platforms-North Sea oil and offshore wind: Opportunity and risk," Ocean. Coast. Manag., vol. 160, pp. 75–85, 2018
92. A. Afifi, S. May, and V. A. Clark, "Computer-Aided Multivariate Analysis," CRC Press, Boca Raton, FL, USA, 2003.
93. W. G. Large, J. Morzel, and G. Crawford, "Accounting for surface wave distortion of the marine wind profile in low-level ocean storms wind measurements," J. Phys. Oceanogr., vol. 25, pp. 2959–2971, 1995.
94. J. F. Manwell, J. G. McGowan, and A. L. Rogers, "Wind Energy Explained: Theory, Design and Application," John Wiley & Sons, Hoboken, NJ, USA, 2010.
95. C. Pérez-Collazo, M. M. Jakobsen, H. Buckland, and J. Fernández-Chozas, "Synergies for a Wave-Wind Energy Concept," University of Plymouth, Plymouth, UK, 2013.
96. P. L. C. Der Valk, "Coupled Simulations of Wind Turbines and Offshore Support Structures: Strategies Based on the Dynamic Substructuring Paradigm," Wöhrmann Print Service, Zutphen, The Netherlands, 2014.

97. S. Astariz and G. Iglesias, "Selecting optimum locations for co-located wave and wind energy farms. Part II: A case study," Energy Convers. Manag., vol. 122, pp. 599–608, 2016.

98. Lu, S.Y., Jason, C.S., Wesnigk, J., Delory, E., Quevedo, E., Hernández, J., Llinás, O., Golmen, L., Papandroulakis, N. and Anastasiadis, P. "Environmental aspects of designing multi-purpose offshore platforms in the scope of the FP7 TROPOS Project". In OCEANS 2014-TAIPEI, pp. 1-8, 2014.

99. Boo, S.Y., Kim, K.H., Lee, K., Park, S., Choi, J.S. and Hong, K., "Design challenges of a Hybrid Platform with multiple wind turbines and wave energy converters," in Proc. SNAME 21st Offshore Symposium, Houston, TX, USA, 16 February 2016.

100. T. Salic, J. F. Charpentier, M. Benbouzid, M. Le Boulluec, "Control strategies for floating offshore wind turbine: Challenges and trends," Electronics, vol. 8, p. 1185, 2019.

101. "IEC 61400-3-1:2019; Turbines—Part 3: Design Requirements for Offshore Wind Turbines," International Organization for Standardization, Geneva, Switzerland, 2019.

102. B. Skaare, T.D. Hanson, and F.G. Nielsen, "Importance of control strategies on fatigue life of floating wind turbines," in Proc. Int. Conf. Offshore Mech. Arct. Eng., 2007, pp. 493–500.

103. A. Pecher and J.P. Kofoed, "Handbook of Ocean Wave Energy," Springer Nature, Berlin, Germany, 2017.

104. J. Abanades, D. Greaves, and G. Iglesias, "Wave farm impact on the beach profile: A case study," Coast. Eng., vol. 86, pp. 36–44, 2014.

105. R. Carballo and G. Iglesias, "Wave farm impact based on realistic wave-WEC interaction," Energy, vol. 51, pp. 216–229, 2013.

106. Q. Gao, N. Ertugrul, B. Ding, and M. Negnevitsky, "Offshore wind, wave and integrated energy conversion systems: A review and future," in Proc. 2020 Australasian Universities Power Engineering Conference, Hobart, Australia, 2020, pp. 1–6.

107. M. Ayub and X. Ma, "Non-linear supertwisting speed control PMSG based Higher Order Sliding Mode Control," in Proc. 2021 26th Int. Conf. Autom. Comput. (ICAC), Portsmouth, UK, 2021, pp. 1–6.

108. E. Rusu and V. Venugopal, "Offshore Renewable Energy: Ocean Waves, Tides and Offshore Wind," Energies, vol. 12, p. 182, 2019.

109. K.-M. Exo, O. Huppop, and S. Garthe, "Birds and offshore wind farms: A hot topic in marine ecology," Bull. Wader Study Group, vol. 100, pp. 50–53, 2003.

110. A.L. Drewitt and R.H.W. Langston, "Assessing the impacts of wind farms on birds," Ibis, vol. 148, pp. 29–42, 2006.

111. A.H. Fayram and A. de Risi, "The potential compatibility of offshore wind power and fisheries: An example using bluefin tuna in the Adriatic Sea," Ocean Coast. Manag., vol. 50, pp. 597–605, 2007.

112. A. Azzellino, V. Ferrante, J.P. Kofoed, C. Lanfredi, and D. Vicinanza, "Optimal siting of offshore wind-power combined with wave energy through a marine spatial planning approach," Int. J. Mar. Energy, vol. 3, pp. e11–e25, 2013.

113. E. Petracca, E. Faraggiana, A. Ghigo, M. Sirigu, G. Bracco, and G. Mattiazzo, "Design and Techno-Economic Analysis of a Novel Hybrid Offshore Wind and Wave Energy System," Energies, vol. 15, p. 2739, 2022.

114. Abhinav, K.A., Collu, M., Benjamins, S., Cai, H., Hughes, A., Jiang, B., Jude, S., Leithead, W., Lin, C., Liu, H. and Recalde-Camacho, L., "Offshore multi-purpose platforms for a Blue Growth: A technological, environmental and socio-economic review," Sci. Total Environ., vol. 734, p. 138256, 2020.

115. Dalton, G., Bardócz, T., Blanch, M., Campbell, D., Johnson, K., Lawrence, G., Lilas, T., Friis-Madsen, E., Neumann, F., Nikitas, N. and Ortega, S.T., "Feasibility of investment in Blue Growth multiple-use of space and multi-use platform projects; results of a novel assessment approach and case studies," Renew. Sustain. Energy Rev., vol. 107, pp. 338–359, 2019.

116. I. Legorburu, K.R. Johnson, and S.A. Kerr, "Multi-use maritime platforms-North Sea oil and offshore wind: Opportunity and risk," Ocean. Coast. Manag., vol. 160, pp. 75–85, 2018.

117. M. A. Abdullah, A. Yatim, C. W. Tan, and R. Saidur, "A review of maximum power point tracking algorithms for wind energy systems," Renewable and Sustainable Energy Reviews, vol. 16, pp. 3220-3227, 2012.

118. Q. Wang and L. Chang, "An intelligent maximum power extraction algorithm for inverter-based variable speed wind turbine systems," IEEE Transactions on Power Electronics, vol. 19, pp. 1242-1249, 2004.

119. J. A. Baroudi, V. Dinavahi, and A. M. Knight, "A review of power converter topologies for wind generators," Renewable Energy, vol. 32, no. 14, pp. 2369-2385, 2007.

120. B. Housseini, A. F. Okou, and R. Beguenane, "Performance comparison of variable speed PMSG-based wind energy conversion system control algorithms," in 2017

Twelfth International Conference on Ecological Vehicles and Renewable Energies (EVER), pp. 1-10, IEEE, 2017.

121. V. Yaramasu, A. Dekka, M. J. Durán, S. Kouro, and B. Wu, "PMSG-based wind energy conversion systems: survey on power converters and controls," IET Electric Power Applications, vol. 11, no. 6, pp. 956-968, 2017.
122. Y. Soufi, S. Kahla, and M. Bechouat, "Feedback linearization control based particle swarm optimization for maximum power point tracking of wind turbine equipped by PMSG connected to the grid," International Journal of Hydrogen Energy, vol. 41, pp. 20950-20955, 2016.
123. Khan, M.A., Ullah, S., Khan, L., Khan, Q., Khan, Z.A., Zaman, H. and Ahmad, S. "Observer Based Higher Order Sliding Mode Control Scheme for PMSG-WECS." 15th International Conference on Emerging Technologies (ICET) IEEE, pp. 1-6, 2019.
124. Y. Bazargan-Lari, M. Eghtesad, and B. Assadsangabi, "Study of internal dynamics stability and regulation of globular spray mode of GMAW process via MIMO feedback-linearization scheme," in International Conference on Intelligent Engineering Systems, pp. 31-36, 2008.
125. Simone, Dominic J. "Modeling a linear generator for energy harvesting applications." Diss. Monterey, California: Naval Postgraduate School, 2014.
126. C. Wei, Z. Zhang, W. Qiao, and L. Qu, "An adaptive network-based reinforcement learning method for MPPT control of PMSG wind energy conversion systems," IEEE Transactions on Power Electronics, vol. 31, pp. 7837-7848, 2016.

127. S. M. Barakati, M. Kazerani, and J. D. Aplevich, "Maximum power tracking control for a wind turbine system including a matrix converter," IEEE Transactions on Energy Conversion, vol. 24, pp. 705-713, 2009.
128. S. M. R. Kazmi, H. Goto, H.-J. Guo, and O. Ichinokura, "Review and critical analysis of the research papers published till date on maximum power point tracking in wind energy conversion system," in IEEE Energy Conversion Congress and Exposition, pp. 4075-4082, 2010.
129. S. M. Barakati, M. Kazerani, and J. D. Aplevich, "Maximum power tracking control for a wind turbine system including a matrix converter," IEEE Transactions on Energy Conversion, vol. 24, pp. 705-713, 2009.
130. M. Simoes, B. K. Bose, and R. J. Spiegel, "Design and performance evaluation of a fuzzy logic based variable speed wind generation system," in IEEE Industry Applications Conference Thirty-First IAS Annual Meeting, pp. 349-356, 1996.
131. Mishra, S., Shukla, S. and Verma, N., "Comprehensive review on maximum power point tracking techniques: wind energy," in Communication, Control and Intelligent Systems (CCIS), 2015, pp. 464-469.
132. M. Simoes, B. K. Bose, and R. J. Spiegel, "Design and performance evaluation of a fuzzy-logic-based variable-speed wind generation system," IEEE Transactions on Industry Applications, vol. 33, pp. 956–965, 1997.
133. M. Pucci and M. Cirrincione, "Neural MPPT control of wind generators with induction machines without speed sensors," IEEE Transactions on Industrial Electronics, vol. 58, pp. 37–47, 2010.

134. Khan, M. A.; Khan, Q.; Khan, L.; Khan, I.; Alahmadi, A. A.; Ullah, N. "Robust Differentiator-Based Neuro Fuzzy Sliding Mode Control Strategies for PMSG-WECS." Energies, vol. 15, p. 7039, 2022.
135. Bazargan-Lari, Y.; Eghtesad, M.; Assadsangabi, B. "Study of internal dynamics stability and regulation of globular-spray mode of GMAW process via MIMO feedback-linearization scheme." In Proceedings of the 2008 International Conference on Intelligent Engineering Systems, IEEE, 2008, pp. 31–36.
136. Khan, I.U.; Khan, L.; Khan, Q.; Ullah, S.; Khan, U.; Ahmad, S. "Neuro-adaptive backstepping integral sliding mode control design for nonlinear wind energy conversion system." Turkish Journal of Electrical Engineering and Computer Sciences, vol. 29, pp. 531–547, 2021.
137. Mat-Noh, M.; Arshad, M.; Mohd-Mokhtar, R.; Khan, Q. "Back-stepping integral sliding mode control (BISMC) application in a nonlinear autonomous underwater glider." In Proceedings of the 2017 IEEE 7th International Conference on Underwater System Technology: Theory and Applications (USYS), IEEE, 2017, pp. 1–6.
138. Khan, Q.; Bhatti, A.I.; Iqbal, S.; Iqbal, M. "Dynamic integral sliding mode for MIMO uncertain nonlinear systems." International Journal of Control, Automation and Systems, vol. 9, pp. 151–160, 2011.
139. N. O. and A. A. US Department of Commerce, “NDBC search and Rescue Data,” National Data Buoy Center, https://www.ndbc.noaa.gov/sar.php?station=62305 (accessed Sep. 6, 2023).

Appendix I

Hybrid offshore wind and wave energy with VSC. The simple inverter is compared with VSI with battery management system.

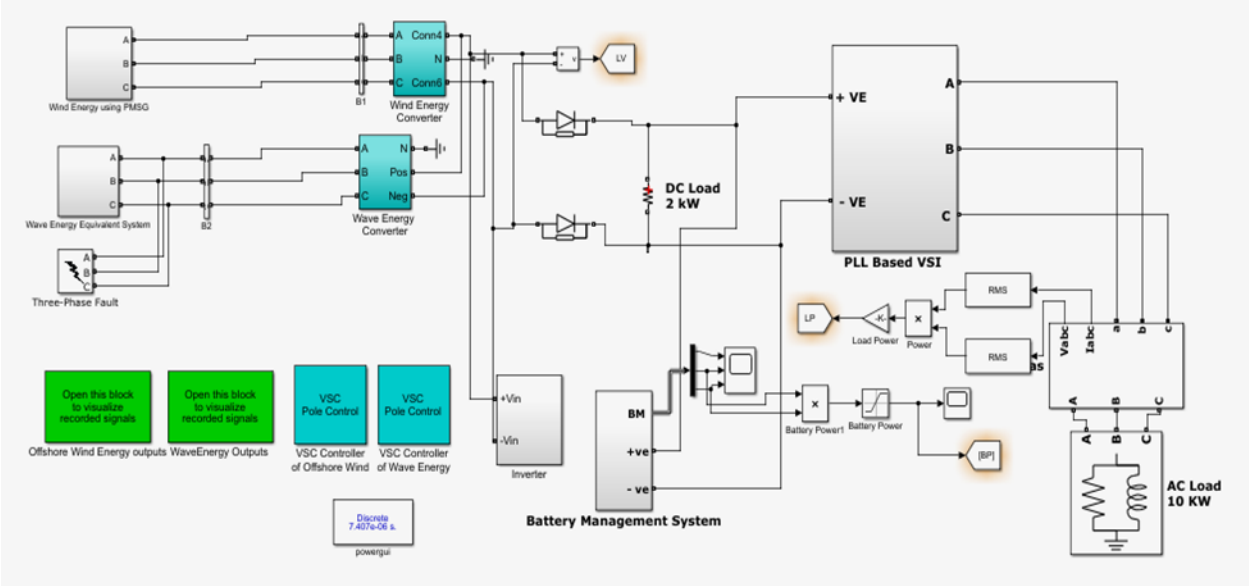

Offshore Wind

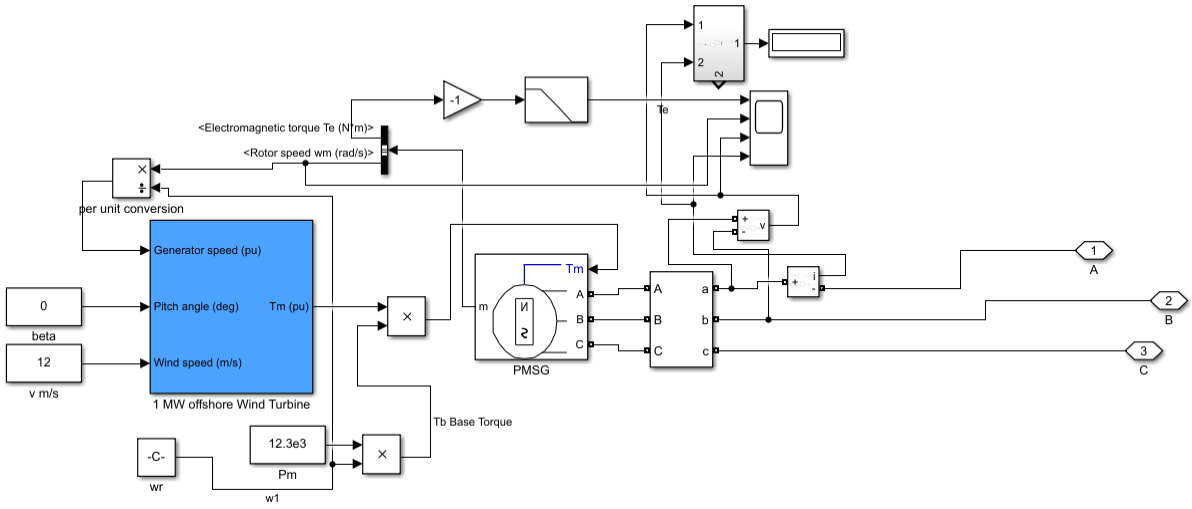

Wave Energy Linear generator

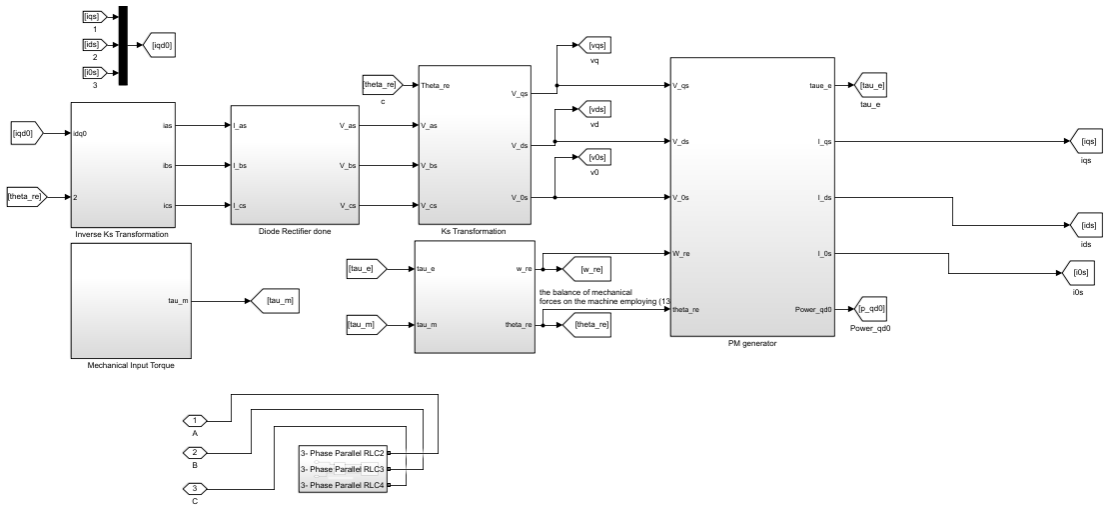

Offshore Wind and Wave Power AC-DC Converter

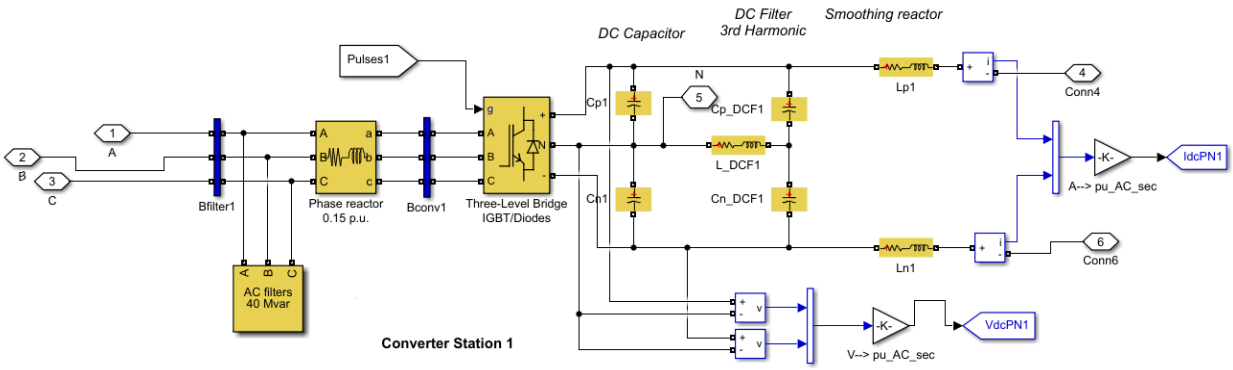

Offshore Wind / Wave Energy Controller Side

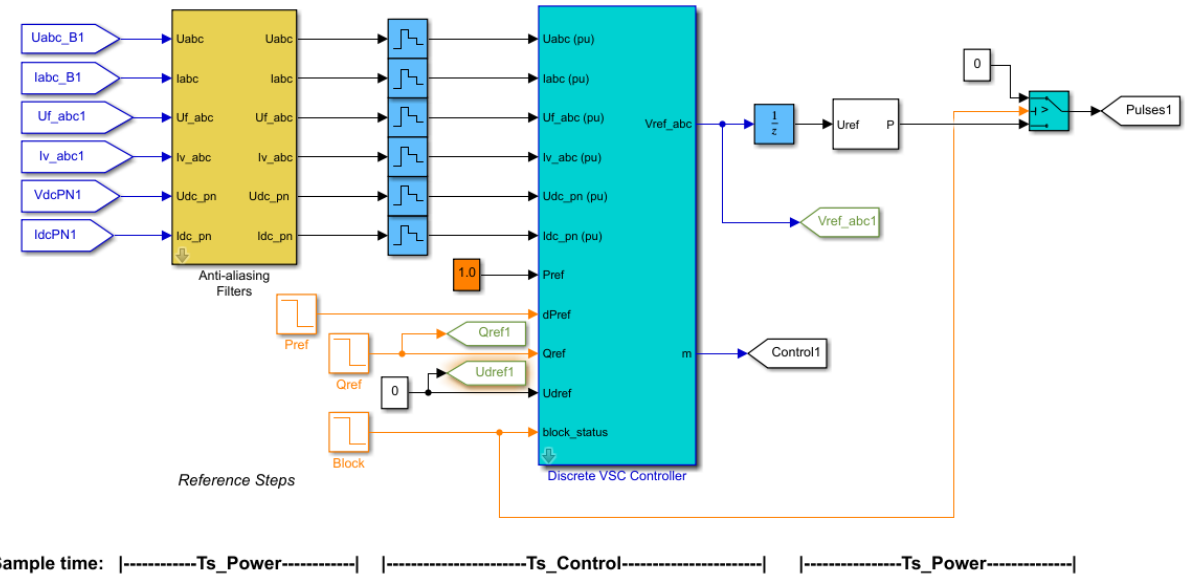

Sample time: |----------Ts_Power----------| |----------Ts_Control----------| |----------Ts_Power----------|

VSC Controller (Station 1)

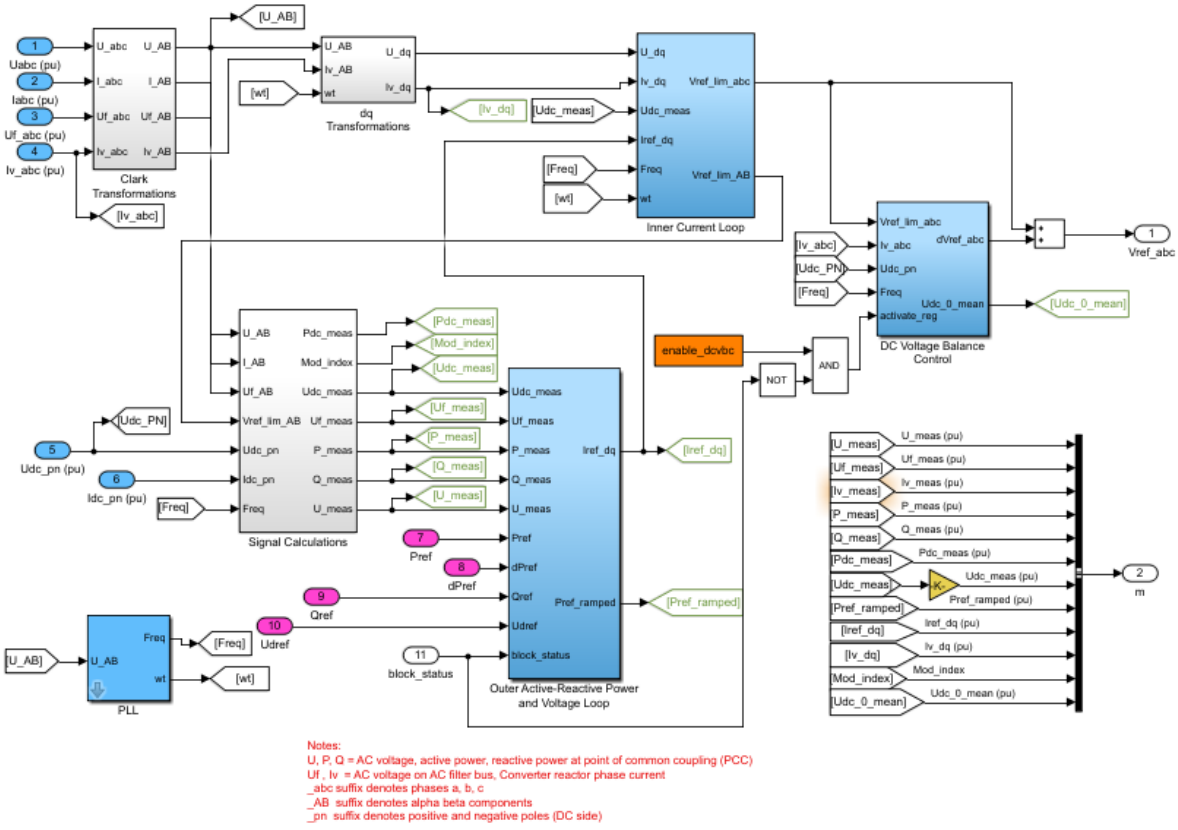

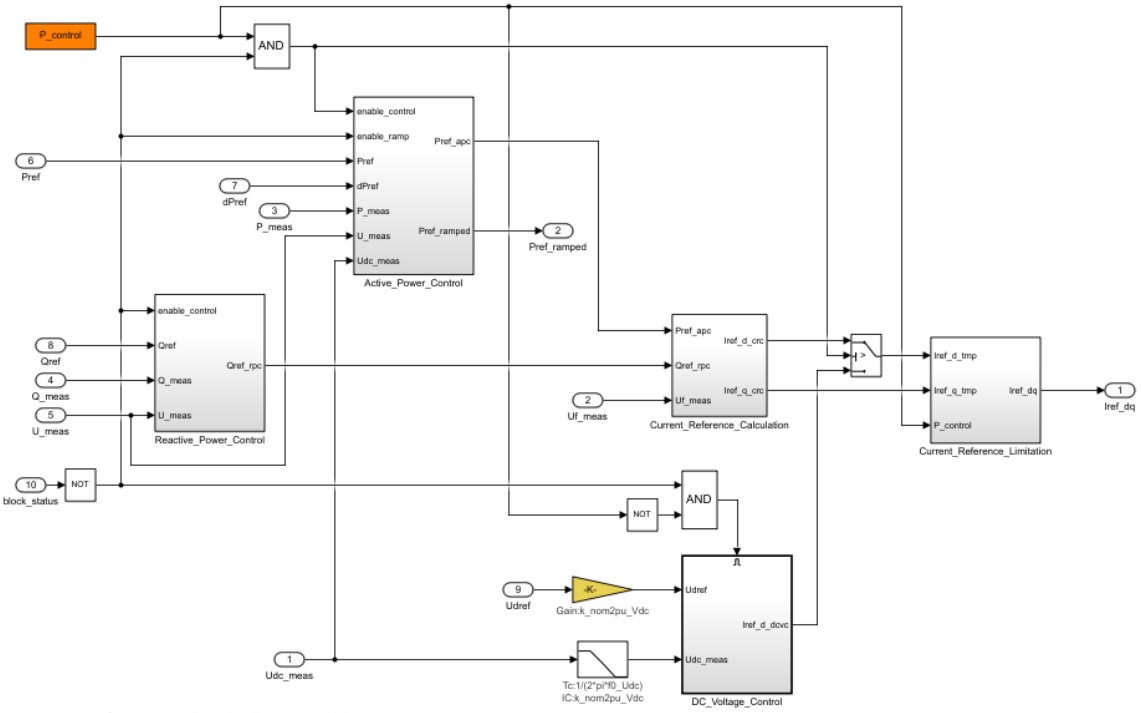

Outer Active-Reactive Power and Voltage Loop

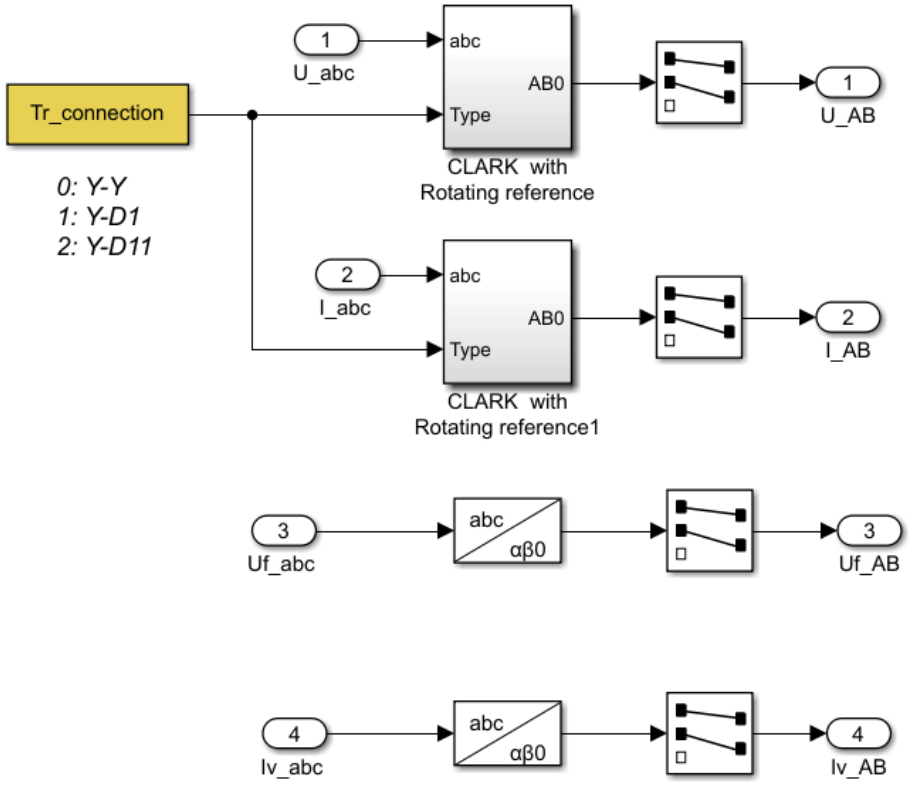

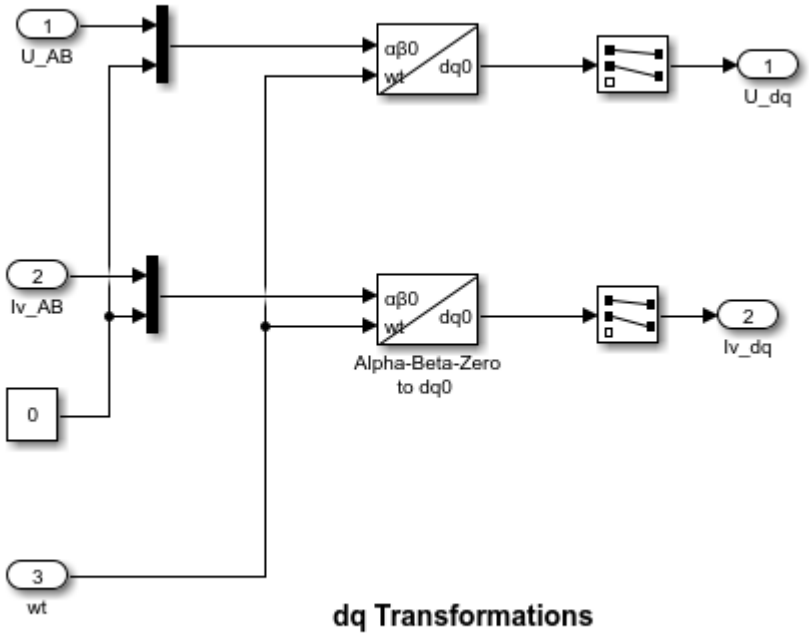

dq Transformations

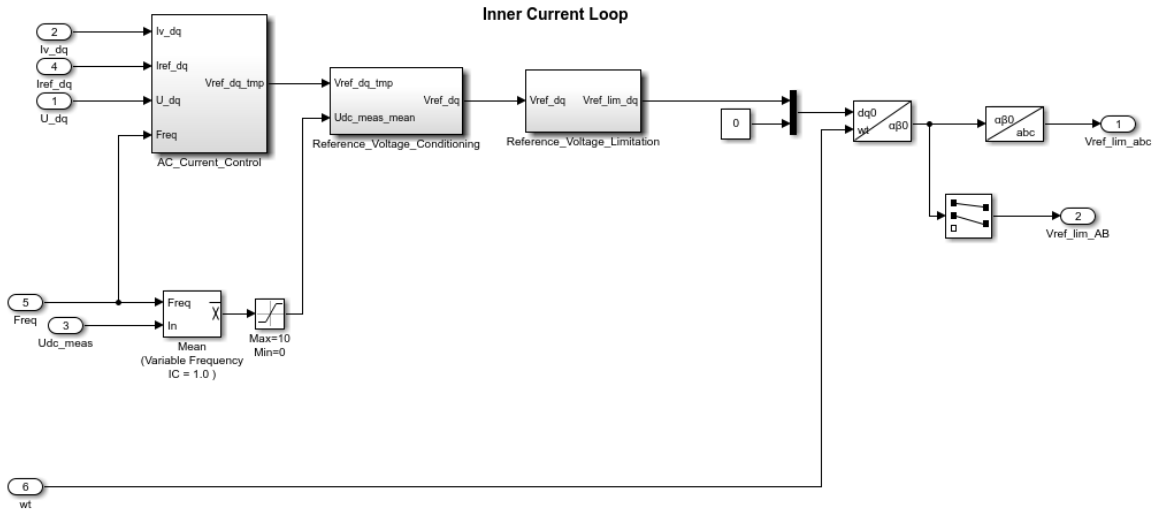

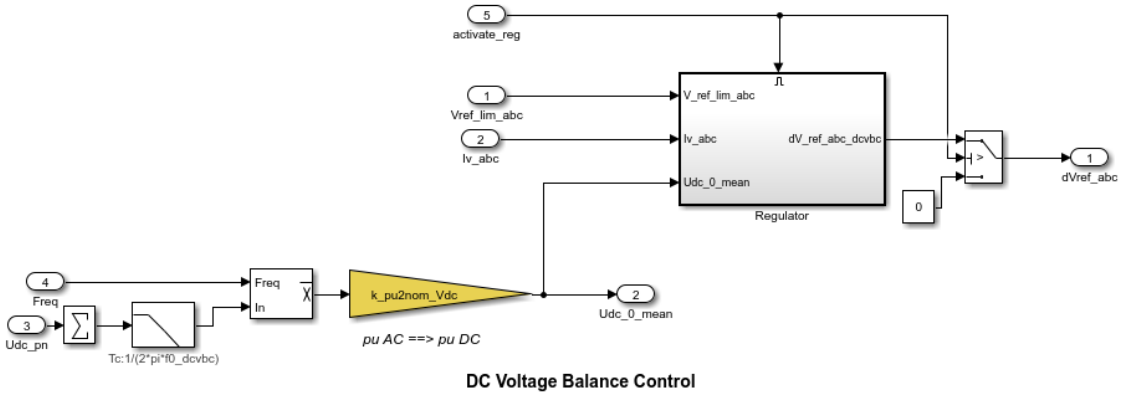

HOWWE Normal Inverter

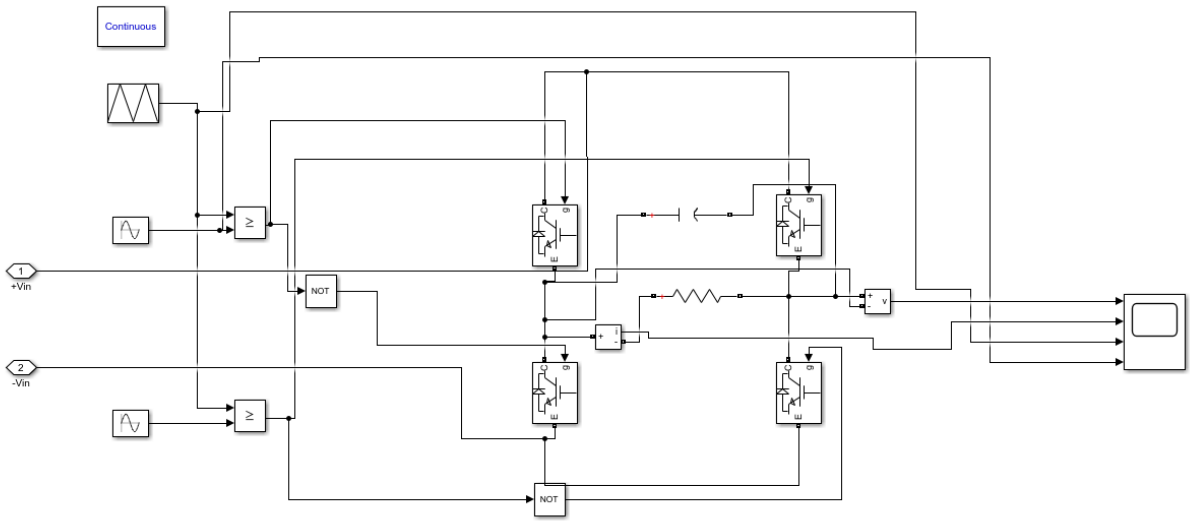

PLL-Based-VSI

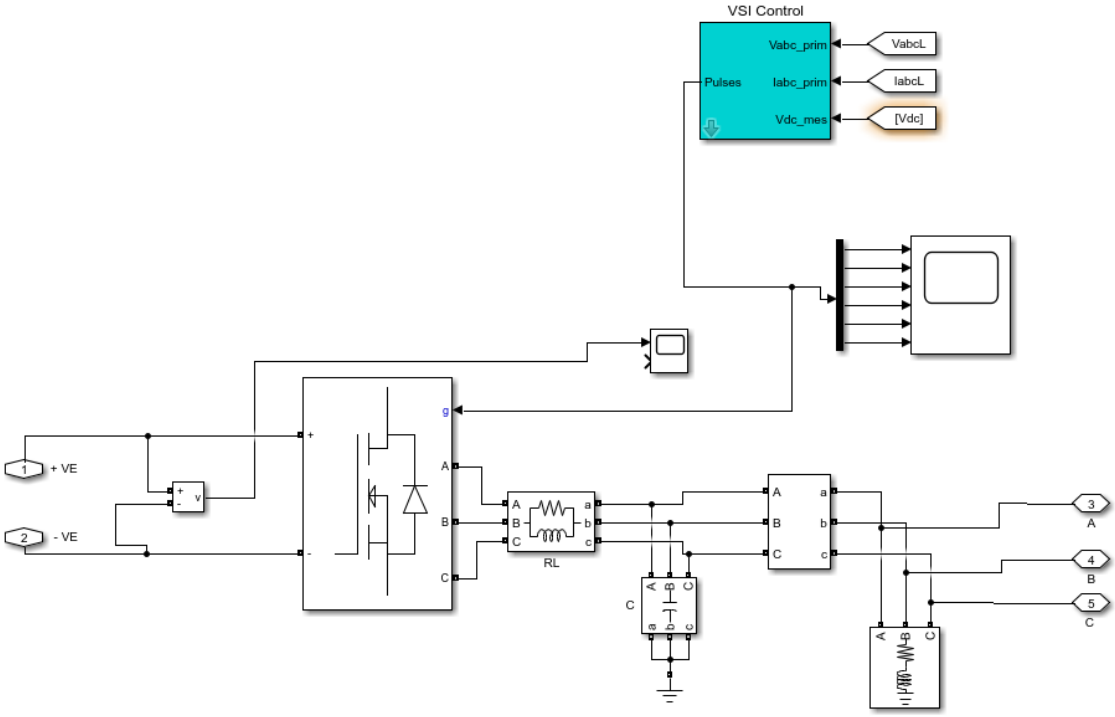

Appendix II

```
% data file for feedback_lin_ctrl.mdl application

% SI units

clear all;

% loading precomputed wind sequece from 'vntu.mat'  (selection is 4)

load vntu, tt=1:length(vK); tt=tt'; vK=vK';

% PMSG parameters

R=3.3                % stator resistance, d,q inductances

Ld=41.56*10^(-3)

Lq=Ld

p=3

Fie=.4382            % ... flux value

% load parameters

Rch_init=80          % initial value of chopper equivalent resistance

Lch=0.08             % inductance

% state-space model parameters, defined in chapter 3.6.2, (3.88)

a1=Ld+Lch

a2=-R/a1

a3=(p*(Lq-Lch))/a1

b1=Lq+Lch

b2=-R/b1

b3=(-p*(Ld+Lch))/b1

b4=(p*Fie)/b1

% wind turbine parameters

ro=1.25              % air density

Rt=2.5               % blade length

lam_opt=7            % optimal ti speed ratio

cp_m=0.47            % maximum power coefficient

i =7                 % transmission ratio

JHSS=0.0042+2.5/(i^2)      % HSS inertia

% parameters of the polynomial approximation of torque coefficient
versus the tip speed, relation (3.82)

alfa1=0.1253;

alfa2=-0.0047;

alfa3=-0.0005;

% parameters of the wind torque expression, relation (3.84)

a=0.5*pi*ro;

d1=alfa1*a*Rt^3;

d2=alfa2*a*Rt^4;

d3=alfa3*a*Rt^5;

% parameter used in the inverse transformation, see (5.37)&(5.38)

d4=p*Fie;

% initial values (states variables - X)

v0=7;

x10=-6.02;

x20=11.09;

x30=137.2;

% new coordinates (Z) state variable initial values

z10=x30;

z20=(d1*v0^2+d2*v0*x30+d3*x30^2-d4*x20);

z30=(1/a1*(x10/x20));

disp('Parameters loaded!')
```

Table 6.2 Real time data of 45 days average wind speed and average sea waves of Silverstone Lightship United Kingdom [139]

Date (UTC)	Average Wind Dir (True)	Average Wind Spd m/s	Wind Obs	Average Seas meters	Wave Obs	Air Temp. (Degrees F.)	Air Temp. Obs	Water Temp. Obs
2023-10-13 0600Z	-	-	0	1.8288	1	62	1	1
2023-10-12 1200Z	-	-	0	1.2192	1	61	1	1
2023-10-11 1200Z	-	-	0	0.9144	2	62	2	2
2023-10-10 1800Z	-	-	0	0.9144	5	61	5	5
2023-10-10 1200Z	-	-	0	0.9144	1	61	1	1
2023-10-10 0000Z	-	-	0	0.9144	5	59	5	5
2023-10-09 1800Z	-	-	0	1.2192	1	61	1	1
2023-10-09 1200Z	140	4.11456	1	1.2192	2	63	2	2
2023-10-09 0000Z	-	-	0	1.524	1	62	1	1
2023-10-08 1800Z	-	-	0	1.524	1	62	1	1
2023-10-08 1200Z	-	-	0	1.524	1	63	1	1
2023-10-08 0600Z	150	5.144	1	1.524	1	62	2	2
2023-10-08 0000Z	-	-	0	1.524	1	63	1	1
2023-10-07 1800Z	-	-	0	1.8288	1	63	1	1
2023-10-07 1200Z	180	7.216	1	1.524	1	62	1	1
2023-10-07 0600Z	-	-	0	1.8288	1	61	1	1
2023-10-07 0000Z	-	-	0	1.8288	1	62	1	1
2023-10-06 1800Z	-	-	0	1.8288	1	62	1	1
2023-10-06 1200Z	190	6.7056	1	2.4384	1	62	1	1
2023-10-06 0600Z	200	5.6636	1	2.1336	1	61	1	1
2023-10-06 0000Z	-	-	0	1.8288	1	61	1	1
2023-10-05 1800Z	-	-	0	1.8288	1	61	1	1
2023-10-05 1200Z	210	9.144	1	1.524	1	61	1	1
2023-10-05 0600Z	-	-	0	1.524	1	61	1	1
2023-10-05 0000Z	-	-	0	1.2192	1	60	1	1
2023-10-04 1800Z	-	-	0	1.2192	1	60	1	1
2023-10-04 1200Z	230	8.2296	1	1.524	1	61	1	1
2023-10-04 0000Z	-	-	0	1.8288	2	60	2	2
2023-10-03 1800Z	-	-	0	1.8288	1	60	1	1
2023-10-03 1200Z	270	9.144	1	1.8288	1	60	1	1
2023-10-01 1800Z	-	-	0	1.2192	3	61	3	3
2023-10-01 1200Z	-	-	0	1.2192	4	61	4	4

2023-09-30 1800Z	-	-	0	1.524	3	62	3	3
2023-09-30 1200Z	-	-	0	1.8288	1	63	1	1
2023-09-30 0000Z	-	-	0	2.1336	5	60	5	5
2023-09-29 1800Z	-	-	0	2.1336	1	60	1	1
2023-09-29 1200Z	260	3.3528	1	2.4384	1	61	1	1
2023-09-29 0600Z	-	-	0	2.4384	1	60	1	1
2023-09-28 1800Z	-	-	0	2.1336	1	62	1	1
2023-09-28 1200Z	-	-	0	2.1336	1	62	1	1
2023-09-27 1800Z	-	-	0	3.6576	1	63	1	1
2023-09-27 1200Z	-	-	0	3.048	1	64	1	1
2023-09-27 0000Z	-	-	0	2.1336	5	62	5	5
2023-09-26 1800Z	-	-	0	2.1336	3	62	3	3
2023-09-26 1200Z	250	3.3528	1	2.7432	1	62	1	1
2023-09-26 0600Z	230	5.5584	1	2.7432	1	61	1	1
2023-09-26 0000Z	-	-	0	3.3528	1	62	1	1
2023-09-25 1800Z	-	-	0	3.3528	1	62	1	1
2023-09-25 1200Z	190	3.3528	1	3.9624	1	62	1	1
2023-09-25 0600Z	210	3.3528	1	3.3528	1	62	1	1
2023-09-24 1800Z	-	-	0	3.9624	1	63	1	1
2023-09-24 1200Z	-	-	0	3.9624	1	64	1	1
2023-09-24 0000Z	-	-	0	1.8288	1	62	1	1
2023-09-23 1800Z	-	-	0	1.524	4	61	4	4
2023-09-23 1200Z	180	7.15872	1	1.2192	1	61	1	1
2023-09-23 0600Z	-	-	0	1.2192	1	59	1	1
2023-09-23 0000Z	-	-	0	1.524	4	59	4	4
2023-09-22 1800Z	-	6.7056	0	2.1336	1	58	1	1
2023-09-22 1200Z	320	5.144	1	2.4384	1	58	1	1
2023-09-22 0600Z	-	-	0	2.1336	1	58	1	1
2023-09-22 0000Z	-	-	0	2.4384	1	60	1	1
2023-09-21 1800Z	-	8.2296	0	2.1336	1	55	1	1
2023-09-21 1200Z	280	-	1	2.7432	1	57	1	1
2023-09-21 0600Z	220	-	1	2.7432	1	56	1	1
2023-09-21 0000Z	-	13.716	0	2.7432	1	60	1	1
2023-09-20 1800Z	-	-	0	3.3528	1	60	1	1
2023-09-20 1200Z	260	-	1	3.048	1	61	1	1
2023-09-20 0000Z	-	10.668	0	3.048	1	64	1	1
2023-09-19 1800Z	-	-	0	2.7432	1	63	1	1
2023-09-19 1200Z	240	-	1	3.3528	1	64	1	1
2023-09-19 0000Z	-	11.5824	0	2.1336	1	61	1	1
2023-09-18 1800Z	-	-	0	2.4384	1	62	1	1
2023-09-18 1200Z	270	-	1	1.8288	1	62	1	1
2023-09-18 0600Z	-	-	0	1.524	1	61	1	1
2023-09-17 1800Z	-	-	0	0.9144	2	64	2	2

2023-09-17 1200Z	110	-	1	0.6096	1	65	1	1
2023-09-17 0000Z	-	6.7056	0	1.524	1	64	1	1
2023-09-16 1800Z	-	-	0	1.524	3	64	3	3
2023-09-16 1200Z	-	-	0	1.2192	1	63	1	1
2023-09-16 0000Z	-	-	0	0.6096	5	63	5	5
2023-09-15 1800Z	-	6.7056	0	0.6096	1	63	1	1
2023-09-15 1200Z	40	-	1	0.6096	1	62	1	1
2023-09-15 0600Z	-	-	0	0.6096	2	62	2	2
2023-09-15 0000Z	-	-	0	0.9144	1	62	1	1
2023-09-14 1800Z	-	1.524	0	0.9144	1	63	1	1
2023-09-14 1200Z	210	2.7432	1	1.2192	1	64	1	1
2023-09-14 0600Z	-	-	0	0.6096	1	63	1	1
2023-09-14 0000Z	-	9.144	0	0.6096	1	63	1	1
2023-09-13 1800Z	-	7.3152	0	0.6096	1	62	1	1
2023-09-13 1200Z	280	5.3344	1	0.9144	1	63	1	1
2023-09-13 0600Z	20	-	1	0.9144	2	61	2	2
2023-09-13 0000Z	-	-	0	1.2192	1	61	1	1
2023-09-12 1800Z	360	1.3716	1	1.524	1	62	1	1
2023-09-12 1200Z	350		1	2.1336	1	62	1	1
2023-09-12 0600Z	300	1.3716	1	1.2192	1	63	1	1
2023-09-12 0000Z	-	-	0	0.9144	1	64	1	1
2023-09-11 1800Z	-	-	0	0.9144	1	65	1	1
2023-09-11 1200Z	220	2.2672	1	1.2192	1	66	1	1
		-		0.9144				
2023-09-11 0600Z	210	-	1	0.9144	1	64	1	1
2023-09-11 0000Z	-	-	0	0.9144	2	65	2	2
2023-09-10 1800Z	-	-	0	0.6096	1	65	1	1
2023-09-10 1200Z	250	-	1	0.9144	1	65	1	1
2023-09-10 0000Z	-	-	0	0.6096	1	67	1	1
2023-09-09 1800Z	-	0.9144	0	0.9144	1	67	1	1
2023-09-09 1200Z	-	1.3716	0	0.9144	1	66	1	1
2023-09-09 0600Z	-	-	0	0.9144	2	65	2	2
2023-09-09 0000Z	-	-	0	0.6096	1	65	1	1
2023-09-08 1800Z	-	3.6576	0	0.6096	1	65	1	1
2023-09-08 1200Z	250	-	1	0.6096	1	66	1	1
2023-09-08 0600Z	110	-	1	0.9144	1	61	1	1
2023-09-08 0000Z	-	-	0	0.9144	1	63	1	1
2023-09-07 1800Z	-	3.048	0	0.9144	1	65	1	1
2023-09-07 1200Z	130	3.048	1	1.2192	1	65	1	1
2023-09-07 0600Z	-	-	0	1.2192	1	66	1	1
2023-09-07 0000Z	-	2.7432	0	1.524	1	66	1	1
2023-09-06 1800Z	-	5.5584	0	1.524	1	66	1	1
2023-09-06 1200Z	110	7.3152	1	1.524	1	65	1	1

2023-09-06 0600Z	120		1	2.1336	2	63	2	2
2023-09-06 0000Z	-	-	0	1.524	1	64	1	1
2023-09-05 1800Z	145	-	2	1.524	2	65	2	2
2023-09-05 1200Z	140	5.5584	1	1.524	1	64	1	1
/// **2023-09-05 0600Z**	120	4.8768	1	1.8288	1	65	1	1
		-		1.2192				
2023-09-05 0000Z	-	3.3528	0	1.2192	1	66	1	1
2023-09-04 1800Z	-	3.048	0	1.8288	1	67	1	1
2023-09-04 1200Z	90	1.524	1	0.6096	1	67	1	1
2023-09-04 0600Z	70	-	1	0.9144	1	65	1	1
2023-09-04 0000Z	-	3.048	0	1.2192	1	67	1	1
2023-09-03 1800Z	55	3.048	2	1.2192	2	65	2	2
2023-09-03 1200Z	40	2.7432	1	1.8288	1	62	1	1
2023-09-03 0600Z	50	-	1	2.1336	1	61	1	1
2023-09-03 0000Z	-	0.6096	0	2.1336	1	62	1	1
2023-09-02 1800Z	10	2.4384	1	1.8288	1	63	1	1
2023-09-02 1200Z	20	1.8288	1	0.9144	1	62	1	1
2023-09-02 0600Z	20	-	1	0.9144	1	61	1	1
2023-09-02 0000Z	-	-	0	1.2192	1	60	1	1
2023-09-01 1800Z	140	-	1	0.9144	1	61	1	1
2023-09-01 1200Z	220	-	1	0.9144	1	62	1	1
2023-09-01 0600Z	230	1.8288	1	1.2192	1	60	1	1
2023-08-31 1800Z	-	-	0	1.524	1	61	1	1
2023-08-31 1200Z	-	5.3344	0	1.2192	1	63	1	1
2023-08-31 0000Z	-	5.3344	0	0.9144	6	61	6	6
2023-08-30 1800Z	-	-	0	1.2192	1	61	1	1
2023-08-30 1200Z	272	-	2	1.8288	2	61	2	2
2023-08-30 0000Z	-	-	0	1.2192	1	61	1	1
2023-08-29 1800Z	310	-	1	0.9144	2	61	2	2
2023-08-29 1200Z	340	-	1	0.9144	1	61	1	1
2023-08-29 0000Z	-	-	0	0.9144	1	61	1	1

Table 6.3 Real time data of 45 days average wind speed and average sea waves of Greenwich Lightship United Kingdom [139]

Date (UTC)	**Average Wind Dir (True)**	**Average Wind Spd m/s**	**Wind Obs**	**Average Seas meters**	**Wave Obs**
2023-10-18 0600Z	97	13.421944	6	0.9144	6
2023-10-18 0000Z	98	12.336576	6	1.524	6
2023-10-17 1800Z	89	14.425312	6	0.9144	6

2023-10-17 1200Z	87	12.8661	6	1.2192	6
2023-10-17 0600Z	90	12.8661	1	0.9144	1
2023-10-17 0000Z	100	11.835912	1	1.2192	1
2023-10-16 1800Z	90	13.421944	1	1.2192	1
2023-10-16 1200Z	90	11.288888	1	0.6096	1
2023-10-16 0600Z	110	10.823144	1	0.6096	1
2023-10-16 0000Z	100	6.687032	1	0.3048	1
2023-10-15 1800Z	60	5.14444	1	0.3048	1
2023-10-15 1200Z	360	4.115552	1	0.3048	1
2023-10-15 0600Z	350	8.749648	1	0.6096	1
2023-10-15 0000Z	350	8.749648	1	0.6096	1
2023-10-14 1800Z	330	9.753056	1	0.6096	1
2023-10-14 1200Z	300	9.065632	1	0.9144	1
2023-10-14 0600Z	300	9.753056	1	0.9144	1
2023-10-14 0000Z	300	10.287312	1	1.2192	1
2023-10-13 1800Z	210	17.474576	1	1.524	1
2023-10-13 1200Z	250	5.67368	1	1.524	1
2023-10-13 0600Z	190	14.425312	1	1.2192	1
2023-10-13 0000Z	170	7.716288	1	0.6096	1
2023-10-12 1800Z	240	8.239872	1	0.6096	1
2023-10-12 1200Z	240	8.749648	1	0.6096	1
2023-10-12 0600Z	230	10.823144	1	0.6096	1
2023-10-12 0000Z	210	7.160064	1	0.3048	1
2023-10-11 1800Z	260	3.086664	1	0.3048	1
2023-10-11 1200Z	200	7.716288	1	0.6096	1
2023-10-11 0600Z	240	9.065632	1	0.6096	1
2023-10-11 0000Z	240	10.287312	1	0.9144	1
2023-10-10 1800Z	250	10.287312	1	0.6096	1
2023-10-10 1200Z	250	9.753056	1	0.3048	1
2023-10-10 0600Z	200	5.14444	1	0.6096	1
2023-10-10 0000Z	240	4.733856	1	0.3048	1
2023-10-09 1800Z	250	5.67368	1	0.6096	1
2023-10-09 1200Z	250	4.733856	1	0.3048	1
2023-10-09 0600Z	260	4.115552	1	0.6096	1
2023-10-09 0000Z	240	6.224368	1	0.6096	1
2023-10-08 1800Z	240	3.601344	1	0.6096	1
2023-10-08 1200Z	320	3.601344	1	0.6096	1
2023-10-08 0600Z	240	3.086664	1	0.6096	1
2023-10-08 0000Z	260	2.057776	1	0.6096	1
2023-10-07 1800Z	240	8.239872	1	0.6096	1
2023-10-07 1200Z	240	8.239872	1	0.6096	1
2023-10-07 0600Z	250	8.239872	1	0.9144	1
2023-10-07 0000Z	250	8.749648	1	0.6096	1

2023-10-06 1800Z	240	10.823144	1	0.9144	1
2023-10-06 1200Z	240	8.239872	1	0.3048	1
2023-10-06 0600Z	240	7.160064	1	0.6096	1
2023-10-06 0000Z	230	7.160064	1	0.3048	1
2023-10-05 1800Z	250	6.705344	1	0.6096	1
2023-10-05 1200Z	240	6.705344	1	0.3048	1
2023-10-05 0600Z	260	8.239872	1	0.6096	1
2023-10-05 0000Z	260	8.239872	1	0.6096	1
2023-10-04 1800Z	250	9.321312	1	0.9144	1
2023-10-04 1200Z	250	10.287312	1	0.6096	1
2023-10-04 0600Z	260	8.239872	1	0.9144	1
2023-10-04 0000Z	270	8.239872	1	0.9144	1
2023-10-03 1800Z	270	9.753056	1	1.2192	1
2023-10-03 1200Z	260	12.336576	1	0.9144	1
2023-10-03 0600Z	300	10.823144	1	0.9144	1
2023-10-03 0000Z	250	12.8661	1	0.9144	1
2023-10-02 1800Z	180	8.239872	1	0.3048	1
2023-10-02 1200Z	270	2.057776	1	0.3048	1
2023-10-02 0600Z	100	2.057776	1	0.3048	1
2023-10-02 0000Z	230	3.086664	1	0.6096	1
2023-10-01 1800Z	280	1.543332	1	0.3048	1
2023-10-01 1200Z	190	4.633808	1	0.6096	1
2023-10-01 0600Z	200	6.682032	1	0.3048	1
2023-10-01 0000Z	180	6.224368	1	0.6096	1
2023-09-30 1800Z	190	6.682032	1	0.3048	1
2023-09-30 1200Z	190	4.633808	1	0.6096	1
2023-09-30 0600Z	160	2.057776	1	0.3048	1
2023-09-30 0000Z	340	3.086664	1	0.6096	1
2023-09-29 1800Z	270	7.226432	1	0.6096	1
2023-09-29 1200Z	280	9.753056	1	0.9144	1
2023-09-29 0600Z	300	12.8661	1	1.2192	1
2023-09-29 0000Z	190	11.288888	1	0.9144	1
2023-09-28 1800Z	180	10.287312	1	1.2192	1
2023-09-28 1200Z	200	8.749648	1	0.9144	1
2023-09-28 0600Z	245	6.224368	2	2.4384	2
2023-09-28 0000Z	250	9.321312	1	1.524	1
2023-09-27 1800Z	240	10.823144	1	0.6096	1
2023-09-27 1200Z	130	4.633808	1	0.3048	1
2023-09-27 0600Z	130	5.14444	1	0.6096	1
2023-09-27 0000Z	280	2.57222	1	0.3048	1
2023-09-26 1800Z	250	2.57222	1	0.9144	1
2023-09-26 1200Z	90	6.224368	1	0.6096	1
2023-09-26 0600Z	180	6.224368	1	0.9144	1

2023-09-26 0000Z	120	6.682032	1	0.6096	1
2023-09-25 1800Z	180	1.543332	1	0.9144	1
2023-09-25 1200Z	240	5.042216	1	0.6096	1
2023-09-25 0600Z	240	6.224368	1	1.2192	1
2023-09-25 0000Z	210	10.823144	1	1.2192	1
2023-09-24 1800Z	170	9.753056	1	1.2192	1
2023-09-24 1200Z	170	10.823144	1	1.2192	1
2023-09-24 0600Z	180	11.835912	1	0.9144	1
2023-09-24 0000Z	200	11.835912	1	0.6096	1
2023-09-23 1800Z	210	6.224368	1	0.6096	1
2023-09-23 1200Z	260	4.733856	1	0.6096	1
2023-09-23 0600Z	300	5.14444	1	0.6096	1
2023-09-23 0000Z	310	8.239872	1	0.9144	1
2023-09-22 1800Z	300	7.160064	1	0.9144	1
2023-09-22 1200Z	270	10.287312	1	0.9144	1
2023-09-22 0600Z	320	6.682032	1	0.6096	1
2023-09-22 0000Z	280	3.086664	1	0.9144	1
2023-09-21 1800Z	240	6.682032	1	0.6096	1
2023-09-21 1200Z	220	7.226432	1	0.9144	1
2023-09-21 0600Z	230	6.682032	1	0.6096	1
2023-09-21 0000Z	230	5.67368	1	2.1336	1
2023-09-20 1800Z	190	15.432576	1	1.8288	1
2023-09-20 1200Z	200	13.986192	1	0.6096	1
2023-09-20 0600Z	200	15.432576	1	0.3048	1
2023-09-20 0000Z	220	13.421944	1	0.6096	1
2023-09-19 1800Z	220	13.708888	1	0.3048	1
2023-09-19 1200Z	230	16.460448	1	0.9144	1
2023-09-19 0600Z	220	14.816896	1	0.6096	1
2023-09-19 0000Z	250	12.8661	1	0.9144	1
2023-09-18 1800Z	260	12.336576	1	0.6096	1
2023-09-18 1200Z	250	16.460448	1	0.9144	1
2023-09-18 0600Z	200	8.749648	1	0.6096	1
2023-09-18 0000Z	170	6.687032	1	1.2192	1
2023-09-17 1800Z	110	6.224368	1	1.2192	1
2023-09-17 1200Z	100	6.224368	1	1.2192	1
2023-09-17 0600Z	70	9.065632	1	1.2192	1
2023-09-17 0000Z	50	10.287312	1	0.9144	1
2023-09-16 1800Z	50	8.239872	1	0.6096	1
2023-09-16 1200Z	60	5.67368	1	0.6096	1
2023-09-16 0600Z	60	5.14444	1	0.6096	1
2023-09-16 0000Z	80	5.67368	1	0.6096	1
2023-09-15 1800Z	50	3.086664	1	0.9144	1
2023-09-15 1200Z	110	2.57222	1	0.9144	1

2023-09-15 0600Z	70	3.601344	1	0.9144	1
2023-09-15 0000Z	60	1.543332	1	0.6096	1
2023-09-14 1800Z	340	1.028888	1	0.9144	1
2023-09-14 1200Z	310	2.057776	1	0.6096	1
2023-09-14 0600Z	320	2.57222	1	0.9144	1
2023-09-14 0000Z	80	2.57222	1	0.9144	1
2023-09-13 1800Z	80	4.114544	1	1.524	1
2023-09-13 1200Z	30	6.682032	1	0.9144	1
2023-09-13 0600Z	10	8.749648	1	1.2192	1
2023-09-13 0000Z	360	9.753056	1	0.9144	1
2023-09-12 1800Z	260	7.160064	1	1.2192	1
2023-09-12 1200Z	250	5.14444	1	1.2192	1
2023-09-12 0600Z	240	3.601344	1	0.6096	1
2023-09-12 0000Z	270	4.114544	1	0.6096	1
2023-09-11 1800Z	240	4.633808	1	0.3048	1
2023-09-11 1200Z	280	4.633808	1	0.3048	1
2023-09-11 0600Z	270	6.224368	1	0.3048	1
2023-09-11 0000Z	280	7.716288	1	0.6096	1
2023-09-10 1800Z	240	2.57222	1	0.6096	1
2023-09-10 1200Z	210	9.753056	1	0.6096	1
2023-09-10 0600Z	90	5.14444	1	0.9144	1
2023-09-10 0000Z	50	5.14444	1	0.9144	1
2023-09-09 1800Z	20	3.601344	1	1.2192	1
2023-09-09 1200Z	110	3.086664	1	1.524	1
2023-09-09 0600Z	40	3.601344	1	1.524	1
2023-09-09 0000Z	40	5.14444	1	1.2192	1
2023-09-08 1800Z	350	3.601344	1	0.6096	1
2023-09-08 1200Z	50	2.57222	1	0.6096	1
2023-09-08 0600Z	50	1.543332	1	0.6096	1
2023-09-08 0000Z	40	2.57222	1	0.6096	1
2023-09-07 1800Z	120	2.57222	1	0.3048	1
2023-09-07 1200Z	60	2.57222	1	0.3048	1
2023-09-07 0600Z	70	3.086664	1	0.6096	1
2023-09-07 0000Z	10	2.85808	1	0.6096	1
2023-09-06 1800Z	10	0.514444	1	0.9144	1
2023-09-06 1200Z	330	0.514444	1	0.6096	1
2023-09-06 0600Z	50	1.028888	1	0.3048	1
2023-09-06 0000Z	30	5.042216	1	0.6096	1
2023-09-05 1800Z	80	6.224368	1	0.3048	1
2023-09-05 1200Z	80	8.239872	1	0.6096	1
2023-09-05 0600Z	70	9.753056	1	0.3048	1
2023-09-05 0000Z	50	10.823144	1	0.6096	1
2023-09-04 1800Z	60	9.753056	1	0.6096	1

2023-09-04 1200Z	50	7.160064	1	0.6096	1
2023-09-04 0600Z	70	6.682032	1	0.6096	1
2023-09-04 0000Z	60	9.753056	1	0.6096	1
2023-09-03 1800Z	60	6.224368	1	0.6096	1
2023-09-03 1200Z	50	5.14444	1	0.6096	1
2023-09-03 0600Z	60	8.239872	1	0.6096	1
2023-09-03 0000Z	50	13.421944	2	0.9144	2

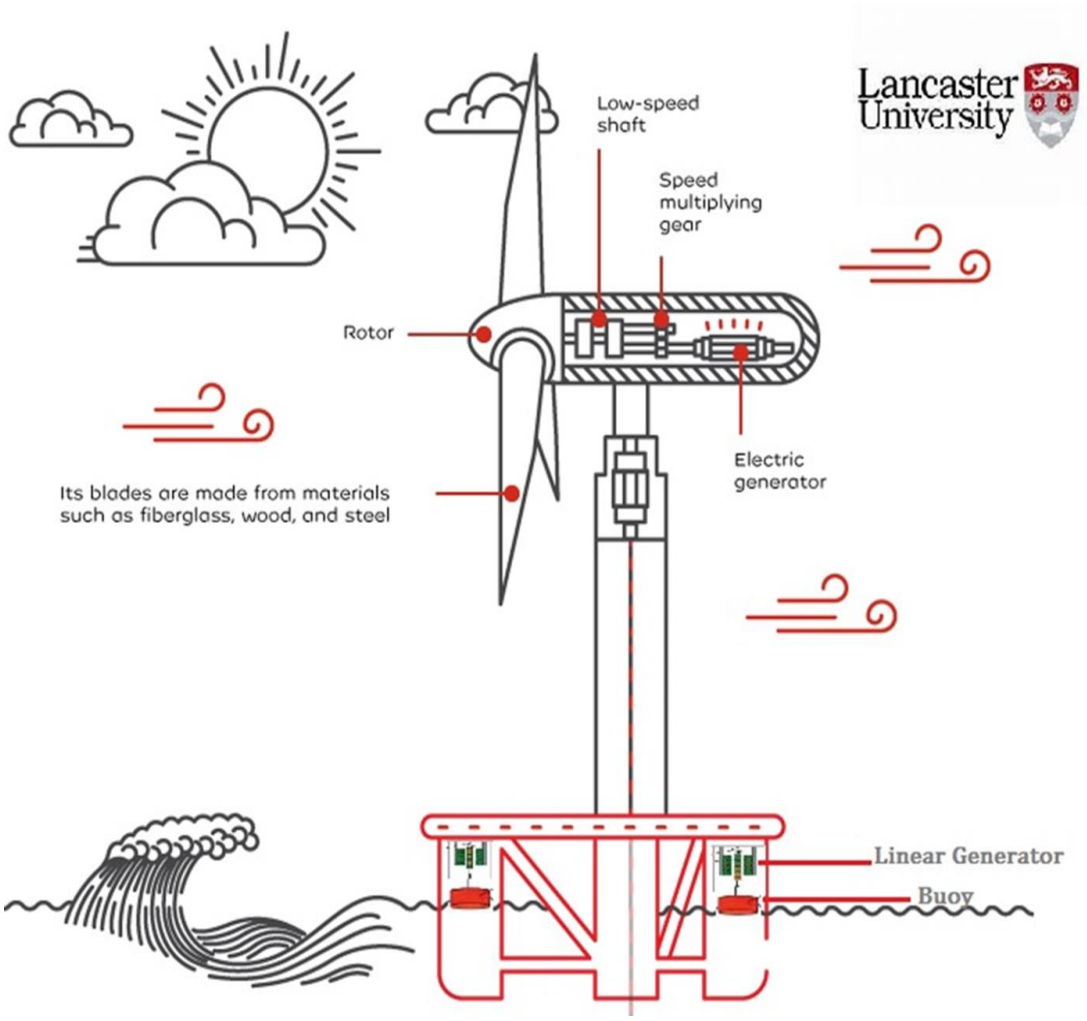
Lancaster University
Low-speed shaft
Speed multiplying gear
Rotor
Electric generator
Its blades are made from materials such as fiberglass, wood, and steel
Linear Generator
Buoy